

Aus der  
Klinik für Diagnostische und Interventionelle Radiologie  
des Universitätsklinikums Bonn  
Direktorin: Univ.-Prof. Dr. Ulrike Attenberger

**Quantitative kardiale Magnetresonanztomographie zur Charakterisierung  
nicht-ischämischer Herzmuskelerkrankungen**

Habilitationsschrift  
Zur Erlangung der Venia Legendi  
der Hohen Medizinischen Fakultät  
der Rheinischen-Friedrich-Wilhelms-Universität Bonn  
für das Lehrgebiet  
„Radiologie“

Vorgelegt von  
**Dr. med. Alexander Isaak**  
Wissenschaftlicher Mitarbeiter  
an der Rheinischen Friedrich-Wilhelms-Universität Bonn  
Bonn 2023

Datum des Habilitationskolloquiums: 4. Mai 2023

*Meiner Familie*

## Zugrunde liegende Arbeiten

Der vorliegenden kumulativen Habilitationsschrift liegen die im Folgenden aufgeführten Publikationen zugrunde. Die Arbeiten untersuchen den diagnostischen Nutzen quantitativer Techniken der kardialen Magnetresonanztomographie zur Charakterisierung nicht-ischämischer Herzmuskelerkrankungen und legen den Schwerpunkt auf inflammatorische Myokardveränderungen.

**Isaak A**, Bischoff LM, Faron A, Endler C, Mesropyan N, Sprinkart AM, Pieper CC, Kuetting D, Dabir D, Attenberger U, Luetkens JA. Multiparametric cardiac magnetic resonance imaging in pediatric and adolescent patients with acute myocarditis. *Pediatric Radiology*. 2021 Dec;51(13):2470-2480. <https://doi.org/10.1007/s00247-021-05169-7>.

**Isaak A**, Ayub TH, Merz WM, Faron A, Endler C, Sprinkart AM, Pieper CC, Kuetting D, Dabir D, Attenberger U, Zimmer S, Becher UM, Luetkens JA. Peripartum Cardiomyopathy: Diagnostic and Prognostic Value of Cardiac Magnetic Resonance in the Acute Stage. *Diagnostics*. 2022 Feb 1;12(2):378. <https://doi.org/10.3390/diagnostics12020378>.

Faron A\*, **Isaak A\***, Mesropyan N, Reinert M, Schwab K, Sirokay J, Sprinkart AM, Bauernfeind FG, Dabir D, Pieper CC, Heine A, Kuetting D, Attenberger U, Landsberg J, Luetkens JA. Cardiac MRI Depicts Immune Checkpoint Inhibitor-induced Myocarditis: A Prospective Study. *Radiology*. 2021 Dec;301(3):602-609. <https://doi.org/10.1148/radiol.2021210814>.

**Isaak A\***, Praktijnjo M\*, Jansen C, Faron A, Sprinkart AM, Pieper CC, Chang J, Fimmers R, Meyer C, Dabir D, Thomas D, Trebicka J, Attenberger U, Kuetting D, Luetkens JA. Myocardial Fibrosis and Inflammation in Liver Cirrhosis: MRI Study of the Liver-Heart Axis. *Radiology*. 2020 Oct;297(1):51-61. <https://doi.org/10.1148/radiol.2020201057>.

*\*geteilte Erstautorenschaft*



*Folgende Publikationen werden in der vorliegenden Habilitationsschrift ebenfalls berücksichtigt:*

Dabir D, Luetkens J, Kuetting DLR, Feisst A, **Isaak A**, Schild HH, Thomas D. Cardiac magnetic resonance including parametric mapping in acute Takotsubo syndrome: Preliminary findings. *European Journal of Radiology*. 2019 Apr;113:217-224.

Luetkens J, Faron A, **Isaak A**, Dabir D, Kuetting D, Feisst A, Schmeel FC, Sprinkart AM, Thomas D. Comparison of Original and 2018 Lake Louise Criteria for Diagnosis of Acute Myocarditis: Results of a Validation Cohort. *Radiology Cardiothoracic Imaging*. 2019 Jul 25;1(3):e190010.

Luetkens JA\*, von Landenberg C\*, **Isaak A**, Faron A, Kuetting D, Gliem C, Dabir D, Kornblum C\*, Thomas D\*. Comprehensive Cardiac Magnetic Resonance for Assessment of Cardiac Involvement in Myotonic Muscular Dystrophy Type 1 and 2 Without Known Cardiovascular Disease. *Circulation Cardiovascular Imaging*. 2019 Jun;12(6):e009100.

Luetkens JA\*, **Isaak A\***, Öztürk C, Mesropyan N, Monin M, Schlabe S, Reinert M, Faron A, Heine A, Velten M, Dabir D, Boesecke C, Strassburg CP, Attenberger U, Zimmer S, Duerr GD, Nattermann J. Cardiac MRI in Suspected Acute COVID-19 Myocarditis. *Radiology Cardiothoracic Imaging*. 2021 Mar 4;3(2):e200628.

**Isaak A**, Feisst A, Luetkens JA. Myocarditis Following COVID-19 Vaccination. *Radiology*. 2021 Oct;301(1):E378-E379.

Kravchenko D, **Isaak A**, Zimmer S, Mesropyan N, Reinert M, Faron A, Pieper CC, Heine A, Velten M, Nattermann J, Kuetting D, Duerr GD, Attenberger UI, Luetkens JA. Cardiac MRI in Patients with Prolonged Cardiorespiratory Symptoms after Mild to Moderate COVID-19. *Radiology*. 2021 Dec;301(3):E419-E425.

Kravchenko D, **Isaak A**, Mesropyan N, Endler C, Bischoff L, Vollbrecht T, Pieper CC, Sedaghat A, Kuetting D, Hart C, Feisst A, Attenberger U, Luetkens JA. Cardiac MRI in Suspected Acute Myocarditis After COVID-19 mRNA Vaccination. *Rofo*. 2022 Mar 10.

*\*geteilte Erstautorenschaft*

## **1. Inhaltsverzeichnis**

<b>1. Inhaltsverzeichnis .....</b>	<b>6</b>
<b>2. Einleitung .....</b>	<b>8</b>
2.1 Nicht-ischämische Kardiomyopathien: Definition und Klassifikation.....	8
2.2 Komplikationen der nicht-ischämischen Kardiomyopathien .....	13
2.3 Kardiale MRT bei nicht-ischämischen Kardiomyopathien .....	15
2.4 Quantitative MRT-Techniken bei nicht-ischämischen Kardiomyopathien.....	19
2.5 Fragestellung.....	23
<b>3. Ergebnisse .....</b>	<b>25</b>
3.1 Quantitative kardiale MRT bei der pädiatrischen Myokarditis .....	25
3.2 Quantitative kardiale MRT bei der peripartalen Kardiomyopathie.....	37
3.3 Quantitative kardiale MRT bei Immun-Checkpoint-Inhibitor-induzierter Myokarditis .	51
3.4 Quantitative kardiale und hepatische MRT bei der Leberzirrhose.....	60
<b>4. Diskussion.....</b>	<b>73</b>
<b>5. Zusammenfassung .....</b>	<b>83</b>
<b>6. Inhaltliche Überlappung mit anderen kumulativen Habilitationsschriften .....</b>	<b>85</b>
<b>7. Bibliographie .....</b>	<b>86</b>
<b>8. Danksagung .....</b>	<b>105</b>

## Abkürzungsverzeichnis

AHA.....	American Heart Association
AUC.....	Area under the curve
b-SSFP.....	Balanced Steady-State Free Precession
COVID-19.....	Coronavirus disease 2019
CT.....	Computertomographie
ECV.....	Extrazelluläre Volumenfraktion
EKG.....	Elektrokardiogramm
ICI.....	Immun-Checkpoint-Inhibitor
LGE.....	Late Gadolinium Enhancement
MRT.....	Magnetresonanztomographie
ROI.....	Region of Interest
SI.....	Signalintensität
STIR.....	Short Tau Inversion Recovery

## 2. Einleitung

### 2.1 Nicht-ischämische Kardiomyopathien: Definition und Klassifikation

Erkrankungen des Herzmuskels können generell in ischämisch oder nicht-ischämisch eingeteilt werden. Ischämische Myokardveränderungen sind in der Regel auf die koronare Herzerkrankung zurückzuführen. Nicht-ischämische Kardiomyopathien sind Herzmuskelerkrankungen, die nach der American Heart Association (AHA) definitionsgemäß nicht Folge einer koronaren Herzerkrankung, einer arteriellen Hypertonie, einer Herzklappenerkrankung oder eines angeborenen Herzfehlers sind (Maron et al., 2006). Der klinisch häufig verwendete Begriff „ischämische Kardiomyopathie“, welcher zur Beschreibung einer erheblichen linksventrikulären Funktionseinschränkung aufgrund einer irreversiblen Myokardinfarzierung im Rahmen der koronaren Herzerkrankung dient, wird demnach nicht als „Kardiomyopathie“ im eigentlichen Sinn definiert (Felker et al., 2002; Maron et al., 2006; Elliott et al., 2008). Nicht-ischämische Kardiomyopathien setzen sich aus unterschiedlichen Krankheitsentitäten zusammen. Die bis heute weitläufig akzeptierte AHA-Klassifikation von 2006 unterscheidet die primären Kardiomyopathien (betreffen ausschließlich oder überwiegend den Herzmuskel) von den sekundären Kardiomyopathien (betreffen im Rahmen diverser systemischer Erkrankungen/Einflüsse mitunter den Herzmuskel) (Maron et al., 2006). Bei der Einteilung der nicht-ischämischen Kardiomyopathien kommt es häufig zu Überschneidungen. Daher bestehen parallel zur AHA-Klassifikation auch andere Klassifikationsempfehlungen, u.a. die der European Society of Cardiology (Elliott et al., 2008), welche den Schwerpunkt vermehrt auf die phänotypische Klassifizierung legt.

#### *Primäre Kardiomyopathien*

Die Unterteilung der primären Kardiomyopathien erfolgt in genetische (u.a. hypertrophe Kardiomyopathie, arrhythmogene rechtsventrikuläre Kardiomyopathie, linksventrikuläre Non-Compaction-Kardiomyopathie), erworbene (u.a. Myokarditis, Takotsubo-Kardiomyopathie, peripartale Kardiomyopathie) und gemischte Formen (u.a. dilatative Kardiomyopathie, restriktive Kardiomyopathie) (Maron et al., 2006) (siehe *Abbildung 1*).

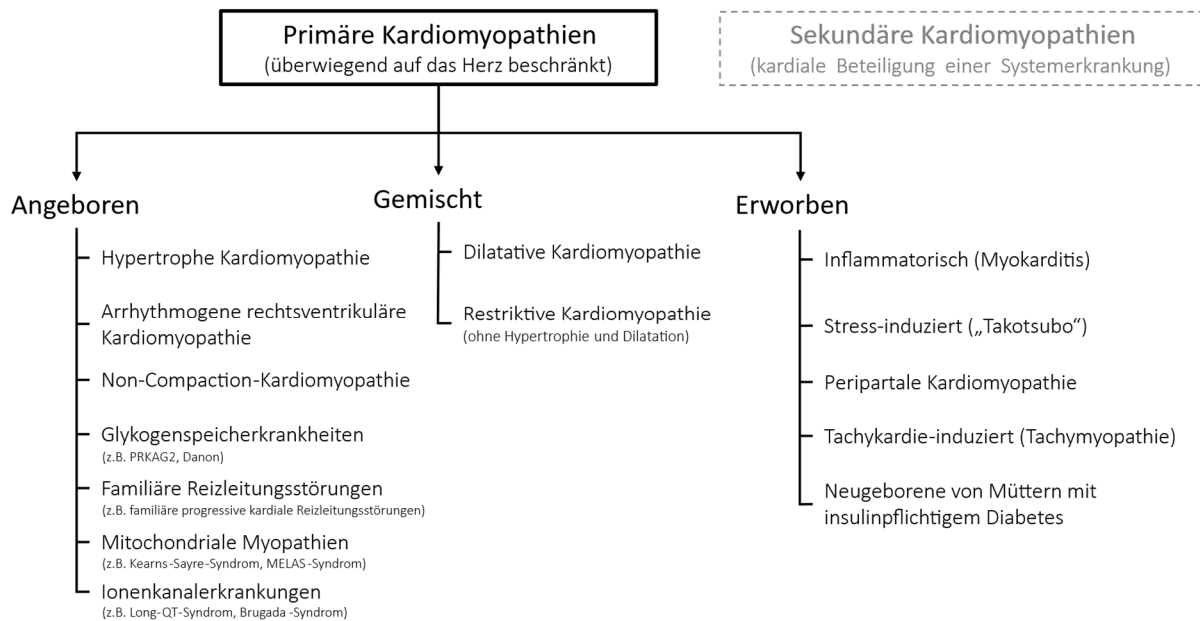


Abbildung 1. Einteilung der primären Kardiomyopathien nach der American Heart Association. Abbildung in Anlehnung an (Maron et al., 2006).

### Angeborene und gemischte primäre Kardiomyopathien

Die Prävalenz der genetischen und gemischten Formen der primären Kardiomyopathien variiert stark zwischen den verschiedenen Typen sowie je nach angewandter Definition. Die beiden häufigsten Formen sind die dilatative und die hypertrophe Kardiomyopathie (Seferović et al., 2019). Die dilatative Kardiomyopathie kann anhand einer ventrikulären Dilatation in Verbindung mit einer verminderten Ejektionsfraktion diagnostiziert werden (Weintraub et al., 2017). Die hypertrophe Kardiomyopathie ist durch die Manifestation einer symmetrischen oder asymmetrischen linksventrikulären Hypertrophie gekennzeichnet, die nicht auf eine erhöhte Nachlast infolge eines Vitiums oder einer arteriellen Hypertonie zurückzuführen ist (Marian and Braunwald, 2017). Darüber hinaus umfassen die genetischen Kardiomyopathien viele weitere, relativ seltene Formen. Die arrhythmogene rechtsventrikuläre Kardiomyopathie ist durch ein meist fettig-fibrotisches Remodelling des rechten Ventrikels mit einem einhergehenden Funktionsverlust gekennzeichnet. Die linksventrikuläre Non-Compaction-Kardiomyopathie wird durch die Störung der myokardialen Verdichtung während der embryonalen Organogenese verursacht und führt zu einer ausgeprägten Trabekularisierung mit aufgelockerter endokardialer Myokardstruktur (Towbin et al., 2015).

### Primäre erworbene Kardiomyopathien

Die häufigste erworbene Form der primären Kardiomyopathien ist die Myokarditis (Inzidenz: ca. 22 Fälle pro 100.000 Einwohner pro Jahr (Vos et al., 2015)), die v.a. junge Erwachsene

betrifft und ein weites Spektrum an klinischen Erscheinungs- und Verlaufsformen bietet (Ammirati et al., 2018). Sie kann u.a. entsprechend ihrer klinischen Präsentation (fulminante, akute, subakute oder chronische Myokarditis), entsprechend der Histologie (Riesenzell-Myokarditis, eosinophile Myokarditis, lymphozytäre Myokarditis) oder auch anhand ihrer Ätiologie (virale, allergische, immun-vermittelte oder toxische Myokarditis) klassifiziert werden (Ammirati et al., 2020). Zudem kann die Myokarditis zur Entwicklung einer dilatativen Kardiomyopathie mit systolischer Funktionseinschränkung führen, welche dann als chronisch-inflammatorische Kardiomyopathie bezeichnet wird (Ammirati et al., 2020). Die peripartale Kardiomyopathie definiert sich über eine akute oder langsam fortschreitende Herzinsuffizienz und manifestiert sich überwiegend in der späten Schwangerschaft und in der Zeit um die Entbindung. Phänotypisch zeigt sich meist das Bild einer dilatativen Kardiomyopathie. Die Takotsubo-Kardiomyopathie (auch: Stress-induzierte Kardiomyopathie oder Broken-Heart Syndrom) geht mit einer akuten, in der Regel jedoch vollständig reversiblen regionalen Wandbewegungsstörung einher, wobei meist die apikalen und mittventrikulären Myokardsegmente betroffen sind (sogenanntes „apical ballooning“) (Templin et al., 2015). Sie betrifft häufig postmenopausale Frauen und ist in den meisten Fällen mit vorausgehenden emotionalen oder physischen Triggern assoziiert (Templin et al., 2015).

### Sekundäre Kardiomyopathien

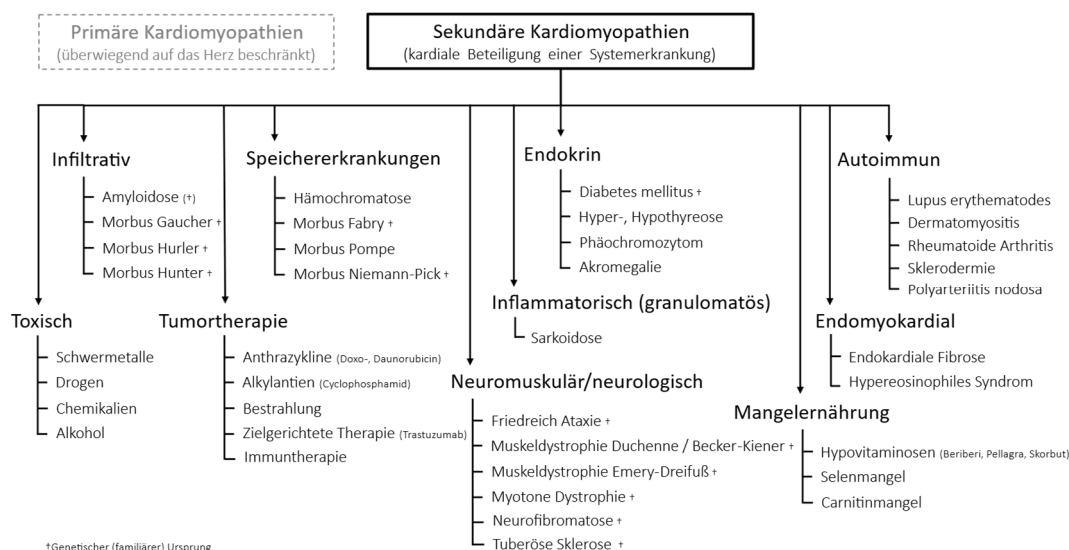


Abbildung 2. Einteilung der sekundären Kardiomyopathien nach der American Heart Association. Abbildung in Anlehnung an (Maron et al., 2006).

Die heterogene Gruppe der sekundären Kardiomyopathien begründet sich auf einer Vielzahl von Systemerkrankungen (u.a. entzündliche, endokrinologische, autoimmun-bedingte,

neurologische und infiltrative Systemerkrankungen sowie Speichererkrankungen) oder auf exogene Einflüsse (v.a. toxische und medikamentöse Ursachen), die meist im Rahmen eines Multiorganbefalls auch das Myokard betreffen können (Maron et al., 2006) (siehe *Abbildung 2*). Die Diagnosefindung bei den sekundären Kardiomyopathien ist aufgrund ihrer unterschiedlichen und überwiegend unspezifischen Morphologie besonders herausfordernd und gelingt in der Regel nur in Verbindung mit der Patientenanamnese.

Speichererkrankungen sind eine wichtige Gruppe der sekundären Kardiomyopathien. Bei diesen Systemerkrankungen kommt es zu intrazellulären Ablagerungen von Substanzen im Gewebe verschiedener Organe, potenziell auch in den Myozyten. Beispiele hierfür sind die Hämochromatose (Akkumulation von Eisen), Morbus Fabry (Akkumulation von Glykosphingolipid) oder auch Morbus Pompe (Akkumulation von Glykogen in den Lysosomen). Zu den in der AHA-Klassifikation als „infiltrativ“ definierten Ursachen der Kardiomyopathien zählt insbesondere die Amyloidose, bei der es im Rahmen einer Myokardbeteiligung zur extrazellulären Ansammlung fehlgefalteter Amyloid-Proteine zwischen den Myozyten kommt. Die meisten infiltrativen Kardiomyopathien zeigen den Phänotyp einer linksventrikulären Hypertrophie, selten kommt es auch zu einer linksventrikulären Dilatation (Seward and Casaclang-Verzosa, 2010). Funktionell sind diese Kardiomyopathien oft durch eine restriktive Funktionseinschränkung charakterisiert (Pereira et al., 2018). Zu den entzündlich-bedingten Ursachen gehört insbesondere auch die Sarkoidose, bei der die Bildung von nicht-verkäsenden Granulomen auch das Myokard betreffen kann. Weitere wichtige Ursachen sekundärer Kardiomyopathien sind endokrinologische Erkrankungen (z.B. der Diabetes mellitus und die Hyper- oder Hypothyreose) (Klein and Danzi, 2007; Jia et al., 2018) und Autoimmunerkrankungen (v.a. rheumatische Erkrankungen, wie die rheumatoide Arthritis, sowie Erkrankungen aus der Gruppe der Kollagenosen, wie der systemische Lupus erythematoses und die Polymyositis und Dermatomyositis) (Prasad et al., 2015). Darüber hinaus können auch neuromuskuläre Erkrankungen mit sekundären Kardiomyopathien assoziiert sein (u.a. Muskeldystrophie Duchenne und Becker-Kiener, Friedreich-Ataxie und myotonen Dystrophien).

Eine nicht unerhebliche Gruppe der sekundären Kardiomyopathien wird durch toxische und medikamentöse Trigger verursacht. Die Mechanismen der toxisch-induzierten Kardiomyopathien sind in Abhängigkeit der jeweiligen Noxen sehr unterschiedlich, führen

aber generell zu Störungen multipler zellulärer und struktureller Funktionen des Myokards (Hantson, 2019). Der führende Phänotyp der toxischen Kardiomyopathien ist die dilatative Kardiomyopathie. Die alkoholische Kardiomyopathie kann bei Personen mit langfristig starkem Alkoholkonsum auftreten und ist oft ein unerkannter Grund einer dilatativen Kardiomyopathie (Gavazzi et al., 2000). Diese unterscheidet sich von der zirrhotischen Kardiomyopathie, welche bei Patient/-innen mit Leberzirrhose unabhängig vom Alkoholabusus auftritt und primär auf hämodynamischen Veränderungen beruht (Møller and Henriksen, 2010). Hauptmanifestation dieses klinischen Syndroms ist die splanchnische Vasodilatation mit resultierender zentraler Hypovolämie und hyperdynamer Zirkulation (niedriger systemischer Gefäßwiderstand, hohes Herzzeitvolumen). Obwohl dieser Zustand in Ruhe oft kompensiert ist, demaskiert sich bei physiologischen und pathophysiologischen Belastungen eine unzureichende myokardiale Reaktionsfähigkeit (Zardi et al., 2010). Zu den Ursachen toxischer Kardiomyopathien zählen auch Kokain (Schwartz et al., 2010) und Methamphetamin (Schürer et al., 2017), welche durch direkte toxische Schädigungen und durch Katecholamin-vermittelte Tachykardien und Vasokonstriktionen zu akuten und chronischen Myokardveränderungen (Myokardinfarkte, Myokarditis und Herzinsuffizienz) führen können (Hantson, 2019).

Hiervon separiert werden therapieassoziierte Myokardveränderungen, vor allem im Rahmen onkologischer Therapien. Im Rahmen des komplexen klinischen Managements onkologischer Patient/-innen spielt die Kardiotoxizität eine entscheidende Rolle hinsichtlich Therapieerträglichkeit und Langzeitprognose und treibt aktuell die Entwicklung der spezifischen Schnittstelle der Kardi-onkologie voran. Klassische Chemotherapeutika wie Anthrazykline und Alkylantien sind mit der Entwicklung einer Kardiomyopathie assoziiert, die primär auf die Zellmembranschädigung durch die Bildung freier Radikale zurückzuführen ist (Hahn et al., 2014). Ferner sind kardiotoxische Effekte auch bei modernen zielgerichteten und immuntherapeutischen Krebstherapien beschrieben, z.B. bei monoklonalen Antikörpern (insbesondere Trastuzumab) und Immun-Checkpoint-Inhibitoren (ICI) (Zamorano et al., 2016). Die hier aufgeführten sekundären Kardiomyopathien repräsentieren nur einen Teil der derzeit bekannten Formen. Insgesamt zeigt die Heterogenität ihrer möglichen Ursachen die immense klinische Relevanz für viele unterschiedliche Fachrichtungen über die Kardiologie hinaus. Die Behandlung richtet sich in erster Linie auf den zugrunde liegenden systemischen



Krankheitsprozess, die Beseitigung der auslösenden Faktoren und die Behandlung der Symptome der Herzinsuffizienz.

## 2.2 Komplikationen der nicht-ischämischen Kardiomyopathien

Trotz ihrer Heterogenität führen alle Formen der Kardiomyopathien zu einer etwaigen Struktur- und Funktionsänderung des Herzmuskelgewebes, die langfristig insbesondere das Risiko für eine Herzinsuffizienz und für Herzrhythmusstörungen erhöht. Nicht-ischämische Kardiomyopathien betreffen häufiger jüngere Menschen und Frauen (DeFilippis et al., 2022). Nahezu 50 % der Menschen, die im Kindes- oder Jugendalter plötzlich sterben oder sich einer Herztransplantation unterziehen, sind von Kardiomyopathien betroffen (McKenna et al., 2017). Zu den allgemeinen klinischen Manifestationen gehören Herzrhythmusstörungen, Kurzatmigkeit, Ödeme der unteren Extremitäten, Synkopen und Brustschmerzen. Im Rahmen der Diagnostik und Risikobewertung wird der Interaktion zwischen genetischen und erworbenen Ursachen immer mehr eine Schlüsselrolle zugeschrieben (McDonagh et al., 2021). Die Identifizierung einer erworbenen Ursache der Kardiomyopathie schließt eine zugrunde liegende pathogene Genvariante nicht aus, und letztere kann eine zusätzliche erworbene Ursache erfordern, um klinisch manifest zu werden (McDonagh et al., 2021). Im Allgemeinen ist die Prognose der nicht-ischämischen Kardiomyopathien besser als die der ischämischen Myokarderkrankung (Corbalan et al., 2019).

### *Herzinsuffizienz*

Die nicht-ischämischen Kardiomyopathien sind eine häufige Ursache für die Entwicklung einer chronischen Herzinsuffizienz (Seferović et al., 2019; McDonagh et al., 2021). Der Anteil der Patient/-innen mit einer Herzinsuffizienz aufgrund nicht-ischämischer Herzmuskelerkrankungen schwankte in größeren Therapiestudien zwischen 18 % und 53 % (Follath, 1999). Die dilatative Kardiomyopathie ist einer der häufigsten Gründe für eine Herzinsuffizienz und die häufigste Indikation für eine Herztransplantation (McKenna et al., 2017; Weintraub et al., 2017). Im Rahmen der Kardiomyopathien können systolische, diastolische oder kombinierte Herzinsuffizienzen vorliegen (McDonagh et al., 2021). Die infiltrativen Kardiomyopathien sind häufig mit einer diastolischen Dysfunktion assoziiert (Pereira et al., 2018). Die akute Myokarditis kann zu einer verbleibenden systolischen Funktionseinschränkung führen (Merlo et al., 2019) und in eine chronisch-inflammatorische

Kardiomyopathie übergehen, wobei die zugrunde liegenden Mechanismen noch unzureichend untersucht sind (Tschöpe et al., 2021). Die peripartale Kardiomyopathie zeigt in der akuten Erkrankungsphase typischerweise das Bild einer dilatativen Kardiomyopathie mit neu auftretender Herzinsuffizienz-Symptomatik. Die meist hochgradige Funktionseinschränkung ist potenziell reversibel, geht bei einem Teil der betroffenen Frauen jedoch in eine chronische Herzinsuffizienz über (Regitz-Zagrosek et al., 2018). Bei einem Großteil der Systemerkrankungen, die mit Kardiomyopathien assoziiert sind, ist der Grad der Herzinsuffizienz letztlich oft der bestimmende Faktor hinsichtlich der Langzeitprognose (Dispenzieri et al., 2003; Birnie et al., 2016; Dunlay et al., 2019).

### *Plötzlicher Herztod*

Als häufigste Ursache für den plötzlichen Herztod stehen die nicht-ischämischen Herzmuskelerkrankungen nach der koronaren Herzkrankheit an zweiter Stelle (Roger et al., 2011). Zusammengefasst machen allein die primären nicht-ischämischen Herzmuskelerkrankungen mehr als ein Drittel der Ursachen für den plötzlichen Herztod aus (Corrado, 2001; McKenna et al., 2017). Die Myokarditis ist dabei mit 8-14 % eine der wichtigsten Ursachen in der jungen Bevölkerung (Corrado, 2001; Harmon et al., 2014; McKenna et al., 2017). Ursächlich sind meist ventrikuläre Tachy- und Bradyarrhythmien. Die Therapie mittels implantierbarem Kardioverter-Defibrillator kann bei selektierten Patient/-innen die Sterblichkeit senken (Desai et al., 2004) und kann bei hämodynamisch signifikanten Arrhythmien oder überlebtem Herzstillstand als Sekundärprävention indiziert sein. Die Studienergebnisse zur Primärprävention durch einen implantierbaren Kardioverter-Defibrillator zeigen hingegen unterschiedliche Ergebnisse und unterstreichen auch die Relevanz einer modernen Herzinsuffizienztherapie bei nicht-ischämischen Kardiomyopathien zur Reduzierung des Mortalitätsrisikos (Kadish et al., 2004; Køber et al., 2016). Die Möglichkeiten zur genauen Risikobewertung des plötzlichen Herztods bei Kardiomyopathien sind bis heute relativ begrenzt und basieren meist auf multiplen bildgebenden, elektrophysiologischen, serologischen und genetischen Markern (Hammersley and Halliday, 2020). Die bildgebende Detektion von myokardialer Fibrose mittels kardialer Magnetresonanztomographie (MRT) spielt dabei eine immer entscheidendere Rolle. Da die frühzeitige Erkennung des strukturellen und funktionellen Ausmaßes einer primären oder

sekundären Herzmuskelerkrankung von erheblicher therapeutischer und prognostischer Relevanz ist, kommt der kardialen MRT heutzutage eine entscheidende Rolle zu.

### 2.3 Kardiale MRT bei nicht-ischämischen Kardiomyopathien

Die Bildgebung im Bereich der nicht-ischämischen Kardiomyopathien stellt den Untersucher vor besondere Herausforderungen, da sich die Phänotypen der Kardiomyopathien trotz gleicher oder ähnlicher Ursache unterscheiden können. Die zugehörige Patientenanamnese und eine zielgerichtete Umfelddiagnostik ist besonders bei der Diagnosefindung der sekundären Kardiomyopathien unabdingbar. Die Unterscheidung ischämischer und nicht-ischämischer Myokardschädigungen ist entscheidend im diagnostischen Algorithmus von Patient/-innen mit akuten und chronischen kardialen Symptomen (Bluemke and Teague, 2019). Bei den meisten älteren Patient/-innen sollte vorrangig eine ischämische Kardiomyopathie in Betracht gezogen und ausgeschlossen werden, bevor es zur weiteren Abklärung einer nicht-ischämischen Kardiomyopathie kommt (Bluemke and Teague, 2019). Die primär eingesetzte Modalität ist die Echokardiographie (ggf. unter physischem oder pharmakologischem Stress), gefolgt von der kardialen Computertomographie (CT) bei geringer bis mittlerer Prätestwahrscheinlichkeit bzw. der Herzkatheteruntersuchung mit Ventrikulographie bei hoher Prätestwahrscheinlichkeit (Collet et al., 2021). Bei unklaren und weiter abklärungsbedürftigen Befunden bzw. bei einem primären Verdacht auf eine nicht-ischämische Kardiomyopathie erfolgt die weiterführende Diagnostik mittels Kardio-MRT, dem derzeitigen Goldstandard in der nicht-invasiven Diagnostik von Kardiomyopathien (Patel and Kramer, 2017; Bluemke and Teague, 2019). Sie ermöglicht eine genaue morphologische Herzbeurteilung, eine exakte Funktionsbestimmung sowie als einzige Modalität eine erweiterte myokardiale Gewebecharakterisierung.

#### *Funktionelle und morphologische Bildgebung (Cine-Bildgebung)*

Die kardiale MRT hat sich aufgrund ihrer exzellenten räumlichen Auflösung zum Referenzstandard bei der Bestimmung der links- und rechtsventrikulären Funktion und Dimension entwickelt. Für die Cine-Bildgebung werden standardmäßig „balanced Steady-State Free Precession“ (b-SSFP) Pulssequenzen eingesetzt. Als „Videosequenzen“ bilden diese einen gesamten Herzzyklus in unterschiedlichen Orientierungen entlang der Herzachse ab. Dies ermöglicht eine genaue morphologische Beurteilung des Myokards und die Bestimmung

und Quantifizierung des Kardiomyopathie-Phänotyps (u.a. Berechnung des ventrikulären end-diastolischen Volumens bei der diastolischen Kardiomyopathie und der ventrikulären Masse bei der hypertrophen Kardiomyopathie). Visuell können so auch segmentale Auffälligkeiten in der Myokardmorphologie detektiert werden (z.B. asymmetrisches Hypertrophie-Muster). Darüber hinaus erlaubt die Cine-Bildgebung die Differenzierung zwischen globalen und regionalen Wandbewegungsstörungen und ermöglicht unter Einbezug der übrigen MRT-Sequenzen die Differenzierung unterschiedlicher Kardiomyopathien (u.a. Tako-Tsubo Kardiomyopathie mit typischem „apical ballooning“, peripartale Kardiomyopathie mit tendenziell globaler Wandbewegungsstörung oder Myokarditis mit häufig nur geringer regionaler Wandbewegungsstörung). Gleichzeitig gilt die Cine-Bildgebung als Goldstandard zur Beurteilung der links- und rechtsventrikulären Ejektionsfraktion (Hundley et al., 2010). Die Graduierung der systolischen Dysfunktion gehört zu den diagnostischen Basiskriterien der Kardiomyopathien. Anhand dieser wird auch der Typ einer potenziell begleitenden Herzinsuffizienz definiert (z.B. Herzinsuffizienz mit reduzierter vs. erhaltener Ejektionsfraktion). Die Quantifizierung der Ejektionsfraktion wirkt sich direkt auf therapeutische Entscheidungen aus. So gehört eine linksventrikuläre Ejektionsfraktion unter 35 % zu den bestimmenden Faktoren für die Indikation eines implantierbaren Kardioverter-Defibrillators oder einer Schrittmachertherapie (Glikson et al., 2021; McDonagh et al., 2021). Die myokardiale Deformationsanalyse (sogenannte „Strain-Analyse“) ist ein Verfahren zur Beurteilung der globalen und regionalen Myokardkontraktilität und kann in longitudinaler, zirkumferentieller und radialer Richtung gemessen werden (Schuster et al., 2016). Die sogenannte „Feature Tracking“ Methode erlaubt die Bestimmung des myokardialen Strains aus den herkömmlichen b-SSFP Funktionssequenzen (Hor et al., 2010). Der myokardiale Strain zeigte in vielen aktuellen Studien bei nicht-ischämischen Kardiomyopathien einen zusätzlichen diagnostischen und prognostischen Mehrwert (Buss et al., 2015; Luetkens et al., 2017; Romano et al., 2018; Fischer et al., 2020).

#### *Ödembildgebung (T2-gewichtete Bildgebung)*

Die Beurteilung des Myokardödems ist eine essenzielle Komponente in der MRT-Diagnostik entzündlicher Herzmuskelerkrankungen. Pathophysiologisch liegt diesem eine erhöhte Permeabilität betroffener Zellmembranen mit einem resultierenden Wasseraustritt in den Extrazellularraum zugrunde (Eitel and Friedrich, 2011). T2-gewichtete „Short Tau Inversion

Recovery“ (STIR) Sequenzen unterdrücken das Signal von fließendem Blut und Fettgewebe und stellen ödematöse bzw. inflammatorische Myokardareale signalreicher dar (Hundley et al., 2010). Ein fokales Myokardödem kann so durch den Kontrastunterschied zum angrenzenden, nicht ödematösen Myokard visuell abgegrenzt werden. Ein diffuses globales Myokardödem ist aufgrund des fehlenden myokardialen Kontrastunterschieds rein visuell nicht zuverlässig detektierbar. Mittels semiquantitativer Analyse kann die Signalintensität (SI) des Myokards mit der eines Referenzgewebes (Skelettmuskel) in derselben Schicht der T2-STIR Sequenz verglichen werden ( $T2\text{-SI-Ratio} = SI_{\text{Myokard}} / SI_{\text{Skelettmuskel}}$ , Normwert:  $< 2,0$ ) (Ferreira et al., 2018). Die Technik zur Detektion einer Hyperämie (sogenannte „Early Gadolinium Enhancement Ratio“) wird in den aktuellen MRT-Diagnoseempfehlungen zur nicht-ischämischen Inflammation (2018 Lake-Louise-Kriterien) nicht mehr empfohlen und wurde durch neuere quantitative Methoden ersetzt (Ferreira et al., 2018). Da ein Großteil der erworbenen primären Kardiomyopathien bzw. sekundären Kardiomyopathien auf inflammatorischen Prozessen beruht, ist deren Detektion in fokaler und insbesondere auch diffuser Form entscheidend (Knockaert, 2007). Die konventionelle qualitative und semiquantitative T2-gewichtete Ödembildgebung hat diesbezüglich jedoch mehrere technische Einschränkungen: Variabilität der Signalintensität durch Phased-Array-Spulen, Signalverlust bei höheren Herzfrequenzen/Arrhythmien, unvollständige Signalunterdrückung von langsam fließendem/myokardnahem Blut und Bewegungsartefakte durch Atmung. Diese wirken sich auch direkt auf die semiquantitative Analyse aus, die darüber hinaus auch durch ein begleitendes Ödem der Skelettmuskulatur (Myositis) beeinträchtigt werden kann. Aus diesem Grund erlaubt die T2-gewichtete Ödembildgebung eine sichere Detektion ödematöser Areale oft nur bei einem fokalen bzw. segmentalen Myokardödem (idealerweise korrespondierend zu hypokinetischen oder nekrotischen Myokardsegmenten) (Giri et al., 2009), und kann ein diffuses Myokardödem nicht sicher beurteilen.

#### *Vitalitätsbildgebung (Late Gadolinium Enhancement)*

Die Vitalitätsbildgebung mittels „Late Gadolinium Enhancement“ (LGE) Technik erlaubt die Darstellung myokardialer Kontrastmittelanreicherungen als Korrelat für myokardiale Narben bzw. Fibrose (chronische Myokardschädigung) oder Nekrosen (akute bzw. subakute Myokardschädigung). Diese basiert standardmäßig auf T1-gewichteten Gradientenecho-Sequenzen, welche etwa 10-15 Minuten nach intravenöser Gabe eines extrazellulären

Gadolinium-basierten Kontrastmittels nach einem vorgeschalteten Inversionspuls akquiriert werden. Der Inversionspuls ermöglicht einen hohen Kontrast zwischen dem signalunterdrückten gesunden Myokard (relativ schnelles „Auswaschen“ des Kontrastmittels aufgrund des relativ kleinen interstitiellen bzw. extrazellulären Volumens) und dem signalreichen geschädigten Myokard (vermehrte Akkumulation bzw. relativ langsames „Auswaschen“ des Kontrastmittels aufgrund des pathologisch vergrößerten interstitiellen bzw. extrazellulären Volumens) (Vogel-Claussen et al., 2006). Anhand der Narbenlokalisierung innerhalb der Herzwand kann nun zuverlässig zwischen ischämischen (primär subendokardiale Lokalisation) und nicht-ischämischen (primär mittmyokardiale und subepikardiale Lokalisation) Myokarderkrankungen differenziert werden (siehe *Abbildung 3*). Darüber hinaus können bestimmte Lokalisationen der Kontrastmittelmehranreicherungen auf spezifische nicht-ischämische Kardiomyopathien hinweisen. Fokale Mehranreicherungen in nicht-ischämischer Lokalisation sind per se jedoch unspezifisch und können z.B. ein Korrelat von Ersatzfibrose, fettig-fibrotischen Veränderungen, epitheloiden Granulomen, entzündlichen Infiltraten und Nekrosen oder von myokardialen Ablagerungen sein (Hashimura et al., 2017).

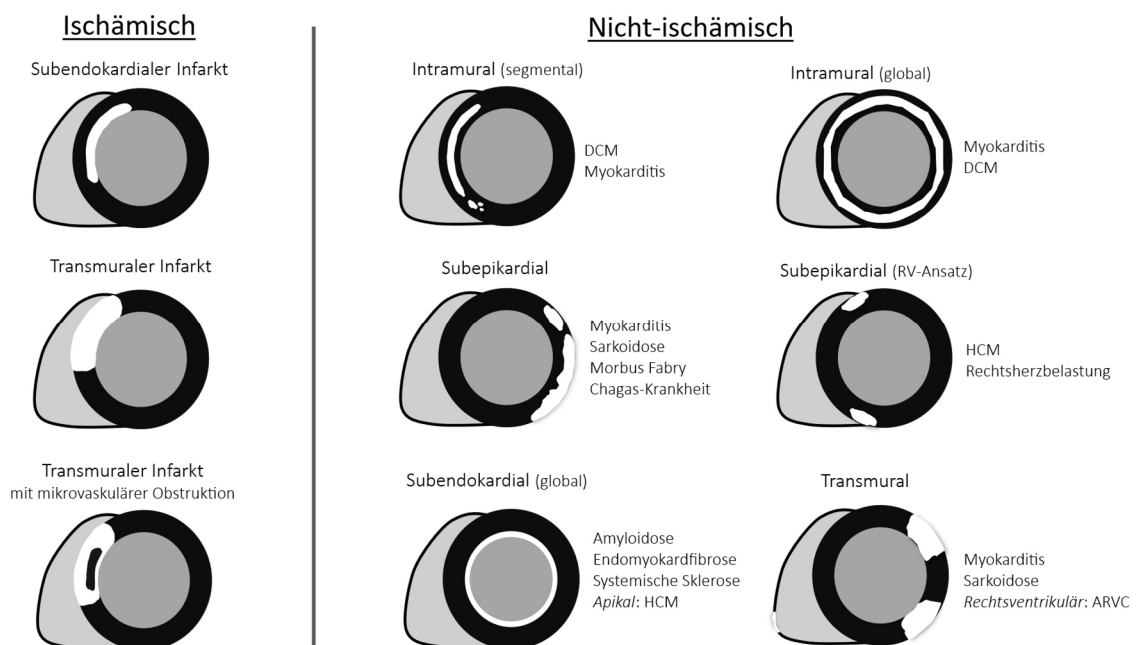


*Abbildung 3. Ischämische und nicht-ischämische Verteilungsmuster in der Vitalitätsbildgebung (Late Gadolinium Enhancement). Abbildung erstellt in Anlehnung an (Mahrholdt et al., 2005; Clinical magnetic resonance imaging, 2006; Karamitsos et al., 2009). DCM, Dilatative Kardiomyopathie; HCM, Hypertrophe Kardiomyopathie; RV, Rechtsventrikulär; ARVC, Arrhythmogene rechtsventrikuläre Kardiomyopathie.*

Neben ihrem diagnostischen Wert hat die Vitalitätsbildgebung auch eine prognostische Bedeutung bei Kardiomyopathien. Die mittels LGE-Bildgebung ermittelte nicht-ischämische

Myokardfibrose gilt als potenziell arrhythmogenes Substrat und dessen Vorhandensein, Ausmaß und Lokalisationsort ist prognostisch relevant (unter anderem verbunden mit einem erhöhten Risiko für Gesamtmortalität, Krankenhausaufenthalte wegen Herzinsuffizienz und plötzlichen Herztod (Greulich et al., 2013; Gulati et al., 2013; Neilan et al., 2013; Disertori et al., 2016; Aquaro et al., 2017; Halliday et al., 2017; Lota et al., 2021)). Weiterhin kann auch das Fehlen einer fokalen myokardialen Kontrastmittelmehranreicherung in Verbindung anderer MRT-Marker (Funktion, Ödem) auf bestimmte Kardiomyopathien hinweisen, wie z.B. die Tako-Tsubo Kardiomyopathie oder die peripartale Kardiomyopathie.

Die LGE-Bildgebung kann eine diffuse bzw. globale Vergrößerung des interstitiellen bzw. extrazellulären Volumens methodenbedingt nicht sicher darstellen, da sie primär auf relativen regionalen Unterschieden zwischen normalem und erkranktem Gewebe beruht. Bei Inversion-Recovery-Sequenzen wird die Inversionszeit so eingestellt, dass das Signal von normal aussehendem bzw. am wenigsten betroffenen Myokard unterdrückt wird (sogenannte „Look-Locker-Technik“ (Look and Locker, 1970)). Bei diffusen Myokardveränderungen kann der sogenannte Nullpunkt des Myokards meist nur auf der Grundlage von abnormalen Werten bestimmt werden. Aus diesem Grund sind auch die vorhandenen semiquantitativen LGE-Auswertungsmethoden (z.B. die „Full Width at Half Maximum“ bzw. die Schwellenwert Methode) nur bedingt zur Bewertung von diffuser Fibrose geeignet (Gräni et al., 2019). Fehlende visuelle Befunde in der LGE-Bildgebung können Pathologien, die in einer diffusen Vergrößerung des interstitiellen Raums resultieren daher nicht sicher ausschließen (z.B. gering degenerierte Kardiomyozyten, interstitielle oder plexiforme Fibrose, diffuse Infiltration durch Entzündungszellen und diffuse Amyloidablagerungen (Hashimura et al., 2017)).

Die aufgeführten diagnostischen Methoden sind in der Abklärung akuter Pathologien zuverlässig, weisen jedoch bei diffusen Herzmuskelveränderungen und bei chronischen Erkrankungen Einschränkungen auf. Die Verwendung aktueller quantitativer Techniken ermöglicht es diese Nachteile zu überwinden und diffuse Myokardveränderungen bei Kardiomyopathien besser zu erkennen (Lurz et al., 2016).

#### 2.4 Quantitative MRT-Techniken bei nicht-ischämischen Kardiomyopathien

Die Entwicklung und klinische Einführung quantitativer Techniken zur direkten Bestimmung der longitudinalen (T1) und transversalen (T2) Relaxationszeit des Myokards (sogenanntes

parametrisches Mapping) haben das diagnostische Potential der kardialen Bildgebung entscheidend erweitert. Sie ermöglichen insbesondere eine verbesserte Detektion diffuser Myokardveränderungen (Karamitsos et al., 2020). Derartige Karten („Maps“) sind parametrisch rekonstruierte Bilder, bei denen jedes Pixel die T1- oder T2-Relaxationszeit des entsprechenden Myokardvoxels enthält (Messroghli et al., 2004; Sprinkart et al., 2015). Die Bildakquisition erfolgt typischerweise in Atemstillstand und mit Elektrokardiogramm (EKG) Triggerung. Meist wird die kurze Herzachse in end-diastolischer Phase abgebildet. Die Relaxationskarten werden üblicherweise direkt am MRT-Scanner erstellt. Das regionale Einzeichnen einer sogenannten „Region of Interest“ (ROI) oder eine globale Messung, beispielsweise unter Einbezug aller Myokardsegmente nach dem 16-Segment Modell der AHA, erlaubt eine zuverlässig reproduzierbare, direkte Quantifizierung der T1- und T2-Relaxationszeiten eines Myokardareals (Dabir et al., 2014). Im Vergleich zu den semiquantitativen Ansätzen (z.B. Berechnung der T2-SI-Ratio) ist kein zusätzliches Referenzgewebe nötig. Dadurch entfallen zusätzliche Störgrößen, die zu falsch positiven oder negativen Ergebnissen führen können (z.B. durch den Signalverlust oder eine begleitende Myositis der Skelettmuskulatur). Durch die Akquisition einer T1-Map vor und nach Kontrastmittelgabe ist die Berechnung der extrazellulären Volumenfraktion (ECV) möglich:

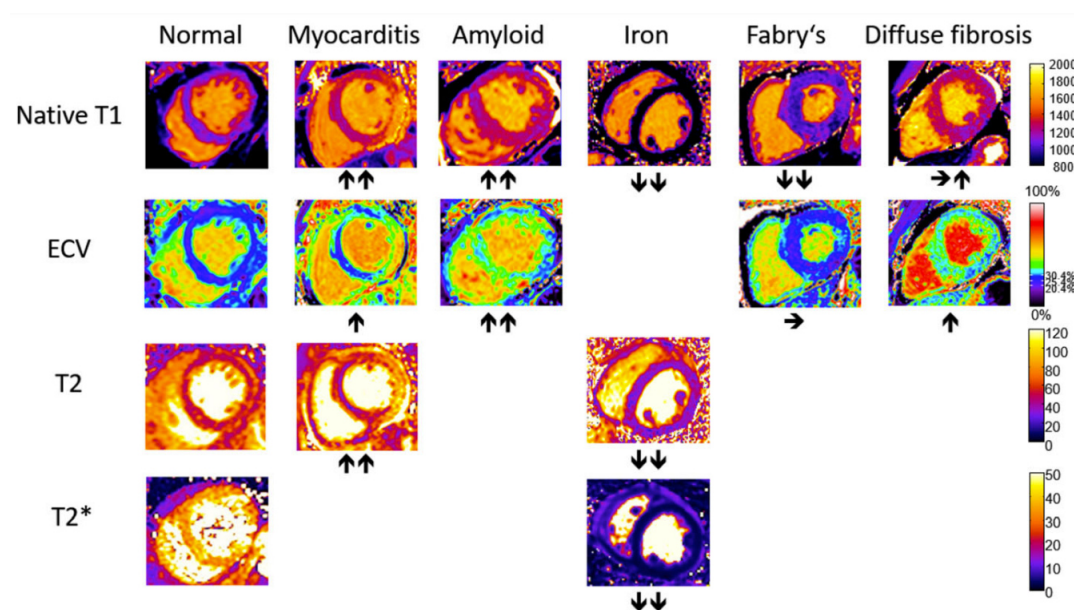
$$ECV = (1 - \text{Hämatokrit}) \frac{\left( \frac{1}{T1_{\text{Myokard nach Kontrastmittel}}} \right) - \left( \frac{1}{T1_{\text{Myokard vor Kontrastmittel}}} \right)}{\left( \frac{1}{T1_{\text{Blut nach Kontrastmittel}}} \right) - \left( \frac{1}{T1_{\text{Blut vor Kontrastmittel}}} \right)}$$

Die ECV entspricht dem Volumenanteil des Herzmuskels, der nicht von Myozyten gebildet wird (z.B. Ödem, Fibrose oder Nekrose). Histologische Untersuchungen bei nicht-ischämischen Kardiomyopathien haben eine deutliche Korrelation zwischen dem myokardialen ECV und der Myokardfibrose gezeigt (Flett et al., 2010; Miller et al., 2013; dem Siepen et al., 2015; Kammerlander et al., 2016). Die native T1-Relaxationszeit repräsentiert sowohl das Signal von Myozyten als auch das des Interstitiums, so dass abnorme Werte unterschiedlichen Pathologien zugrunde liegen können (Zunahme z.B. bei Vorhandensein von Ödem, Fibrose, Amyloid; Abnahme z.B. bei Vorhandensein von Eisen, Fett/Glykosphingolipid) (Messroghli et al., 2017). Damit ist das T1-Mapping sehr sensitiv für diverse Myokardpathologien, als alleiniger Marker jedoch recht unspezifisch. Das T2-Mapping ist ein besonders sensitiver und spezifischer Marker für das Vorliegen eines Myokardödems und kann so insbesondere akute



und inflammatorische Myokardschädigungen detektieren (Eitel and Friedrich, 2011; Messroghli et al., 2017). Wichtig ist, dass die quantitativen Parameter immer im klinischen Kontext sowie in Verbindung mit den übrigen kardialen MRT-Markern interpretiert werden.

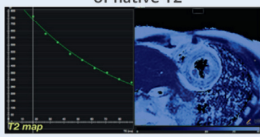
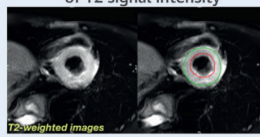
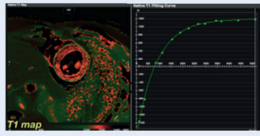
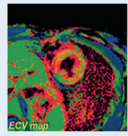
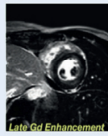
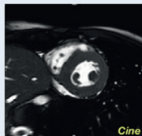
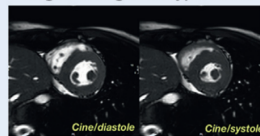
Aufgrund ihrer breitflächigen Verfügbarkeit, ihrer einfachen Integrierbarkeit auf klinischen MRT-Scannern, ihrer relativ kurzen Aufnahmezeit (ein Atemkommando pro Schicht der Map) und ihrer vielfältigen Anwendungsbereiche wurden die Mapping-Sequenzen in den letzten Jahren zunehmend in die klinische Routine implementiert. Besonders nützlich haben sie sich für die Beurteilung von entzündlichen Herzmuskelerkrankungen, Speicherkrankheiten und von fibrotischen Myokardveränderungen im Rahmen diverser Kardiomyopathien erwiesen (Messroghli et al., 2017; Karamitsos et al., 2020) (siehe *Abbildung 4*). Neben der Erstdiagnostik ermöglichen die quantitativen Methoden auch eine Verlaufsbeurteilung der inflammatorischen myokardialen Aktivität (Luetkens et al., 2016c; Luetkens et al., 2016b).



*Abbildung 4. Typisches Erscheinungsbild von T1-, T2-, T2\*- und ECV-Maps bei gesunden Probanden und bei Patienten mit verschiedenen Herzmuskelerkrankungen. Die Pfeile zeigen die Tendenz der relativen Veränderung in den parametrischen Maps. Originale Abbildung aus (Messroghli et al., 2017).*

Seit 2018 sind die quantitativen Techniken fester Bestandteil der Diagnosekriterien für die nicht-ischämische myokardiale Inflammation bzw. Myokarditis (Lake-Louise-Kriterien) (Ferreira et al., 2018). Diese basieren auf zwei Hauptkriterien, bestehend aus einer nicht-ischämischen Myokardschädigung (positiver Befund im LGE oder erhöhte T1-Relaxationszeit oder erhöhtes ECV) und dem Nachweis eines Myokardödems (sichtbares Myokardödem/erhöhte T2-SI-Ratio oder erhöhte T2-Relaxationszeit) (siehe *Abbildung 5*). Ist

pro Hauptkriterium mindestens ein Merkmal erfüllt, kann die Diagnose einer akuten myokardialen Inflammation gestellt werden.

CENTRAL ILLUSTRATION Overview of the Updated Lake Louise Criteria			
	2018 Lake Louise Criteria	CMR Image Examples	
Main Criteria	<b>Myocardial Edema</b> (T2-mapping or T2W images)	Regional or global increase of native T2 	Regional or global increase of T2 signal intensity 
	<b>Non-ischemic Myocardial Injury</b> (Abnormal T1, ECV, or LGE)	Regional or global increase of native T1 	Regional or global increase of ECV  OR Regional LGE signal increase 
Supportive Criteria	<b>Pericarditis</b> (Effusion in cine images or abnormal LGE, T2, or T1)	Pericardial effusion 	Regional or global hypokinesis 
	<b>Systolic LV Dysfunction</b> (Regional or global wall motion abnormality)		

Ferreira, V.M. et al. J Am Coll Cardiol. 2018;72(24):3158-76.

ECV = extracellular volume; LGE = late gadolinium enhancement; T2W = T2-weighted.

Abbildung 5. 2018 Lake-Louise-Kriterien. Die Diagnose der nicht-ischämischen myokardialen Inflammation (Myokarditis) erfolgt anhand von zwei Hauptkriterien: Vorhandensein eines Myokardödems (positiv wenn die T2-Relaxationszeiten pathologisch erhöht sind oder wenn regional hohe Signalintensitäten auf T2-gewichteten Bildern bzw. ein erhöhtes globales T2-Signalintensitätsverhältnis vorliegt) und Zeichen der nicht-ischämischen Myokardschädigung (positiv wenn eine pathologische Erhöhung der nativen T1-Relaxationszeiten oder des extrazellulären Volumens vorliegt oder im Falle eines positiven Befundes im Late Gadolinium Enhancement). CMR, cardiac magnetic resonance; T2W, T2-weighted; LV, left ventricular; Gd = Gadolinium; ECV, extracellular volume fraction; LGE, Late gadolinium enhancement. Originale Abbildung aus (Ferreira et al., 2018).

Die diagnostischen Kriterien für eine nicht-ischämische myokardiale Inflammation können prinzipiell nicht nur auf die klassische akute Myokarditis, sondern auch auf andere erworbene und sekundäre Kardiomyopathien angewendet werden. Basiert die Diagnostik der genetischen und gemischten primären Kardiomyopathien hauptsächlich auf phänotypischen Merkmalen (z.B. Hypertrophie, Dilatation, Hypertrabekularisierung), sind bei den erworbenen primären sowie den sekundären Kardiomyopathien strukturelle Myokardveränderungen (insbesondere Inflammation, Fibrose, Ablagerungen) die hauptsächlichen Diagnosekriterien.

Erworbene und sekundäre Kardiomyopathien sind also nicht morphologisch anhand eines einheitlichen Phänotyps charakterisierbar. Zudem liegen die oben aufgeführten myokardialen Veränderungen bei sekundären Kardiomyopathien oft nur „subklinisch“ vor (milde bis

unterschwellige Symptome, welche klinisch nur schwer erkennbar sind) und sind bildgebend geringer ausgeprägt als Veränderungen bei akuter Myokardschädigung. Die Detektion sekundärer Kardiomyopathien ist demnach klinisch und bildgebend herausfordernd und verlangt nach möglichst sensitiven Bildgebungsmethoden. Klinisch relevante Beispiele sind z.B. die frühzeitige Erkennung einer aktiven kardialen Beteiligung im Rahmen von Systemerkrankungen (z.B. Sarkoidose, Amyloidose, Kollagenosen) oder von kardiotoxischen Effekten im Rahmen onkologischer Therapien (Puntmann et al., 2013; Crouser et al., 2016; Luetkens et al., 2016a; Plana et al., 2018; Harries et al., 2020; Dabir et al., 2021).

## 2.5 Fragestellung

In den vorangegangenen Ausführungen wurde die klinische Relevanz der kardialen MRT in Bezug auf die nicht-ischämischen Kardiomyopathien dargelegt. Aufgrund des Fehlens einfacher spezifischer phänotypischer Merkmale erfordert die Diagnose von erworbenen primären Kardiomyopathien sowie sekundären Kardiomyopathien eine möglichst umfassende Charakterisierung des Herzmuskelgewebes. Die Anwendung der modernen quantitativen Kardio-MRT Verfahren für die myokardiale Gewebecharakterisierung (insbesondere in Bezug auf die diffuse Inflammation) ist in dieser heterogenen Gruppe zum Teil noch unzureichend untersucht.

Die beiden ersten Arbeiten befassen sich mit der MRT-basierten quantitativen Charakterisierung von erworbenen primären Kardiomyopathien; die beiden letzten Arbeiten mit der von sekundären Kardiomyopathien. In der ersten Arbeit werden Anwendung und Nutzen einer umfassenden kardialen MRT inklusive neuer quantitativer Inflammationsmarker bei der pädiatrischen Myokarditis ermittelt. Die Hauptfragestellung ist, ob die revidierten Lake-Louise-Kriterien in dieser speziellen Kohorte einen zusätzlichen Nutzen gegenüber den konventionellen Kriterien aufweisen. Die darauffolgende Arbeit untersucht den diagnostischen Wert einer umfassenden MRT bei einer seltenen erworbenen primären Kardiomyopathie, der peripartalen Kardiomyopathie. Die wesentliche Fragestellung bezieht sich auf die MRT-gestützte Charakterisierung des Krankheitsphänotyps bzw. des myokardialen Gewebes, mit besonderem Fokus auf dem Myokardödem. Die dritte Arbeit charakterisiert eine neuartige, Tumortherapie-assoziierte sekundäre Kardiomyopathie, die Immun-Checkpoint-Inhibitor Myokarditis. Das Hauptaugenmerk liegt auf der Evaluierung einer frühen (subklinischen) Detektion von myokardialer Inflammation als Zeichen kardiotoxischer

Veränderungen. In der letzten Arbeit wird die umfassende MRT-basierte Charakterisierung der zirrhotischen Kardiomyopathie mittels kombinierter multiparametrischer Herz-Leber-MRT evaluiert. Dabei wird insbesondere das Vorhandensein myokardialer Inflammation und Fibrose bei Studienteilnehmer/-innen mit Leberzirrhose untersucht und mit dem Schweregrad der Lebererkrankung korreliert.

Das übergeordnete Ziel der vorgelegten Habilitationsschrift ist die Evaluation der klinischen Anwendung quantitativer Kardio-MRT Verfahren zur Charakterisierung erworbener primärer sowie sekundärer Kardiomyopathien mit besonderem Fokus auf bildbasierte Biomarker der myokardialen Inflammation.

### 3. Ergebnisse

#### 3.1 Quantitative kardiale MRT bei der pädiatrischen Myokarditis

*“Multiparametric cardiac magnetic resonance imaging in pediatric and adolescent patients with acute myocarditis”*

Isaak A, Bischoff LM, Faron A, Endler C, Mesropyan N, Sprinkart AM, Pieper CC, Kuetting D, Dabir D, Attenberger U, Luetkens JA.

Erschienen in *Pediatric Radiology*. 2021 Dec;51(13):2470-2480.

**Zielsetzung und Methoden** – Ziel dieser Arbeit war es die diagnostische Leistung der 2018 Lake-Louise-Kriterien bei Kindern und Jugendlichen mit klinisch suszipierter akuter Myokarditis zu evaluieren und den Nutzen der quantitativen kardialen MRT für die Nachsorge zu bestimmen. Dazu wurden MRT-Untersuchungen von Patient/-innen mit dem klinischen Verdacht auf eine akute Myokarditis und von gesunden Kontrollpatient/-innen retrospektiv unter Anwendung der originalen und der revidierten Lake-Louise-Kriterien analysiert.

**Ergebnisse** – Insgesamt wurden 43 Patient/-innen mit dem klinischen Verdacht auf eine akute Myokarditis (Altersspanne: 8-21 Jahre; 33 männlich) und 13 Kontrollpatient/-innen in die Analyse eingeschlossen. In der Gruppe der Patient/-innen mit verfügbarem T1/T2-Mapping (26/43, 60 %) ergab dessen Integration eine signifikant höhere diagnostische Performance („Area under the curve“ [AUC]: 0,944 vs. 0,870; Sensitivität: 89 % vs. 73 %; Spezifität: 100 % vs. 100 %; siehe *Figure 2* (Isaak et al., 2021a)). Ein „kontrastmittelfreier“ Mapping-Score zeigte ebenfalls eine hohe diagnostische Leistung (AUC: 0,920; Sensitivität: 85 %; Spezifität: 100 %). Die MRT-Nachuntersuchungen (verfügbar in 27/43 Fällen, 63 %) ergaben rückläufige T1- und T2-Relaxationszeiten passend zu einem Rückgang der aktiven myokardialen Inflammation, trotz der häufig noch persistierenden LGE-Läsionen (siehe *Figure 3* und *Figure 4*, (Isaak et al., 2021a)). Es bestanden signifikante Korrelationen zwischen den quantitativen Inflammationsmarkern und dem Schweregrad der Erkrankung, wie z.B. der linksventrikulären Funktionseinschränkung. Die myokardiale T2-Relaxationszeit korrelierte mit dem Aufenthalt und der Dauer auf der Intermediate-Care-Station.

**Schlussfolgerungen** – Die Hinzunahme quantitativer MRT-Marker erhöht die diagnostische Performance für die akute Myokarditis im Kindes- und Jugendalter, erlaubt Rückschlüsse auf die Erkrankungsschwere und ermöglicht die Überwachung der entzündlichen Krankheitsaktivität.



# Multiparametric cardiac magnetic resonance imaging in pediatric and adolescent patients with acute myocarditis

Alexander Isaak<sup>1,2</sup> · Leon M. Bischoff<sup>1,2</sup> · Anton Faron<sup>1,2</sup> · Christoph Endler<sup>1,2</sup> · Narine Mesropyan<sup>1,2</sup> · Alois M. Sprinkart<sup>1,2</sup> · Claus C. Pieper<sup>1</sup> · Daniel Kuetting<sup>1,2</sup> · Darius Dabir<sup>1,2</sup> · Ulrike Attenberger<sup>1</sup> · Julian A. Luetkens<sup>1,2</sup>

Received: 14 October 2020 / Revised: 10 May 2021 / Accepted: 31 July 2021

© The Author(s) 2021

## Abstract

**Background** The diagnostic value of cardiac magnetic resonance imaging (MRI) employing the 2018 Lake Louise criteria in pediatric and adolescent patients with acute myocarditis is undefined.

**Objective** To evaluate the diagnostic value of the Lake Louise criteria in pediatric and adolescent patients with suspected acute myocarditis and to show the utility of cardiac MRI for follow-up in this patient cohort.

**Materials and methods** Forty-three patients (age range: 8–21 years) with suspected acute myocarditis and 13 control patients who underwent cardiac MRI were retrospectively analyzed. T2-weighted and late gadolinium enhancement imaging were performed in all patients. T1 and T2 mapping were available in 26/43 patients (60%). The Lake Louise criteria were assessed. In 27/43 patients (63%), cardiac MRI follow-up was available. Receiver operating characteristic analysis, Pearson's correlation coefficient and paired Student's *t*-test were used for statistical analysis.

**Results** In the total cohort, the Lake Louise criteria achieved a sensitivity of 86% (95% confidence interval [CI]: 72–95%) and a specificity of 100% (95% CI: 79–100%) for the diagnosis of acute myocarditis. In the subgroup of patients with available mapping parameters, the diagnostic performance of the Lake Louise criteria was higher when mapping parameters were implemented into the score (area under the receiver operating characteristic curve: 0.944 vs. 0.870;  $P=0.033$ ). T2 relaxation times were higher in patients with admission to the intermediate care unit and were associated with the length of intermediate care unit stay ( $r=0.879$ ,  $P=0.049$ ). Cardiac MRI markers of active inflammation decreased on follow-up examinations (e.g., T1 relaxation times: 1,032±39 ms vs. 975±33 ms,  $P<0.001$ ; T2 relaxation times: 58±5 ms vs. 54±5 ms,  $P=0.003$ ).

**Conclusion** The Lake Louise criteria have a high diagnostic performance for the diagnosis of acute myocarditis and are a valuable tool for follow-up in pediatric and adolescent patients. The mapping techniques enhance the diagnostic performance of the 2018 Lake Louise criteria.

**Keywords** Adolescents · Cardiac magnetic resonance imaging · Children · Heart · Lake Louise criteria · Myocarditis · T1 mapping · T2 mapping · Young adults

## Introduction

Acute myocarditis is an inflammatory disorder of the myocardium primarily caused by infections, autoimmune processes,

systemic diseases, drugs or toxins and can affect both adults and children [1]. Because subclinical manifestation is common, the true incidence of acute myocarditis in children is unknown. Estimated incidence rates range between 1 and 2 per 100,000 children [2, 3]. Males seem to be affected more often [2, 4]. Although incidence of acute myocarditis is relatively low in children, it accounts for about one-third of childhood dilated cardiomyopathies [5] and is related to sudden cardiac death in young patients [6, 7]. Diagnosis of myocarditis is challenging because of the wide spectrum of clinical presentation. Furthermore, children particularly may show atypical manifestations [8]. The clinical course is

✉ Julian A. Luetkens  
julian.luetkens@ukbonn.de

<sup>1</sup> Department of Diagnostic and Interventional Radiology, University Hospital Bonn, Venusberg-Campus 1, 53127 Bonn, Germany

<sup>2</sup> Quantitative Imaging Lab Bonn (QILaB), University Hospital Bonn, Bonn, Germany

heterogeneous, varying from fast convalescence to delayed recovery or chronic heart failure and, rarely, serious long-term morbidity [8, 9]. Due to its invasiveness and possible sampling error, endomyocardial biopsy — the diagnostic reference standard — is used infrequently in clinical practice. Nowadays, cardiac magnetic resonance imaging (MRI) plays an important role for diagnostic work-up in patients with suggested myocarditis. Cardiac MRI is a noninvasive and radiation-free technique that is suitable for pediatric and adolescent patients and can be of particular value to differentiate acute myocarditis from myocardial infarction, primary cardiomyopathy or congenital heart disease to spare young patients from coronary angiography [10, 11]. The Lake Louise criteria were established in 2009 for the diagnosis of myocarditis by cardiac MRI. They include three aspects of myocardial inflammation (edema, hyperemia and necrosis) in a two-out-of-three approach (high signal intensities on T2-weighted images, early gadolinium enhancement and late gadolinium enhancement) [12]. In 2018, the implementation of quantitative mapping techniques led to a revision of the original Lake Louise criteria [13–15]. According to the 2018 Lake Louise criteria, diagnosis of myocarditis can be made when two main criteria are fulfilled, at least one T1-based criterion (increased myocardial T1 relaxation time, increased extracellular volume fraction or positive late gadolinium enhancement) and one T2-based criterion (increased myocardial T2 relaxation time or visual myocardial edema/increased T2 signal intensity ratio) [16]. Previous studies evaluated the performance of cardiac MRI diagnostic parameters primary in adults, but the diagnostic value of quantitative parameters remains undetermined in children and adolescents.

The purpose of this cardiac MRI study was to evaluate (1) the diagnostic performance of the 2018 Lake Louise criteria for acute myocarditis in pediatric and adolescent patients and (2) to assess the value of cardiac MRI for follow-up of the disease.

## Materials and methods

This retrospective, case-control study was approved by the institutional ethics committee and the requirement for written informed consent was waived. Patients with clinically defined acute myocarditis and control patients were included in this study. The department's registry was searched for children and adolescents (ages 2 to 21 years old, according to the American Academy of Pediatrics [17]) who had undergone cardiac MRI for the evaluation of acute myocarditis on the same clinical whole-body MRI system between January 2014 and April 2020. Patients with preexisting cardiovascular disease were excluded. The diagnosis of myocarditis was made according to current criteria for clinically suspected myocarditis as recommended by the European Society of

Cardiology Working Group on Myocardial and Pericardial Diseases [8]. The main criteria for clinical diagnosis were acute chest pain, signs of acute myocardial injury (electrocardiogram [ECG] changes and/or elevated troponin), and a constellation of signs associated with infection (elevated leucocytes and/or C-reactive protein and/or confirmed infectious disease). This clinical validation approach was used for the diagnosis of acute myocarditis in this study as previously reported [14–16, 18]. Clinical evidence was the reference standard against which the diagnostic performance of cardiac MRI parameters was tested. As a control group, outpatients were retrospectively reviewed for those who had been referred for nonspecific cardiac symptoms or thoracic discomfort to rule out structural heart disease. All control patients had an unremarkable past medical history of cardiovascular disease. Electrocardiographic and echocardiographic results were unremarkable and no cardiac risk factors were present. All control participants had normal cardiac MRI results without structural abnormalities.

## Cardiac magnetic resonance

All investigations were performed on a clinical whole-body MRI system (Ingenia 1.5 tesla; Philips Healthcare, Best, the Netherlands). For signal reception, a 32-channel torso coil with digital interface was used. ECG-gated steady state free precession cine images were acquired in short-axis, four-chamber and two-chamber views. T2-weighted short tau inversion recovery (STIR) sequences were acquired in short-axis, two-chamber and transversal views to visualize myocardial edema and calculate the T2 signal intensity ratio. Late gadolinium enhancement imaging was based on segmented inversion recovery gradient echo sequences in short-axis, two-chamber and four-chamber orientation. Cardiac MRI protocol consisted of myocardial T1 and T2 mapping acquired in end-diastole in apical, midventricular and basal short-axis views. Post-contrast myocardial T1 maps were performed 10 min after contrast injection in the same orientation. T1 mapping was based on a standard 3(3)3(3)5 modified Look-Locker inversion recovery (MOLLI) acquisition scheme [19]. A 6-echo gradient spin echo (GraSE) sequence allowed acquisition of T2 mapping [20]. For contrast enhancement, a single bolus of 0.2 mmol/kg body weight of gadobutrol (Gadovist; Bayer Healthcare, Berlin, Germany) was given. For extracellular volume fraction estimation, the hematocrit blood levels on the cardiac MRI day were available. A detailed description of the cardiac MRI sequence parameters is provided in Online Supplementary Material 1.

## Cardiac image analysis

Images were analyzed by two radiologists (J.A.L. and A.I., with 8 and 3 years of experience in cardiac MRI, respectively)



using dedicated software (IntelliSpace Portal version 10.1; Philips Medical System, Best, the Netherlands). Readers were blinded to the clinical information. All volumes and masses were indexed to body surface area using the Mosteller method. Visual analysis of T2 STIR and late gadolinium enhancement images was evaluated separately by consensus agreement of the two readers for focal myocardial hyperintensity as markers for myocardial edema and necrosis, respectively. Semiquantitative analysis allowed for determination of quantitative T2 signal intensity ratio (global myocardial edema) [12, 14]. Myocardial relaxation maps were motion corrected using FEIR (fast elastic image registration) by dedicated software (IntelliSpace Portal version 10.1, Philips Medical System). Myocardial T1 and T2 relaxation times and hematocrit corrected extracellular volume fraction values (using pre- and post-contrast T1 values) were calculated using a segmental approach as previously described [14–16]. The 2018 Lake Louise criteria were applied as recommended [13].

### Statistical analysis

Prism (version 8.4.3; GraphPad Software, San Diego, CA), SPSS Statistics (version 26; IBM Corp., Armonk, NY) and MedCalc (version 18.11.3; MedCalc Software bvba, Ostend, Belgium) were used for statistical analysis. The Kolmogorov-Smirnov test was applied to assess normality. Continuous patient characteristics are presented as mean±standard deviation or as absolute frequency. Continuous variables between the two groups were compared using the Student's *t*-test. Dichotomous variables were compared using the Fisher exact test. For intraindividual comparisons, the paired Student's *t*-test and McNemar's test were used. Correlation analysis was performed using Pearson's correlation coefficient. A receiver operating characteristic (ROC) analysis was performed to calculate area under the curve (AUC). Optimal cutoff values were determined using the Youden index and sensitivities and specificities were calculated. Differences between ROC curves were tested using the DeLong method. The level of statistical significance was set to  $P<0.05$ .

## Results

### General characteristics

Fifty-nine subjects, 43 patients with acute myocarditis (77% males, mean age: 17±3 years, range: 8–21 years) and 16 age-matched control patients (50% males, mean age: 17±4 years, range: 5–21 years) were included in this study (Table 1). Cardiac MRI was performed 4±5 days after clinical diagnosis of suspected myocarditis. Acute thoracic pain was present in 26/43 (60%), abnormal ECG in 35/43 (81%) and infectious disease in 31/43 (72%) patients. Coronary angiography was

performed in 11/43 patients (26%) to rule out coronary stenosis. Patients had significantly elevated blood markers of troponin, white blood cell count and C-reactive protein when compared to healthy controls (Table 1). Nine of the 43 (21%) patients with acute myocarditis were admitted to the intensive care unit (length of stay: 7±8 days) during their hospital stay.

### Cardiac magnetic resonance imaging results

No significant differences were observed in left ventricular ejection fraction (LVEF; 57±8% vs. 59±5%;  $P=0.32$ ), left ventricular end-diastolic volume index (83±15 mL/m<sup>2</sup> vs. 78±12 mL/m<sup>2</sup>;  $P=0.17$ ), or cardiac index (3.3±0.6 L/min/m<sup>2</sup> vs. 3.4±0.5 L/min/m<sup>2</sup>;  $P=0.72$ ) between patients with acute myocarditis and control patients (Table 1). Twenty-nine of the 43 (67%) myocarditis patients had preserved LVEF ≥55%. Pericardial effusion was present in 17/43 (40%) patients (controls: 0/16, 0%;  $P<0.001$ ). Focal high intensities on T2 STIR images were detected in 32/43 (74%) patients with acute myocarditis (controls: 0/16, 0%;  $P<0.001$ ), and T2 signal intensity ratio was elevated in the myocarditis group compared to the control group (2.10±0.49 vs. 1.54±0.29,  $P<0.001$ ). Late gadolinium enhancement in a nonischemic distribution was found in 36/43 (84%) patients (controls: 0/16, 0%;  $P<0.001$ ). Positive late gadolinium enhancement was observed more frequently in patients with reduced LVEF (<55%) than in patients with preserved LVEF (≥55%) (14/14, 100% vs. 22/29, 76%;  $P=0.048$ ).

T1 and T2 mapping was available in a subgroup of 26/43 patients and in all control patients. Myocardial native T1 relaxation time as a marker of acute myocardial injury was higher in patients with acute myocarditis than in healthy controls (1,031±46 ms vs. 962±17 ms;  $P<0.001$ ) (Fig. 1).

T2 relaxation time, as a marker of diffuse myocardial edema, was higher in patients compared to controls (58±5 ms vs. 51±2 ms;  $P<0.001$ ). No difference was observed in extracellular volume fraction values between both groups (29.2±5.9% vs. 26.5±2.8%;  $P=0.058$ ). Quantitative parameters of myocardial inflammation were higher in patients with reduced LVEF (T1 relaxation time: 1,066±17 ms vs. 1,008±58 ms,  $P=0.001$ ; T2 relaxation time: 63±6 ms vs. 56±4 ms,  $P=0.010$ ). Patients with admission to the intermediate care unit had more elevated T1 (1,063±26 ms vs. 1,017±58 ms;  $P=0.011$ ) and T2 relaxation times (64±6 ms vs. 56±4 ms;  $P=0.015$ ), but no significant differences in extracellular volume fraction (32.1±5.8% vs. 26.1±5.5%;  $P=0.057$ ), LVEF (51±11% vs. 59±6%;  $P=0.059$ ) or troponin level (787±702 ng/L vs. 739±783 ng/L;  $P=0.90$ ) when compared to patients without admission to the intermediate care unit. T2 relaxation time as a parameter of myocardial edema was associated with the length of intermediate care unit stay ( $r=0.879$ ,  $P=0.049$ ) and inflammatory laboratory parameters (C-reactive protein:  $r=0.532$ ,  $P=0.009$ ;



**Table 1** Clinical and cardiac magnetic resonance imaging (MRI) characteristics of pediatric and adolescent patients with acute myocarditis and control patients

Variable	Patients (n=43)	Controls (n=16)	P-value
<b>Clinical parameters</b>			
Age (years)	17±3	17±4	0.35
Men	33 (77%)	8 (50%)	0.061
Weight (kg)	72±19	61±20	0.068
Height (cm)	168±17	160±16	0.10
Heart rate (bpm)	73±15	76±10	0.46
Hematocrit (%)	39±6	39±3	0.67
Elevated troponin	40 (93%)	0 (0%)	<0.001
White blood cell count (10 <sup>3</sup> /μL)	10.8±5.0	8.6±1.6	0.021
C-reactive protein (mg/L)	62±1	2±2	<0.001
<b>General cardiac MRI parameters</b>			
Left ventricular ejection fraction (%)	57±8	59±5	0.32
Left ventricular end-diastolic volume index (mL/m <sup>2</sup> )	83±15	78±12	0.17
Cardiac index (L/min/m <sup>2</sup> )	3.3±0.6	3.4±0.5	0.72
Interventricular septal thickness (mm)	8.3±1.4	7.5±1.4	0.20
Pericardial effusion	17 (40%)	0 (0%)	<0.001
T2 signal intensity ratio	2.10±0.49	1.54±0.29	<0.001
Visual focal myocardial edema	32 (74%)	0 (0%)	<0.001
Visual late gadolinium enhancement	36 (84%)	0 (0%)	<0.001
<b>Mapping cardiac MRI parameters</b>			
T1 relaxation time, native (ms)	1,031±46	962±17	<0.001
Extracellular volume fraction (%)	29.2±5.9	26.5±2.8	0.058
T2 relaxation time (ms)	58±5	51±2	<0.001

Continuous variables are given as mean±standard deviation. Dichotomous variables are given as absolute frequency with percentages in parentheses. P-values were obtained using a Student's *t*-test,  $\chi^2$  test (cell count >5) or Fisher exact test (cell count ≤5). T1 and T2 relaxation times and extracellular volume fraction were available in 26/43 patients and all controls

white blood cell count:  $r=0.589$ ,  $P=0.002$ ). T1 relaxation times correlated with troponin levels ( $r=0.558$ ,  $P=0.016$ ). Patients younger than 18 years old displayed lower parameters of myocardial edema (T2 relaxation time: 55±3 ms vs. 59±6 ms,  $P=0.035$ ; T2 signal intensity ratio: 1.88±0.34 vs 2.23±0.53,  $P=0.012$ ), but no difference was found in T1 relaxation time (1,035±40 ms vs. 1,024±61 ms;  $P=0.59$ ) when compared to myocarditis patients ages ≥18 years.

### Diagnostic performance

In the total cohort ( $n=43$ ), the 2018 Lake Louise criteria could only be applied in a limited way because mapping parameters were not available in 17/43 patients. The application of the 2018 Lake Louise criteria in the total cohort reached a sensitivity of 37/43 (86%, 95% confidence interval [CI]: 72–95%) and a specificity of 16/16 (100%, 95% CI: 79–100%) with an AUC of 0.930. Single parameters alone showed lower sensitivity (late gadolinium enhancement: 36/43 [84%, 95% CI: 69–93%], visual focal edema: 32/43 [74%, 95% CI: 59–

87%], T2 signal intensity ratio: 34/43 [79%, 95% CI: 64–90%]).

In the subgroup analysis of patients with available mapping parameters ( $n=26/43$ ), high diagnostic performance was achieved by T2 mapping with an AUC of 0.899 (sensitivity: 23/26 [88%, 95% CI: 70–98%], specificity: 13/16 [88%, 95% CI: 62–98%]), by T1 mapping with an AUC of 0.873 (sensitivity: 21/26 [82%, 95% CI: 62–94%], specificity: 16/16 [100%, 95% CI: 79–100%]), and by T2 signal intensity ratio with an AUC of 0.868 (sensitivity: 20/26, [77%, 95% CI: 64–90%], specificity: 15/16 [94%, 95% CI: 70–100%]). Extracellular volume fraction had an AUC of 0.687 (sensitivity: 15/26 [58%, 95% CI: 37–77%], specificity: 14/16 [88%, 95% CI: 62–98%]). In this subgroup, the 2018 Lake Louise criteria yielded a significantly higher diagnostic performance (AUC: 0.944, sensitivity: 89%, specificity: 100%) compared to the modified 2018 Lake Louise criteria with exclusion of mapping parameters (AUC: 0.870, sensitivity: 73%, specificity: 100%;  $P=0.034$ ). Mapping parameters allowed for the diagnosis of acute myocarditis in four additional patients. Furthermore, a combined non-contrast score of native T1

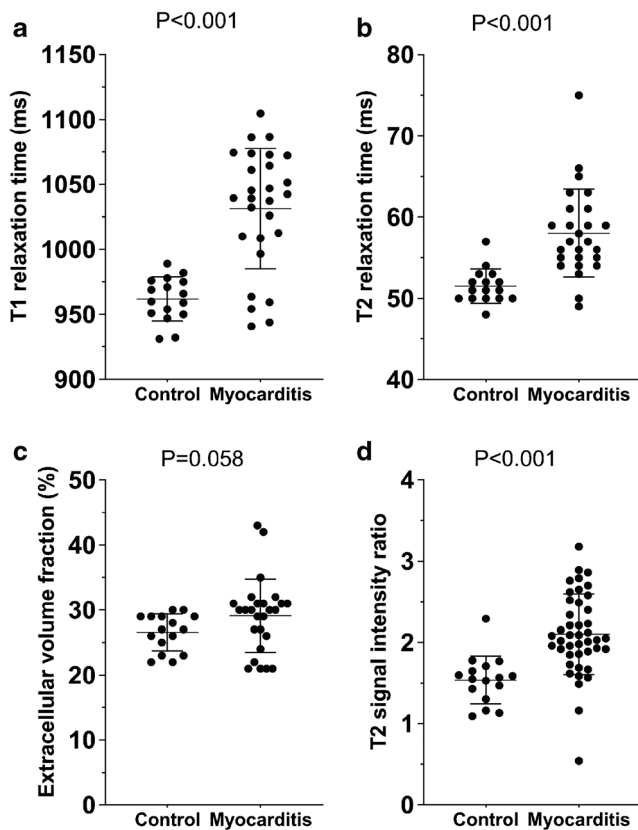


**Fig. 1** Graphs with individual plotted values show the distribution of myocardial magnetic resonance parameters in controls and in the subgroup of patients with myocarditis and available mapping parameters (26/43 patients and 16/16 controls). **a** T1 relaxation time. **b** T2 relaxation time. **c** Extracellular volume fraction. **d** T2 signal intensity ratio. T2 signal intensity ratio was available in all patients and controls. Individual values are represented as single dots. The horizontal lines show the mean values with error bars representing one standard deviation. *P*-values were obtained using an unpaired Student’s *t*-test

and T2 relaxation times yielded an AUC of 0.920 and a sensitivity of 22/26 (85%, 95% CI: 64–96%) and a specificity of 16/16 (100%, 95% CI: 79–100%). Comparison of the ROC curves of this non-contrast score and the 2018 Lake Louise criteria showed no significant difference in diagnostic performance (*P*=0.15).

Table 2 summarizes all cutoff values, sensitivities and specificities with confidence intervals for all evaluated parameters. Figure 2 visualizes the AUC values for single variables and the 2018 Lake Louise criteria of the total cohort, and a combined score of native quantitative myocardial parameters.

### Cardiac magnetic resonance imaging follow-up

Cardiac MRI follow-up was performed in 27/43 patients with acute myocarditis. Mapping parameters were available in 17/27 follow-up scans. Median time to cardiac MRI follow-up was 53 days (range: 20–322 days). LVEF improved at follow-up (58±7% vs. 61±4%; *P*=0.039). Visual myocardial edema

was initially observed in 17/27 (63%) patients and was still present in 12/27 (44%) patients at follow-up. Late gadolinium enhancement was visible in 25/27 (93%) patients at baseline cardiac MRI and in 20/27 (74%) patients at follow-up. Native T1 (1,032±39 ms vs. 975±33 ms; *P*<0.001) and T2 relaxation times (58±5 ms vs. 54±5 ms; *P*=0.003) decreased at follow-up. Baseline and follow-up parameters are presented in Table 3 and Fig. 3. Representative clinical cardiac MRI examples of patients with acute myocarditis are presented in Fig. 4 (case with a typical pattern of acute myocarditis) and Fig. 5 (case with a diffuse pattern of acute myocarditis, which was diagnosed by mapping parameters according to the 2018 Lake Louise criteria).

### Discussion

In this study, we evaluated the diagnostic performance of current cardiac MRI criteria for acute myocarditis in pediatric and adolescent patients. The main finding is that the 2018 Lake Louise criteria have a high performance for the diagnosis of acute myocarditis in pediatric and adolescent patients, especially when mapping parameters are implemented. Monitoring of disease/follow-up is feasible with cardiac MRI, especially with mapping parameters. Extensive increase of T2 relaxation times is associated with a severe course of disease. Furthermore, a combined non-contrast score solely based on native mapping parameters yielded a diagnostic accuracy comparable to the 2018 Lake Louise criteria. Therefore, the use of a non-contrast cardiac MRI protocol in children may be a viable option in cases where intravenous contrast is sought to be avoided.

Several studies have investigated the diagnostic performance of myocardial T1 and T2 mapping and extracellular volume fraction in adults [14, 21–24]. However, cardiac MRI studies evaluating pediatric myocarditis are underrepresented. The published cutoff values for mapping parameters in acute myocarditis show a wide heterogeneity because myocardial T1 and T2 relaxation times depend on different center-specific technical parameters as well as on the employed scanning sequence, field strength, manufacturer, software and type of analysis [25]. Furthermore, physiological factors may influence T1 and T2 relaxation times, e.g., sex, age, heart rate or even hydration status [26–29]. Previous studies have shown an age-related impact on myocardial T1 relaxation times. Rosmini et al. [30] found that native T1 relaxation times were slightly lower with increasing age. Plausible reasons might be myocardial lipofuscin or hemosiderin accumulation. Roy et al. [28] described higher T1 and extracellular volume fraction values in male participants of increased age, probably related to diffuse myocardial fibrosis. The determined cutoff values for the diagnosis of acute myocarditis in children and adolescents in our study differ from cutoff values for adults, which

**Table 2** Diagnostic performance of single and combined cardiac magnetic resonance imaging parameters for diagnosis of acute myocarditis in pediatric and adolescent patients

Variable	AUC	Cutoff	Sensitivity (%)	Specificity (%)
<u>Qualitative/semiquantitative parameters</u>				
Visual late gadolinium enhancement	0.919 (0.818–0.974)		84 (69–93)	100 (79–100)
Visual focal myocardial edema	0.872 (0.759–0.945)		74 (59–87)	100 (79–100)
T2 signal intensity ratio	0.868 (0.755–0.942)	>1.78	79 (64–90)	94 (70–100)
<u>Quantitative parameters</u>				
T1 relaxation time	0.873 (0.736–0.955)	>993 ms	82 (62–94)	100 (79–100)
Extracellular volume fraction	0.687 (0.526–0.821)	>29%	58 (37–77)	88 (62–98)
T2 relaxation time	0.899 (0.766–0.970)	>53 ms	88 (70–98)	88 (62–98)
<u>Combinations (total cohort)</u>				
2018 Lake Louise criteria	0.930 (0.833–0.980)		86 (72–95)	100 (79–100)
<u>Combinations (subgroup cohort<sup>a</sup>)</u>				
2018 Lake Louise criteria	0.944 (0.872–1.000)		89 (72–96)	100 (81–100)
2018 Lake Louise criteria excluding mapping	0.870 (0.763–0.978)		73 (55–87)	100 (81–100)
Non-contrast score (native T1 + T2 mapping)	0.920 (0.792–0.982)		85 (64–96)	100 (79–100)

Data are given as percentages with 95% confidence intervals. AUC area under the curve

<sup>a</sup> Mapping parameters were available in 26/43 patients and in all controls

were determined in a previous study by applying the same mapping sequences and overall technical parameters [15], which might imply that appropriate cutoff values are needed for specific patient cohorts.

**2018 Lake Louise criteria**

In a previous adult study, the 2018 Lake Louise criteria (sensitivity: 87.5%, specificity: 96.2%) outperformed the original

2009 Lake Louise criteria (sensitivity: 72.5%, specificity: 96.2%) for diagnosis of acute myocarditis [16]. In a pediatric cardiac MRI study by Cornicelli et al. [31], only 57% of patients met the original 2009 Lake Louise criteria, but the additional use of mapping parameters yielded a higher diagnostic performance. In particular, a combined score of global native T1 and T2 relaxation times yielded a sensitivity of 83% and a specificity of 96% [31]. However, the appropriate application of the 2018 Lake Louise criteria could not be done

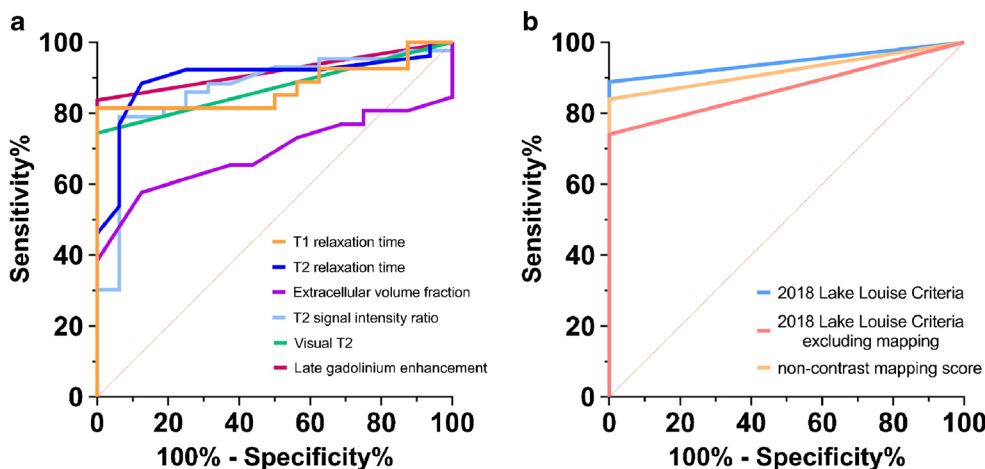


**Fig. 2** Graphs show receiver operating characteristic (ROC) curves for the subgroup cohort of patients (26/43) and control patients (16/16) with available mapping parameters. **a** The individual performance of different cardiac magnetic resonance parameters are presented: native T1 relaxation time (area under the curve [AUC]: 0.873), T2 relaxation time (AUC: 0.899), extracellular volume (AUC: 0.687), T2 signal intensity

ratio (AUC: 0.868) and late gadolinium enhancement (AUC: 0.919). **b** The performance of combined scores is visualized: 2018 Lake Louise criteria (AUC: 0.944), 2018 Lake Louise criteria excluding mapping parameters (AUC: 0.870), and a non-contrast score of native T1 and T2 relaxation times only (AUC: 0.920)

**Table 3** Cardiac magnetic resonance imaging characteristics of pediatric and adolescent patients with acute myocarditis at baseline and follow-up

Variable	Baseline (n=27)	Follow-up (n=27)	P-value
Left ventricular ejection fraction (%)	58±7	61±4	0.039
Left ventricular end-diastolic volume index (mL/m <sup>2</sup> )	83±14	82±15	0.53
Cardiac index (L/min/m <sup>2</sup> )	3.4±0.5	3.4±0.6	1.0
Interventricular septal thickness (mm)	8.6±1.3	8.5±1.3	0.14
T2 signal intensity ratio	2.25±0.43	1.91±0.35	0.001
Visual myocardial edema	17 (63%)	12 (44%)	0.016
Visual late gadolinium enhancement	25 (93%)	20 (74%)	0.063
T1 relaxation time, native (ms)	1,032±39	975±33	<0.001
Extracellular volume fraction (%)	27.9±5.9	25.6±3.5	0.053
T2 relaxation time (ms)	58±5	54±5	0.003

Continuous variables are given as mean±standard deviation. Dichotomous variables are given as absolute frequency with percentages in parentheses. P-values were obtained using a paired Student's *t*-test or McNemar's test. T1 and T2 relaxation times and extracellular volume fraction were available in 17/27 patients

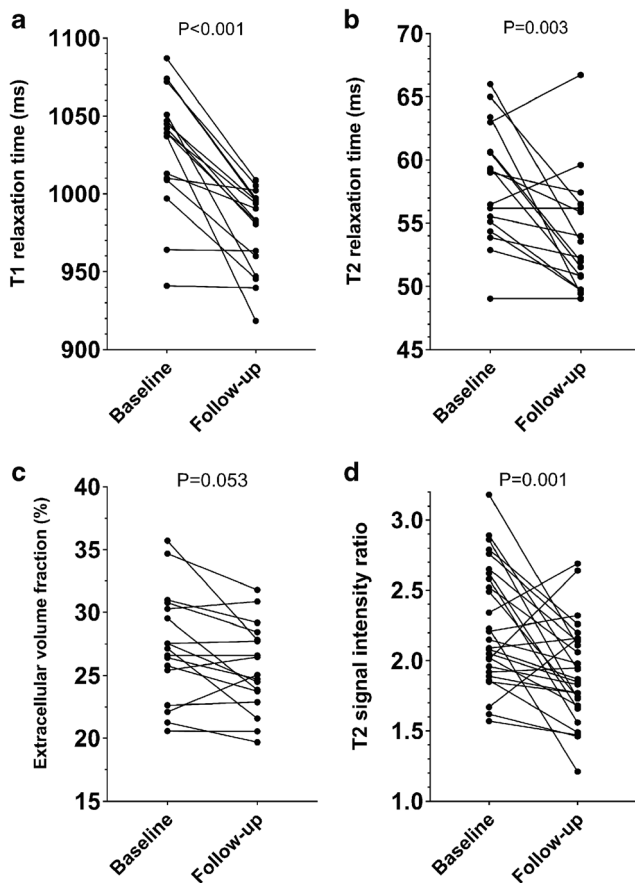


**Fig. 3** Line graphs show the chronological course of T1 relaxation time (a), T2 relaxation time (b), extracellular volume fraction (c) and T2 signal intensity ratio (d) at baseline and follow-up (follow-up was available in n=27; mapping parameters were available in n=17). Individual values are represented by the dots at baseline and follow-up cardiac magnetic resonance. The connecting lines show the tendency of change in quantitative parameters over time. P-values were obtained using a paired Student's *t*-test

due to its later release. In our study, we also could confirm high diagnostic accuracy for 2018 Lake Louise criteria for a pediatric and adolescent cohort, which was significantly higher when mapping parameters were implemented into the score (sensitivity: 89% vs. 73%, specificity: 100% vs. 100%).

### T1 mapping

T1 mapping as a single parameter achieved high diagnostic values according to a recent meta-analysis in adults with acute myocarditis (pooled sensitivity: 85%, pooled specificity: 86%) [32]. High sensitivity (91%) and specificity (86%) of T1 mapping were also observed in the reported pediatric cohort by Cornicelli et al. [31]. We could also show a comparable diagnostic performance of T1 mapping with an AUC of 0.873 and a slightly lower sensitivity (sensitivity: 82%, specificity: 100%) in our cohort. These results show that myocardial T1 mapping is a valuable tool for detecting acute myocarditis in a pediatric cohort. An increase of myocardial T1 values is mainly driven by intracellular or extracellular edema, hyperemia and necrosis in acute myocarditis. However, it is also increased in systemic or chronic diseases related to protein deposition, e.g., in diffuse fibrosis causes like chronic myocarditis or ischemic and nonischemic cardiomyopathies [33, 34]. Therefore, myocardial T1 mapping as a single parameter is not specific for acute myocarditis and should always be interpreted in clinical context.

### Extracellular volume fraction

Extracellular volume fraction was implemented as another T1-based criterion in the 2018 Lake Louise criteria [13]. It reflects the volume of cell-free heart tissue, including the intracapillary plasma volume, which is increased in acute myocarditis [33]. However, it also includes the space occupied



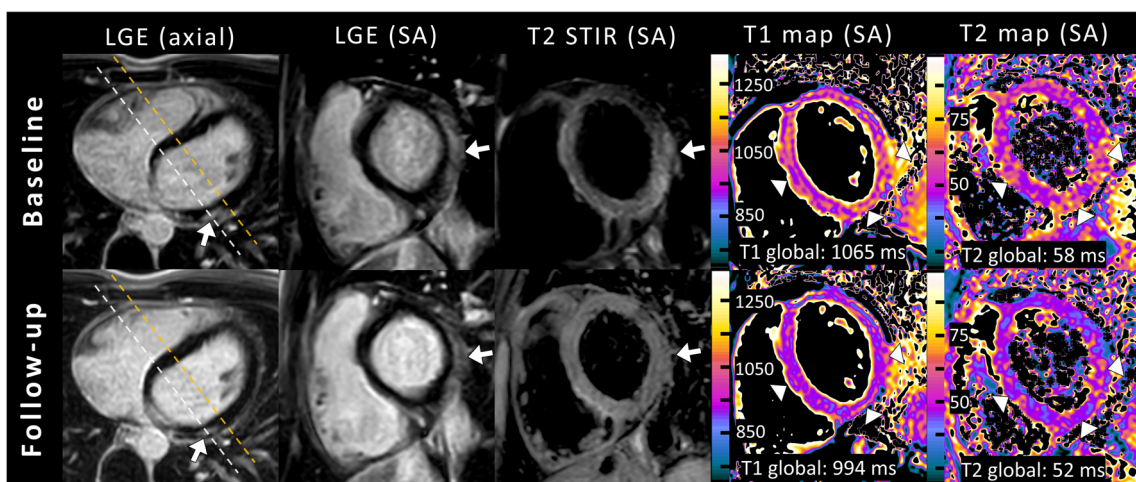


**Fig. 4** A clinical example of cardiac magnetic resonance imaging (MRI) in a 15-year-old boy with the typical appearance of acute myocarditis on cardiac MRI at baseline and with recovery on follow-up after 2 months. Cardiac MRI in end-diastole shows subepicardial enhancement of the basal lateral wall on late gadolinium enhancement (LGE) images in axial and short-axis (SA) orientation with associated focal myocardial edema (arrows) on fat-suppressed (T2-weighted short TI inversion recovery [T2 STIR]) images (white dashed lines in axial LGE images represent the imaging plane of LGE and T2 STIR). T2 STIR images at

follow-up show normalization of focal myocardial edema. Mapping parameters displayed high myocardial native T1 and T2 relaxation times at baseline cardiac MRI and normalization at follow-up. Notably, in this example, T1 and T2 maps cover the transition between the basal and mid segments outside the visible late gadolinium enhancement lesions (orange dashed lines in axial LGE images represent the imaging plane of the quantitative maps) and detected additionally diffuse myocardial alterations in the septal and inferior wall, which normalized at follow-up (arrowheads)

by the extracellular matrix, and is therefore a surrogate for myocardial fibrosis [32, 33]. In our study, the diagnostic performance of extracellular volume fraction (AUC: 0.687, sensitivity: 58%, specificity: 88%) was lower compared to T1 or T2 mapping, which differs from the pediatric study of Cornicelli et al. [31]. However, a recent meta-analysis also showed lower overall performance of extracellular volume

fraction compared to native T1 and T2 mapping [18]. Furthermore, previous studies could demonstrate a strong correlation between extracellular volume fraction values and histological myocardial fibrosis [33, 35]. Thus, extracellular volume fraction could still be normal in the early stage of disease and probably increase in severe or chronic courses of myocarditis.

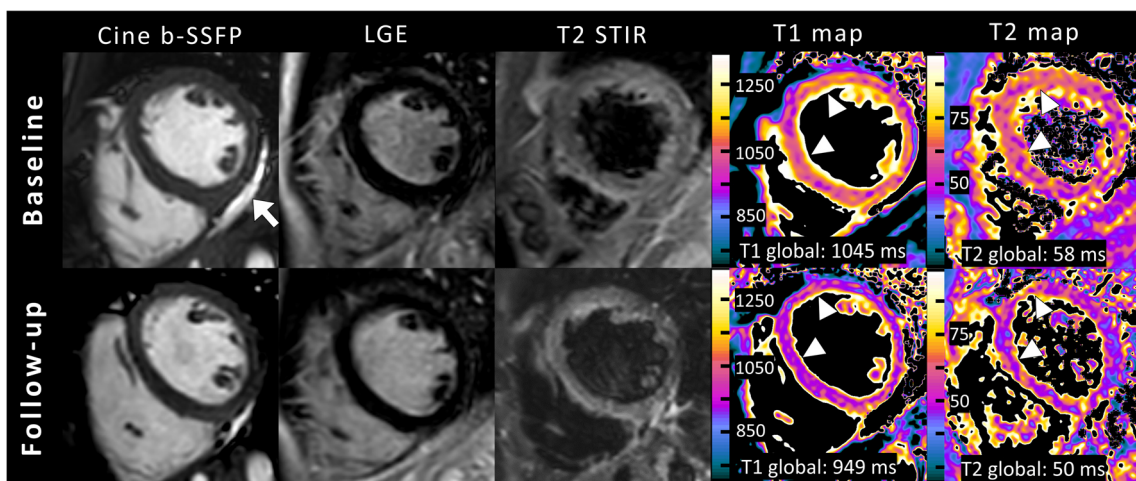


**Fig. 5** A clinical example of cardiac magnetic resonance imaging (MRI) in short-axis view in a 16-year-old boy. Cine images (balanced steady state free precession [b-SSFP]) show normal left ventricular ejection fraction (LVEF; 58%, no segmental hypokinesia) and pericardial effusion basal inferior (arrow). No focal or diffuse enhancement was identified on late gadolinium enhancement (LGE). No focal myocardial edema was visible on fat-suppressed (T2-weighted short TI inversion

recovery [T2 STIR]) images. Mapping parameters displayed high global myocardial native T1 and T2 relaxation times at baseline cardiac MRI and normalization at follow-up (arrowheads show the most affected segments). The diagnosis of acute diffuse myocarditis in this patient was only possible using quantitative parameters according to 2018 Lake Louise criteria and would have been missed by the original Lake Louise criteria

## T2 mapping

While neither extracellular volume fraction nor native T1 mapping strictly represent acute myocardial injury and are also biomarkers of myocardial fibrosis, T2 mapping has shown high sensitivity for detecting myocardial edema (e.g., inflammatory or ischemic causes) and is considered specific for acute myocardial diseases [20, 22]. Therefore, applying T2 mapping as a parameter of myocardial edema can help to discriminate between acute and convalescent myocarditis and also between chronic myocarditis and noninflammatory dilated cardiomyopathy [22, 36, 37]. For this reason, it was implemented in the 2018 Lake Louise criteria as a T2-based criterion [13]. In our study, T2 relaxation times reached the highest sensitivity (88%) of all single parameters and showed the highest diagnostic performance of all quantitative markers (AUC: 0.899), which is in line with the results of previous adult and pediatric studies [15, 16, 31, 32]. Although T2 mapping is less dependent on field strength compared to T1 mapping, most of the above-mentioned technical and physiological limitations also apply to T2 mapping.

## Non-contrast score

According to the 2018 Lake Louise criteria, the diagnosis of acute myocarditis can be principally based on native parameters only (increased native T1 and T2 relaxation times). In our cohort, a combined native score of T1 and T2 mapping showed a high diagnostic performance (AUC: 0.920, sensitivity: 85%, specificity: 100%), which was comparable to the original 2018 Lake Louise criteria (AUC: 0.944, sensitivity: 89%, specificity: 100%). Although complications regarding gadolinium-based contrast agents are rare, especially since the introduction of new-generation agents, the application has several drawbacks. Peripheral intravenous insertion in children is often a traumatic procedure and extravasation may occur. Furthermore, anaphylactic reaction and nephrogenic systemic fibrosis in end-stage renal disease are extremely rare but serious complications [38]. Given the recent literature on gadolinium retention within the brain and body of adults and children after repetitive contrast-enhanced MRI scans, long-term effects and clinical implications remain unclear [38]. Therefore, guidelines recommend cautious use of gadolinium contrast agents in children. Our results indicate that a non-contrast cardiac MRI protocol is a viable option for the diagnosis of acute myocarditis in cases where intravenous contrast is sought to be avoided. Furthermore, our follow-up results indicate that a non-contrast score can sufficiently track disease activity or therapeutic response. But late gadolinium enhancement imaging remains an essential part of diagnostics in acute

myocarditis, especially for detecting focal myocarditis (which may be missed by native quantitative mapping parameters), for discriminating between ischemic and nonischemic cardiomyopathies as well as risk stratification based on visualization and quantification of myocardial scar formation [39–41].

## Clinical correlations

Because the clinical manifestation of myocarditis varies with broad spectrums of symptoms ranging from asymptomatic courses to fulminant presentations with cardiogenic shock, the diagnosis of myocarditis might be difficult. Therefore, in clinical routine, myocarditis is often diagnosed using a multimodal approach with clinical, laboratory, imaging-based and pathological parameters. Our results show correlations between quantitative parameters and disease severity. T1 and T2 values were higher in patients with reduced LVEF. Patients requiring intermediate care unit treatment presented with higher T1 and T2 relaxation times, but without significant differences in extracellular volume fraction, LVEF or troponin level, when compared to patients not requiring intermediate care unit treatment. Notably, T2 relaxation times were directly associated with the duration of intermediate care unit treatment and the extent of systemic inflammation (C-reactive protein, white blood cell count). These findings indicate the diagnostic value of mapping parameters regarding the detection of severe courses of myocarditis, which are associated with increased mortality [42]. Furthermore, quantitative parameters have been shown to be appropriate markers to discriminate between active inflammation and the convalescent stage of the disease [22]. Our results also show that markers of active inflammation (T1 and T2 relaxation times, T2 signal intensity ratio) decreased at follow-up. However, visual myocardial edema and late gadolinium enhancement were still present in most patients. Therefore, mapping parameters seem to be a valuable tool to track disease activity or therapeutic response.

## Limitations

Our study has some limitations. First, endomyocardial biopsy was not available as a reference standard because it is not routinely used in the diagnostic work-up of acute myocarditis at our institution due to relevant disadvantages, e.g., sampling error leading to false-negative results in focal myocarditis or its periprocedural risks, especially in sick children [43, 44]. Therefore, clinical evidence for myocarditis was the reference standard used in this study, which has some drawbacks because this might have influenced the patient composition. Second, most included patients showed an infarct-like pattern of myocarditis. However, cutoff values might be different in patients with more chronic symptoms. Third, clinical data are

partially incomplete because of the retrospective study design. Fourth, infants and young children are underrepresented in our cohort; however, the overall incidence rate of acute myocarditis is very low in this age group. Fifth, our single-center cohort is small, therefore additional prospective studies are needed before our results can be generalized.

## Conclusion

The 2018 Lake Louise criteria including mapping parameters have a high performance for the diagnosis of acute myocarditis in children and adolescents and should be implemented into routine diagnostic work-up. Mapping parameters might be especially useful in tracking inflammatory disease activity.

**Supplementary Information** The online version contains supplementary material available at <https://doi.org/10.1007/s00247-021-05169-7>.

**Funding** Open Access funding enabled and organized by Projekt DEAL.

## Declarations

**Conflicts of interest** Claus C. Pieper declares only activities not related to the present article: He is a consultant for and has grants/grants pending with Guerbet and has received payment for lectures including service on speakers' bureaus from Philips Healthcare, Bayer Vital, and Guerbet. Ulrike Attenberger declares only activities not related to the present article: She has received payment for lectures including service on speakers bureaus from Siemens Healthineers. The remaining authors declare no conflicts of interest. Julian A. Luetkens declares only activities not related to the present article: He has received payment for lectures including service on speakers bureaus from Philips Healthcare.

**Open Access** This article is licensed under a Creative Commons Attribution 4.0 International License, which permits use, sharing, adaptation, distribution and reproduction in any medium or format, as long as you give appropriate credit to the original author(s) and the source, provide a link to the Creative Commons licence, and indicate if changes were made. The images or other third party material in this article are included in the article's Creative Commons licence, unless indicated otherwise in a credit line to the material. If material is not included in the article's Creative Commons licence and your intended use is not permitted by statutory regulation or exceeds the permitted use, you will need to obtain permission directly from the copyright holder. To view a copy of this licence, visit <http://creativecommons.org/licenses/by/4.0/>.

## References

- Richardson P, McKenna W, Bristow M et al (1996) Report of the 1995 World Health Organization/International Society and Federation of Cardiology Task Force on the definition and classification of cardiomyopathies. *Circulation* 93:841–842
- Arola A, Pikkarainen E, Sipilä JO et al (2017) Occurrence and features of childhood myocarditis: a nationwide study in Finland. *J Am Heart Assoc* 6:e005306
- Levine MC, Klugman D, Teach SJ (2010) Update on myocarditis in children. *Curr Opin Pediatr* 22:278–283
- Kindermann I, Barth C, Mahfoud F et al (2012) Update on myocarditis. *J Am Coll Cardiol* 59:779–792
- Canter CE, Simpson KE (2014) Diagnosis and treatment of myocarditis in children in the current era. *Circulation* 129:115–128
- Corrado D, Basso C, Thiene G (2001) Sudden cardiac death in young people with apparently normal heart. *Cardiovasc Res* 50:399–408
- Lyng TH, Nielsen TS, Gregers Winkel B et al (2019) Sudden cardiac death caused by myocarditis in persons aged 1–49 years: a nationwide study of 14 294 deaths in Denmark. *Forensic Sci Res* 4:247–256
- Caforio ALP, Pankuweit S, Arbustini E et al (2013) Current state of knowledge on aetiology, diagnosis, management, and therapy of myocarditis: a position statement of the European Society of Cardiology Working Group on myocardial and pericardial diseases. *Eur Heart J* 34:2636–2648 2648a-2648d
- Simpson KE, Canter CE (2011) Acute myocarditis in children. *Expert Rev Cardiovasc Ther* 9:771–783
- Biesbroek PS, Hirsch A, Zweerink A et al (2018) Additional diagnostic value of CMR to the European Society of Cardiology (ESC) position statement criteria in a large clinical population of patients with suspected myocarditis. *Eur Heart J Cardiovasc Imaging* 19:1397–1407
- Grigoratos C, Di Bella G, Aquaro GD (2019) Diagnostic and prognostic role of cardiac magnetic resonance in acute myocarditis. *Heart Fail Rev* 24:81–90
- Friedrich MG, Sechtem U, Schulz-Menger J et al (2009) Cardiovascular magnetic resonance in myocarditis: a JACC white paper. *J Am Coll Cardiol* 53:1475–1487
- Ferreira VM, Schulz-Menger J, Holmvang G et al (2018) Cardiovascular magnetic resonance in nonischemic myocardial inflammation: expert recommendations. *J Am Coll Cardiol* 72:3158–3176
- Luetkens JA, Doerner J, Thomas DK et al (2014) Acute myocarditis: multiparametric cardiac MR imaging. *Radiology* 273:383–392
- Luetkens JA, Homs R, Sprinkart AM et al (2016) Incremental value of quantitative CMR including parametric mapping for the diagnosis of acute myocarditis. *Eur Heart J Cardiovasc Imaging* 17:154–161
- Luetkens JA, Faron A, Isaak A et al (2019) Comparison of original and 2018 Lake Louise criteria for diagnosis of acute myocarditis: results of a validation cohort. *Radiol Cardiothorac Imaging* 1:e190010
- Hardin AP, Hackell JM, Committee on Practice and Ambulatory Medicine (2017) Age limit of pediatrics. *Pediatrics* 140:e20172151
- Kotanidis CP, Bazmpani M-A, Haidich A-B et al (2018) Diagnostic accuracy of cardiovascular magnetic resonance in acute myocarditis: a systematic review and meta-analysis. *JACC Cardiovasc Imaging* 11:1583–1590
- Messroghli DR, Radjenovic A, Kozerke S et al (2004) Modified Look-Locker inversion recovery (MOLLI) for high-resolution T1 mapping of the heart. *Magn Reson Med* 52:141–146
- Sprinkart AM, Luetkens JA, Träber F et al (2015) Gradient spin echo (GraSE) imaging for fast myocardial T2 mapping. *J Cardiovasc Magn Reson* 17:12
- Radunski UK, Lund GK, Stehning C et al (2014) CMR in patients with severe myocarditis: diagnostic value of quantitative tissue markers including extracellular volume imaging. *JACC Cardiovasc Imaging* 7:667–675
- Luetkens JA, Homs R, Dabir D et al (2016) Comprehensive cardiac magnetic resonance for short-term follow-up in acute myocarditis. *J Am Heart Assoc* 5:e003603
- Dabir D, Vollbrecht TM, Luetkens JA et al (2019) Multiparametric cardiovascular magnetic resonance imaging in acute myocarditis: a



- comparison of different measurement approaches. *J Cardiovasc Magn Reson* 21:54
24. Ferreira VM, Piechnik SK, Dall'Armellina E et al (2013) T(1) mapping for the diagnosis of acute myocarditis using CMR: comparison to T2-weighted and late gadolinium enhanced imaging. *JACC Cardiovasc Imaging* 6:1048–1058
  25. Hamlin SA, Henry TS, Little BP et al (2014) Mapping the future of cardiac MR imaging: case-based review of T1 and T2 mapping techniques. *Radiographics* 34:1594–1611
  26. Bönner F, Janzarik N, Jacoby C et al (2015) Myocardial T2 mapping reveals age- and sex-related differences in volunteers. *J Cardiovasc Magn Reson* 17:9
  27. Rauhalahti SMO, Mangion K, Barrientos PH et al (2016) Native myocardial longitudinal (T1) relaxation time: regional, age, and sex associations in the healthy adult heart. *J Magn Reson Imaging* 44: 541–548
  28. Roy C, Slimani A, de Meester C et al (2017) Age and sex corrected normal reference values of T1, T2, T2\* and ECV in healthy subjects at 3T CMR. *J Cardiovasc Magn Reson* 19:72
  29. Luetkens JA, Voigt M, Faron A et al (2020) Influence of hydration status on cardiovascular magnetic resonance myocardial T1 and T2 relaxation time assessment: an intraindividual study in healthy subjects. *J Cardiovasc Magn Reson* 22:63
  30. Rosmini S, Bulluck H, Captur G et al (2018) Myocardial native T1 and extracellular volume with healthy ageing and gender. *Eur Heart J Cardiovasc Imaging* 19:615–621
  31. Comicelli MD, Rigsby CK, Rychlik K et al (2019) Diagnostic performance of cardiovascular magnetic resonance native T1 and T2 mapping in pediatric patients with acute myocarditis. *J Cardiovasc Magn Reson* 21:40
  32. Pan JA, Lee YJ, Salerno M (2018) Diagnostic performance of extracellular volume, native T1, and T2 mapping versus Lake Louise criteria by cardiac magnetic resonance for detection of acute myocarditis: a meta-analysis. *Circ Cardiovasc Imaging* 11:e007598
  33. Moon JC, Messroghli DR, Kellman P et al (2013) Myocardial T1 mapping and extracellular volume quantification: a Society for Cardiovascular Magnetic Resonance (SCMR) and CMR Working Group of the European Society of Cardiology consensus statement. *J Cardiovasc Magn Reson* 15:92
  34. Isaak A, Praktiknojo M, Jansen C et al (2020) Myocardial fibrosis and inflammation in liver cirrhosis: MRI study of the liver-heart axis. *Radiology* 297:51–61
  35. de Meester de Ravenstein C, Bouzin C, Lazam S et al (2015) Histological validation of measurement of diffuse interstitial myocardial fibrosis by myocardial extravascular volume fraction from modified Look-Locker imaging (MOLLI) T1 mapping at 3 T. *J Cardiovasc Magn Reson* 17:48
  36. Lurz P, Luecke C, Eitel I et al (2016) Comprehensive cardiac magnetic resonance imaging in patients with suspected myocarditis: the MyoRacer-trial. *J Am Coll Cardiol* 67:1800–1811
  37. von Knobelsdorff-Brenkenhoff F, Schüller J, Dogangüzel S et al (2017) Detection and monitoring of acute myocarditis applying quantitative cardiovascular magnetic resonance. *Circ Cardiovasc Imaging* 10:e005242
  38. Schieda N, van der Pol CB, Walker D et al (2020) Adverse events to the gadolinium-based contrast agent gadoteric acid: systematic review and meta-analysis. *Radiology* 297:565–572
  39. Gräni C, Eichhorn C, Bière L et al (2017) Prognostic value of cardiac magnetic resonance tissue characterization in risk stratifying patients with suspected myocarditis. *J Am Coll Cardiol* 70: 1964–1976
  40. Aquaro GD, Perfetti M, Camastra G et al (2017) Cardiac MR with late gadolinium enhancement in acute myocarditis with preserved systolic function: ITAMY study. *J Am Coll Cardiol* 70:1977–1987
  41. Berg J, Kottwitz J, Baltensperger N et al (2017) Cardiac magnetic resonance imaging in myocarditis reveals persistent disease activity despite normalization of cardiac enzymes and inflammatory parameters at 3-month follow-up. *Circ Heart Fail* 10:3004262
  42. Ammirati E, Cipriani M, Lilliu M et al (2017) Survival and left ventricular function changes in fulminant versus nonfulminant acute myocarditis. *Circulation* 136:529–545
  43. Pophal SG, Sigfusson G, Booth KL et al (1999) Complications of endomyocardial biopsy in children. *J Am Coll Cardiol* 34:2105–2110
  44. Hauck AJ, Kearney DL, Edwards WD (1989) Evaluation of post-mortem endomyocardial biopsy specimens from 38 patients with lymphocytic myocarditis: implications for role of sampling error. *Mayo Clin Proc* 64:1235–1245

**Publisher's note** Springer Nature remains neutral with regard to jurisdictional claims in published maps and institutional affiliations.



### 3.2 Quantitative kardiale MRT bei der peripartalen Kardiomyopathie

*“Peripartum Cardiomyopathy: Diagnostic and Prognostic Value of Cardiac Magnetic Resonance in the Acute Stage”*

Isaak A, Ayub TH, Merz WM, Faron A, Endler C, Sprinkart AM, Pieper CC, Kuetting D, Dabir D, Attenberger U, Zimmer S, Becher UM, Luetkens JA.

Erschienen in *Diagnostics*. 2022 Feb 1;12(2):378.




**Zielsetzung und Methoden** – Die peripartale Kardiomyopathie ist eine sehr seltene erworbene primäre Kardiomyopathie mit führender Symptomatik der Herzinsuffizienz und dilatativem Kardiomyopathie-Phänotyp. Ziel dieser Studie war es den diagnostischen und prognostischen Wert der quantitativen kardialen MRT in dieser Entität zu untersuchen. MRT-Untersuchungen von Patientinnen mit peripartaler Kardiomyopathie zum Zeitpunkt der akuten Symptomatik und von gesunden Frauen wurden retrospektiv untersucht. Echokardiographische Nachuntersuchungen wurden durchgeführt. Eine funktionelle Erholung wurde als eine linksventrikuläre Auswurffraktion von mindestens 50 % definiert.

**Ergebnisse** – Patientinnen mit peripartaler Kardiomyopathie ( $33 \pm 5$  Jahre; 17 Frauen) zeigten eine linksventrikuläre/-atriale Dilatation und eine biventrikuläre systolische Dysfunktion inklusive Einschränkung der myokardialen Strainparameter im Vergleich zur gesunden Kontrollgruppe ( $33 \pm 8$  Jahre; 15 Frauen). Fokale Mehranreicherungen in der LGE-Bildgebung wurden nur bei 12 % der Patientinnen detektiert. Ein fokales Myokardödem war bei 59 % der Patientinnen sichtbar. Die semiquantitativen und quantitativen myokardialen Gewebeparameter zeigten im Vergleich zur Kontrollgruppe deutliche Zeichen des globalen diffusen Myokardödems (siehe *Figure 1* (Isaak et al., 2022)). Bei Patientinnen mit Kardio-MRT Nachuntersuchung konnte eine Normalisierung des diffusen Myokardödems beobachtet werden (siehe klinisches Beispiel in *Figure 3* (Isaak et al., 2022)). Bei insgesamt 76 % der Patientinnen erholte sich die linksventrikuläre Funktion vollständig (Mediane Zeit zur Funktionserholung: 45 Tage). Das Fehlen eines visuellen Myokardödems und die Beeinträchtigung der linksventrikulären Strainparameter waren mit einer verzögerten Erholung der linksventrikulären Funktion assoziiert (siehe *Figure 4* (Isaak et al., 2022)).

**Schlussfolgerungen** – Das diffuse Myokardödem scheint eine Hauptkomponente in der akuten Phase der peripartalen Kardiomyopathie zu sein und zusammen mit den linksventrikulären Strainparametern einen prognostischen Wert für die Erholung der linksventrikulären Funktion zu haben.

## Article

# Peripartum Cardiomyopathy: Diagnostic and Prognostic Value of Cardiac Magnetic Resonance in the Acute Stage

Alexander Isaak <sup>1,2</sup>, Tiyasha H. Ayub <sup>3</sup>, Waltraut M. Merz <sup>3</sup>, Anton Faron <sup>1,2</sup>, Christoph Endler <sup>1,2</sup>, Alois M. Sprinkart <sup>1,2</sup>, Claus C. Pieper <sup>1</sup>, Daniel Kuetting <sup>1,2</sup>, Darius Dabir <sup>1,2</sup>, Ulrike Attenberger <sup>1</sup>, Sebastian Zimmer <sup>4</sup>, Ulrich M. Becher <sup>4</sup> and Julian A. Luetkens <sup>1,2,\*</sup>

- <sup>1</sup> Department of Diagnostic and Interventional Radiology, University Hospital Bonn, 53127 Bonn, Germany; alexander.isaak@ukbonn.de (A.I.); anton.faron@ukbonn.de (A.F.); christoph.endler@ukbonn.de (C.E.); sprinkart@uni-bonn.de (A.M.S.); claus\_christian.pieper@ukbonn.de (C.C.P.); daniel.kuetting@ukbonn.de (D.K.); darius.dabir@ukbonn.de (D.D.); ulrike.attenberger@ukbonn.de (U.A.)
- <sup>2</sup> Quantitative Imaging Lab Bonn (QILab), University of Bonn, 53127 Bonn, Germany
- <sup>3</sup> Department of Obstetrics and Prenatal Medicine, University Hospital Bonn, 53127 Bonn, Germany; tiyasha\_hosne.ayub@ukbonn.de (T.H.A.); waltraut.merz@ukbonn.de (W.M.M.)
- <sup>4</sup> Department of Internal Medicine II-Cardiology, University Hospital Bonn, 53127 Bonn, Germany; sebastian.zimmer@ukbonn.de (S.Z.); ulrich.becher@ukbonn.de (U.M.B.)
- \* Correspondence: julian.luetkens@ukbonn.de; Tel.: +49-(0)228-287-19860; Fax: +49-(0)228-287-16093

**Abstract:** This study aimed to evaluate the diagnostic and prognostic value of cardiac magnetic resonance in acute peripartum cardiomyopathy (PPCM). A total of 17 patients with PPCM in the acute stage and 15 healthy controls were retrospectively analyzed regarding myocardial function, edema, late gadolinium enhancement (LGE), and T1 and T2 mappings (T1, T2). Echocardiographic follow-ups were performed. Functional recovery was defined as a left ventricular ejection fraction (LVEF) of  $\geq 50\%$ . Patients with PPCM displayed biventricular dysfunction with reduced myocardial strain parameters and left ventricular and atrial dilatation, as well as diffuse myocardial edema (T2 signal intensity ratio:  $2.10 \pm 0.34$  vs.  $1.58 \pm 0.21$ ,  $p < 0.001$ ; T1:  $1070 \pm 51$  ms vs.  $980 \pm 28$  ms,  $p = 0.001$ ; T2:  $63 \pm 5$  ms vs.  $53 \pm 2$  ms,  $p < 0.001$ ). Visual myocardial edema was present in 10 patients (59%). LGE was positive in 2 patients (12%). A total of 13 patients (76%) showed full LVEF recovery. The absence of visual myocardial edema and impairment of strain parameters were associated with delayed LVEF recovery. Multivariable Cox regression analysis revealed global longitudinal strain as an independent prognostic factor for LVEF recovery. In conclusion, biventricular systolic dysfunction with diffuse myocardial edema seems to be present in acute PPCM. Myocardial edema and strain may have prognostic value for LVEF recovery.



**Citation:** Isaak, A.; Ayub, T.H.; Merz, W.M.; Faron, A.; Endler, C.; Sprinkart, A.M.; Pieper, C.C.; Kuetting, D.; Dabir, D.; Attenberger, U.; et al. Peripartum Cardiomyopathy: Diagnostic and Prognostic Value of Cardiac Magnetic Resonance in the Acute Stage. *Diagnostics* **2022**, *12*, 378. <https://doi.org/10.3390/diagnostics12020378>

Academic Editor: Jan Fedacko

Received: 26 December 2021

Accepted: 28 January 2022

Published: 1 February 2022

**Publisher's Note:** MDPI stays neutral with regard to jurisdictional claims in published maps and institutional affiliations.



**Copyright:** © 2022 by the authors. Licensee MDPI, Basel, Switzerland. This article is an open access article distributed under the terms and conditions of the Creative Commons Attribution (CC BY) license (<https://creativecommons.org/licenses/by/4.0/>).

**Keywords:** peripartum cardiomyopathy; pregnancy; heart failure; cardiac magnetic resonance imaging; myocardial edema; mapping; strain

## 1. Introduction

Peripartum cardiomyopathy (PPCM) is a rare and potentially life-threatening condition. It is defined as development of new-onset cardiomyopathy during the peripartum episode (the majority of patients present postpartum, mostly during the week after delivery) with an initial left ventricular (LV) ejection fraction (EF) of  $<45\%$  and without other identifiable cause of heart failure [1,2]. The incidence of PPCM varies depending on ethnic or regional factors (e.g., ranging from 1 in 1000 to 1 in 4000 deliveries in the United States) [3–5]. Although different genetic, inflammatory, and immunologic hypotheses have been discussed, the exact pathogenic mechanisms of PPCM are still incompletely understood [1]. Diagnosis is primarily made by exclusion of more common differential diagnoses, such as pulmonary embolism, acute myocarditis, takotsubo syndrome, or pre-existing valvular or congenital heart disease [1]. Prognosis of PPCM is highly variable, and clinical course can vary from

mild to severe [5]. The majority of patients show LVEF recovery within 6 months after diagnosis, but full LVEF recovery can be delayed, and there might even be a need for an implantable cardioverter defibrillator [1,6,7].

Although transthoracic echocardiography (TTE) is the first-line diagnostic imaging modality in case of suspected PPCM [5], cardiac magnetic resonance (CMR) is often employed in the diagnostic workup of these patients. CMR is considered the gold standard for the determination of functional and structural myocardial parameters and plays a key role in the accurate diagnosis of nonischemic cardiomyopathies, especially for the detection of acute inflammatory disease [8]. Quantitative techniques such as T1 and T2 mappings and also extracellular volume (ECV) have been shown to quantify diffuse myocardial tissue pathologies (e.g., edema) in nonischemic cardiomyopathies [9]. Furthermore, myocardial strain analysis can quantify functional alterations of the myocardium [10]. The presence of late gadolinium enhancement (LGE) in PPCM was controversially discussed in the last years; however, recent multicenter studies showed that LGE seems to be uncommon in PPCM patients (prevalence of about 4–5%) [11,12]. A few TTE-based studies in PPCM patients showed decreased strain parameters [13], which were associated with worse clinical outcome [14]. Evidence of myocardial edema was found in a few case series using T2-weighted sequences [15,16]. However, the prognostic factors and the role of myocardial edema remain poorly understood. In addition, imaging in previous studies was sometimes not performed in the acute phase of PPCM, so the full extent of myocardial alterations may have been missed.

The purpose of our study was (1) to evaluate the diagnostic value of CMR in the acute stage of PPCM and (2) to find prognostic indicators for recovery.

## 2. Materials and Methods

### 2.1. Study Population

Patients with acute PPCM and healthy control participants were included in this study. From February 2010 to January 2020, the department's CMR registry contained 17 comprehensive scans of patients with clinical diagnosis of PPCM. All CMR scans were performed postpartum. Acute PPCM was diagnosed based on recent diagnostic criteria (occurrence of heart failure with an LVEF of <45% during the peripartum without other identifiable cause of heart failure) [1]. Serial TTE follow-ups (up to 3 years) from the clinical information system were available in 16/17 (94%) patients. An LVEF of  $\geq 50\%$  at TTE follow-up was defined as full LVEF recovery. CMR follow-ups were available in 6/17 patients (35%).

Due to ethical reasons, the control group consisted of healthy female controls instead of females with a normal pregnancy. All included controls were volunteers or outpatients presenting with nonspecific symptoms. All control participants had an unremarkable past medical history of cardiovascular disease. Electrocardiographic (ECG) results were unremarkable, and no cardiac risk factors were present. All control participants had normal cardiac MRI results without structural abnormalities.

### 2.2. Cardiac Magnetic Resonance Imaging

All investigations were performed on a clinical whole-body MRI system (Ingenia 1.5 Tesla, Philips Healthcare, Best, The Netherlands). A 32-channel torso coil with a digital interface was used for signal reception. Cardiac scan protocol included ECG-gated steady-state free precession cine images in short-axis, four-chamber, three-chamber, and two-chamber views. T2-weighted short-tau inversion-recovery (STIR) sequence was acquired in short-axis, two-chamber, and transversal views for the visualization of myocardial edema and for the calculation of the T2 signal intensity ratio, as previously described [8]. LGE imaging was based on a segmented inversion-recovery gradient-echo sequence and acquired in short-axis, two-chamber, and four-chamber views. Myocardial T1 and T2 maps were obtained at end diastole in apical, midventricular, and basal short-axis orientation [17,18]. Postcontrast myocardial T1 maps were performed 10 min after contrast injection. For contrast

enhancement, a single bolus of 0.2 mmol/kg body weight of gadobutrol (Gadovist, Bayer HealthCare, Leverkusen, Germany) was applied. For ECV calculation, the hematocrit level on the day of the CMR scan was used. A detailed description of the CMR sequence parameters is provided in the Supplementary Materials Appendix S1 and Table S1 (online-only supplement).

### 2.3. Cardiac Image Analysis

Images were evaluated by two radiologists (J.A.L. and A.I., with 8 and 3 years of experience in CMR, respectively) using dedicated software (IntelliSpace Portal Version 10.1, Philips Medical Systems, Hamburg, Germany). Ventricular and atrial volume and mass parameters were calculated according to recent guidelines and indexed to body surface area using the Mosteller method [19]. The presence of high signal intensities on T2 STIR and on LGE images was assessed visually by consensus agreement of the two readers. The semiquantitative T2 signal intensity ratio [20] and semiquantitative enhanced volume percentage (performed in short-axis LGE images) using the full-width half-maximum technique were calculated [19]. Myocardial relaxation maps were motion-corrected using FEIR (fast elastic image registration) software (IntelliSpace Portal Version 10.1, Philips Medical Systems, Hamburg, Germany). T1 and T2 relaxation times and hematocrit-corrected ECV values (using pre- and postcontrast T1 values) were calculated as previously described [20]. Dedicated software (Image-Arena 4.6, TomTec Imaging Systems, Unterschleißheim, Germany) was used to perform feature tracking strain measurements derived from cine images in four-chamber and short-axis views to assess LV global longitudinal (GLS), circumferential (GCS), and radial strain (GRS) [10].

### 2.4. Statistical Analysis

Prism (version 8.4.3; GraphPad Software, San Diego, CA, USA) and SPSS Statistics (version 26; IBM, Armonk, NY, USA) were used for statistical analysis. The Kolmogorov–Smirnov test was applied for the assessment of normal distribution. Continuous patient characteristics are presented as mean  $\pm$  standard deviation or as absolute frequency. Continuous variables between two groups were compared by using Student's *t*-test. Due to the exploratory study design, no adjustments for multiple comparisons were made [21]. Dichotomous variables were compared by using the  $\chi^2$  test (with a cell count  $>$  five) or Fisher exact test (with a cell count  $\leq$  five). For intraindividual comparisons, paired Student's *t*-test and McNemar's test were used. Univariable and multivariable Cox regression analyses were applied to test the impact of imaging variables for the prediction of LVEF recovery. After forward selection, significant covariates with  $p < 0.05$  at univariable analysis were added to a multivariable cox regression model to further fit the impact of variables. The results are presented as hazard ratios (HRs) with 95% confidence interval (95% CIs). The cohort was also binarized based on the prevalence of visual myocardial edema and based on median values of LV myocardial dysfunction (LVEF: 27%, GLS:  $-11.2\%$ , GCS:  $-9.5\%$ ). The Kaplan–Meier method with log-rank tests was used to compare the “time to LVEF recovery” between these groups.  $p < 0.05$  was defined to indicate statistical significance.

## 3. Results

### 3.1. General Characteristics

A total of 32 female subjects, 17 females with acute PPCM ( $33 \pm 5$  years) and 15 female control subjects ( $33 \pm 8$  years) were included in this study. No difference between patients and healthy controls was observed in body mass index ( $p = 0.077$ ) or heart rate ( $p = 0.052$ ) (Table 1). Clinical diagnosis of PPCM was made postpartum in the majority of patients (15/17, 88%; range: 1–48 days) and during the last week before delivery in only 2 patients (2/17, 12%; 1 and 3 days before delivery, respectively). In all patients, CMR was performed after delivery (range: 4–48 days; median: 10 days) and during the acute stage of disease (time between clinical diagnosis and CMR ranged from 0 to 9 days; median: 3 days). A total of 6/17 (38%) patients had cesarean section, and 1/17 (6%) patient had a twin gestation.

All patients had symptoms of heart failure (NYHA class II: 5/17, 29%; class III: 9/17, 53%; class IV: 3/17, 18%) and elevated levels of serum N-terminal pro-B-type natriuretic peptide (NT-proBNP) (Table 1). Accompanying conditions were preeclampsia (4/17, 24%), HELLP (hemolysis, elevated liver enzymes, and low platelets) syndrome (2/17, 12%), uterine atony (2/17, 12%), gestational diabetes (3/17, 18%), and gestational hypertension (3/17, 18%). None had a history of cardiac disease, diabetes, or arterial hypertension before pregnancy. All patients had sinus rhythm, and 2 patients had sinus tachycardia on initial TTE. All patients were treated based on available recommendations for acute or subacute heart failure with reduced ejection fraction. Management of heart failure was individually adapted according to the clinical scenario and the course of disease. A total of 5/17 (17%) women received bromocriptine in addition to standard heart failure treatment.

### 3.2. CMR Imaging Results

Patients with PPCM displayed reduced LVEF ( $31 \pm 10\%$  vs.  $61 \pm 6\%$ ,  $p < 0.001$ ) and right ventricular ejection fraction (RVEF) ( $32 \pm 13\%$  vs.  $57 \pm 7\%$ ,  $p < 0.001$ ), increased LV end-diastolic volume index ( $121 \pm 43 \text{ mL/m}^2$  vs.  $73 \pm 9 \text{ mL/m}^2$ ,  $p < 0.001$ ), higher left atrium volume index ( $75 \pm 24 \text{ mL/m}^2$  vs.  $40 \pm 10 \text{ mL/m}^2$ ,  $p < 0.001$ ), and higher LV mass index ( $71 \pm 19 \text{ g/m}^2$  vs.  $41 \pm 7 \text{ g/m}^2$ ,  $p < 0.001$ ) when compared with healthy controls (Figure 1). Global hypokinesia was seen in 15/17 (88%), and focal hypokinesia was seen in 2/17 (12%) patients but in none of the controls. No difference was observed in the right ventricular end-diastolic volume index ( $82 \pm 24 \text{ mL/m}^2$  vs.  $75 \pm 11 \text{ mL/m}^2$ ,  $p = 0.300$ ) or in the cardiac index ( $3.0 \pm 0.7 \text{ L/min/m}^2$  vs.  $3.3 \pm 0.7 \text{ L/min/m}^2$ ,  $p = 0.228$ ). Myocardial strain parameters were impaired in PPCM patients (GLS:  $-11.8 \pm 4.8\%$  vs.  $-22.3 \pm 4.2\%$ ,  $p < 0.001$ ; GCS:  $-12.3 \pm 6.3\%$  vs.  $-24.1 \pm 3.6\%$ ,  $p < 0.001$ ; GRS:  $22.8 \pm 14.7\%$  vs.  $37.1 \pm 10.2\%$ ,  $p = 0.004$ ). A total of 4/17 patients (24%) had moderate pericardial effusion (10–20 mm), and 8/17 patients (47%) had small pericardial effusion (<10 mm). Pleural effusion was present in 11/17 patients (65%). None of the patients in our cohort had evidence of LV thrombus.

Visual myocardial edema was observed in 10/17 patients (59%, controls: 0%,  $p < 0.001$ ), and T2 signal intensity ratio was increased in the PPCM group ( $2.10 \pm 0.34$  vs.  $1.58 \pm 0.21$ ,  $p < 0.001$ ). Visual LGE was present in 2/17 patients (12%, controls: 0%,  $p = 0.484$ ) and showed a predominantly patchy pattern of enhancement in the subepi- and midmyocardium. Quantified LGE percentages were higher in patients than in healthy controls ( $3.9 \pm 4.7\%$  vs.  $0.6 \pm 0.7\%$ ,  $p = 0.013$ ). Myocardial native T1 relaxation times ( $1070 \pm 51 \text{ ms}$  vs.  $980 \pm 28 \text{ ms}$ ,  $p = 0.001$ ) and T2 relaxation times ( $63 \pm 5 \text{ ms}$  vs.  $53 \pm 2 \text{ ms}$ ,  $p < 0.001$ ) were increased in the PPCM group when compared with the control group. However, there was no significant difference in ECV between the two groups ( $31.7 \pm 7.1\%$  vs.  $27.7 \pm 3.2\%$ ,  $p = 0.235$ ).

### 3.3. Subgroup Analyses of CMR Parameters in Patients with Follow-Up

CMR follow-up was performed in 6/17 patients (35%; median time to follow-up: 14 weeks; range: 7 to 132 weeks). Between baseline and follow-up CMR, improvement in LVEF ( $38 \pm 9\%$  vs.  $55 \pm 17\%$ ,  $p = 0.011$ ) and RVEF ( $40 \pm 18\%$  vs.  $55 \pm 11\%$ ,  $p = 0.023$ ) was observed (see Figure 2). There were no statistically significant differences in biventricular volumes, left atrium volumes or in LV mass index (Table 2). Interventricular septal thickness decreased on follow-up ( $10.5 \pm 2.8 \text{ mm}$  vs.  $9.1 \pm 2.0 \text{ mm}$ ,  $p = 0.047$ ). On CMR follow-up, no visual myocardial edema was detected in any of the patients (3/6, 50% vs. 0/6, 0%,  $p = 0.25$ ). One focal LGE lesion was still visible on follow-up CMR. Myocardial strain parameters improved between baseline and follow-up CMR (GLS:  $-13.5 \pm 4.8\%$  vs.  $-19.8 \pm 5.8\%$ ,  $p = 0.039$ ; GCS:  $-15.6 \pm 8.1\%$  vs.  $-18.7 \pm 9.5\%$ ,  $p = 0.009$ ). T1 and T2 mappings were only available in two follow-up cases and were therefore excluded from the follow-up subgroup analysis. However, the presented clinical example showed a tendency towards decreasing T1 and T2 relaxation times at follow-up, indicating myocardial recovery (Figure 3).

**Table 1.** Clinical and cardiac magnetic resonance imaging characteristics of patients with acute peripartum cardiomyopathy (PPCM) and healthy controls.

Variable	Patients with PPCM (n = 17)	Healthy Female Controls (n = 15)	p-Value
<i>Clinical parameters</i>			
Age (years)	33 ± 5	33 ± 8	0.892
Weight (kg)	77 ± 19	67 ± 13	0.088
Height (cm)	170 ± 8	170 ± 7	0.972
Body mass index (kg/m <sup>2</sup> )	27 ± 7	23 ± 4	0.077
Heart rate (bpm)	78 ± 27	75 ± 11	0.052
NT-proBNP (pg/mL)	8792 ± 12,308	NA	-
Troponin I (ng/L)	0.12 ± 0.25	NA	-
C-reactive protein (mg/L)	15.0 ± 11.1	NA	-
White blood cells (G/L)	10.5 ± 3.7	NA	-
<i>CMR parameters</i>			
Left ventricular ejection fraction (%)	31 ± 10	61 ± 6	<b>&lt;0.001</b>
Left ventricular end-diastolic volume index (mL/m <sup>2</sup> )	121 ± 43	73 ± 9	<b>&lt;0.001</b>
Right ventricular ejection fraction (%)	32 ± 13	57 ± 7	<b>&lt;0.001</b>
Right ventricular end-diastolic volume index (mL/m <sup>2</sup> )	82 ± 24	75 ± 11	0.300
Cardiac index (L/min/m <sup>2</sup> )	3.0 ± 0.7	3.3 ± 0.7	0.228
Left atrium volume index (mL/m <sup>2</sup> )	75 ± 24	40 ± 10	<b>&lt;0.001</b>
Left ventricular mass index (g/m <sup>2</sup> )	71 ± 19	41 ± 7	<b>&lt;0.001</b>
Interventricular septal thickness (mm)	10.3 ± 1.9	7.9 ± 1.1	<b>&lt;0.001</b>
T2 signal intensity ratio	2.10 ± 0.34	1.58 ± 0.21	<b>&lt;0.001</b>
Visual myocardial edema	10 (59%)	0 (0%)	<b>&lt;0.001</b>
Visual late gadolinium enhancement	2 (12%)	0 (0%)	0.484
Late gadolinium enhancement (%)	3.9 ± 4.7	0.6 ± 0.7	<b>0.013</b>
Global longitudinal strain (%)	−11.8 ± 4.8	−22.3 ± 4.2	<b>&lt;0.001</b>
Global circumferential strain (%)	−12.3 ± 6.3	−24.1 ± 3.6	<b>&lt;0.001</b>
Global radial strain (%)	22.8 ± 14.7	37.1 ± 10.2	<b>0.004</b>
T1 relaxation time, native (ms)	1070 ± 51	980 ± 28	<b>0.001</b>
Extracellular volume fraction (%)	31.7 ± 7.1	27.7 ± 3.2	0.235
T2 relaxation time (ms)	63 ± 5	53 ± 2	<b>&lt;0.001</b>

Continuous variables are given as mean ± standard deviation. Dichotomous variables are given as absolute frequency with percentages in parentheses. p-Values were obtained using Student's *t*-test and Fisher exact test. NT-proBNP = N-terminal pro-B-type natriuretic peptide. Mapping parameter (T1 and T2 relaxation times and extracellular volume fraction) were available in 8 patients. Values in bold denote statistical significance.



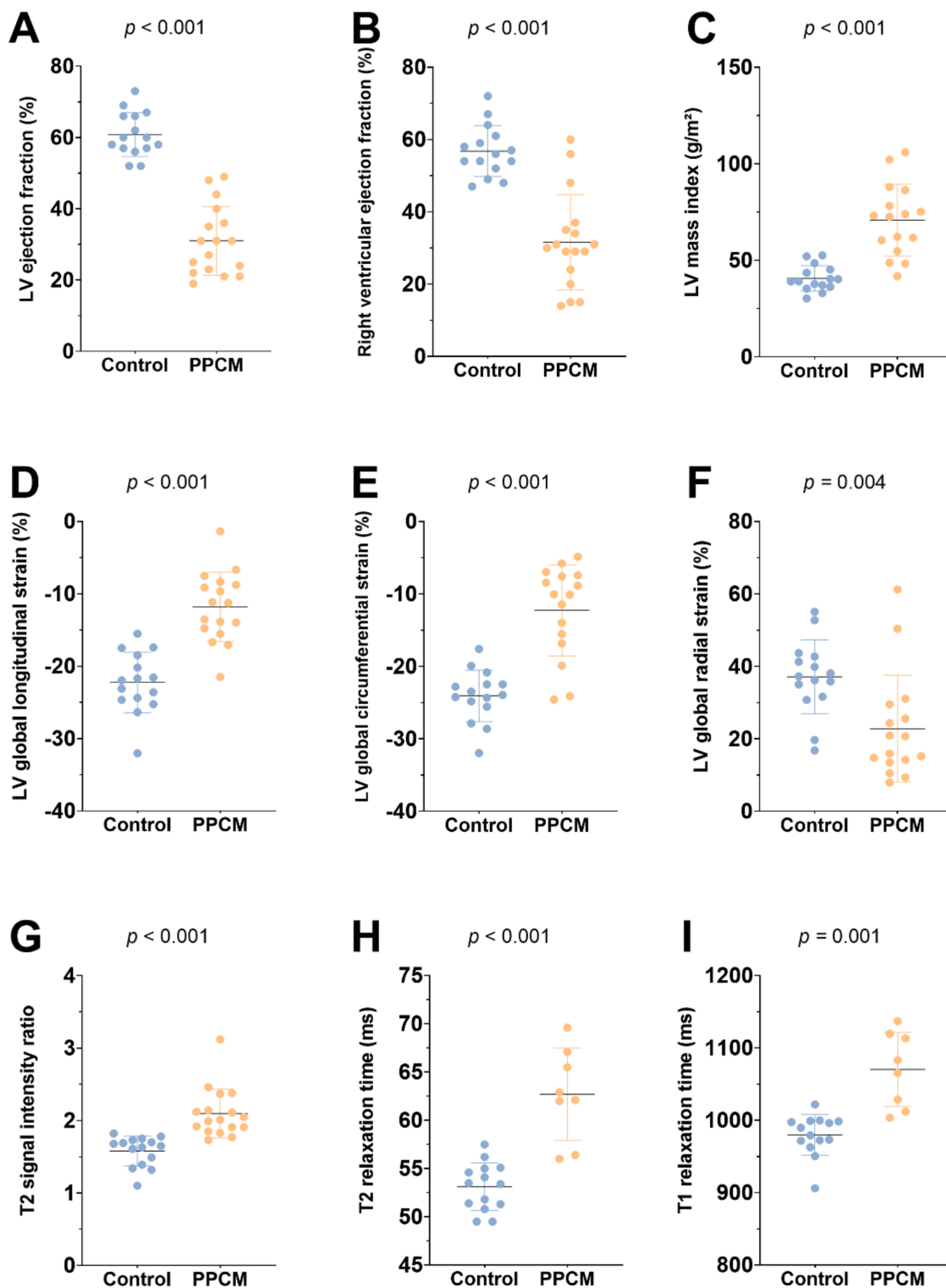


**Figure 1.** Graphs with individual plotted values show distribution of functional (A–F) and structural (G–I) cardiac MRI parameters in the control and the peripartum cardiomyopathy group (PPCM). Individual values are represented as single-colored dots. The horizontal lines show the mean values with error bars representing one standard deviation.  $p$ -Values were obtained using unpaired Student’s  $t$ -test. LV = left ventricular.

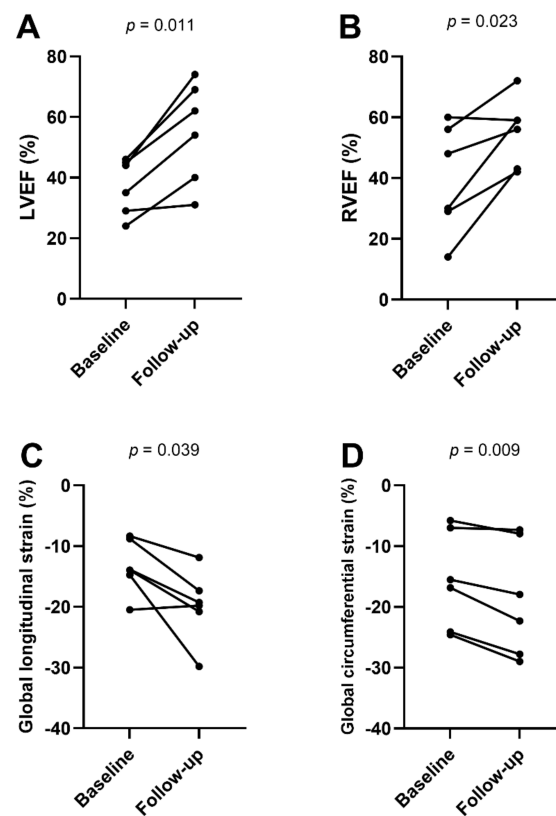


**Figure 2.** Line graphs show functional cardiac magnetic resonance parameters (A–D) at baseline ( $n = 6$ ) and follow-up ( $n = 6$ ). Individual values are represented by the dots at baseline and follow-up MRI. The connecting lines show the tendency of change in functional parameters over time.  $p$ -Values were obtained using paired Student's  $t$ -test. LVEF = left ventricular ejection fraction, RVEF = right ventricular ejection fraction.

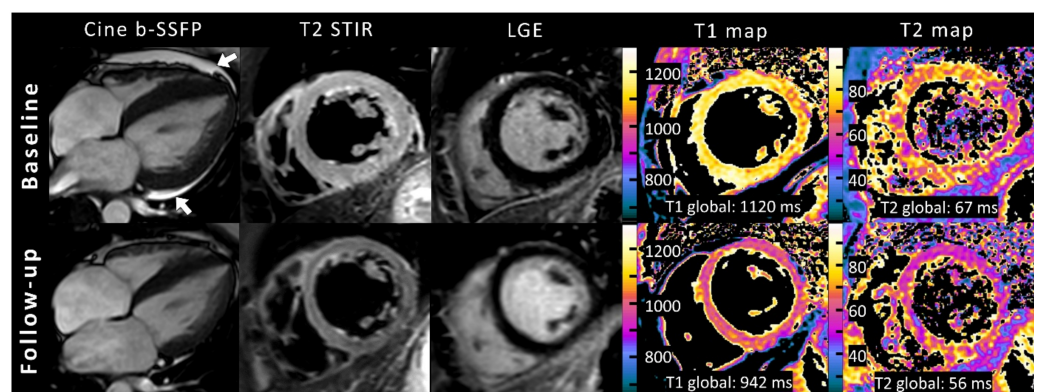


**Figure 3.** Representative example of cardiac magnetic resonance in a 32-year-old female with acute peripartum cardiomyopathy and recovery at follow-up after 2 months. Cine images (balanced steady-state free precession, b-SSFP) are oriented in horizontal long-axis view and at end systole and showed highly reduced left ventricular ejection fraction (35%) with global hypokinesia, left ventricular dilatation (left ventricular end-diastolic volume index:  $118 \text{ mL/m}^2$ ), and pericardial effusion (white arrows). Baseline fat-suppressed images (T2-weighted short TI inversion recovery, T2-STIR) at end diastole revealed extensive diffuse myocardial edema, which normalized at follow-up. No focal enhancement was identified on initial or follow-up late gadolinium enhancement (LGE) imaging. Quantitative mapping showed high global myocardial native T1 and T2 relaxation times at baseline MRI and normalization at follow-up.



**Table 2.** Cardiac magnetic resonance imaging characteristics of patients with acute peripartum cardiomyopathy at baseline and follow-up.

Variable	Baseline (n = 6)	Follow-Up (n = 6)	p-Value
Left ventricular ejection fraction (%)	38 ± 9	55 ± 17	<b>0.011</b>
Left ventricular end-diastolic volume index (mL/m <sup>2</sup> )	89 ± 28	85 ± 27	0.651
Right ventricular ejection fraction (%)	40 ± 18	55 ± 11	<b>0.023</b>
Right ventricular end-diastolic volume index (mL/m <sup>2</sup> )	66 ± 13	71 ± 15	0.370
Left atrium volume index (mL/m <sup>2</sup> )	56 ± 18	42 ± 10	0.051
Left ventricular mass index (g/m <sup>2</sup> )	61 ± 14	52 ± 8	0.176
Interventricular septal thickness (mm)	10 ± 2.8	9.1 ± 2.0	<b>0.047</b>
T2 signal intensity ratio	2.1 ± 0.3	1.7 ± 0.3	0.126
Visual myocardial edema	3 (50%)	0 (0%)	0.25
Visual late gadolinium enhancement	1 (20%)	0 (0%)	0.99
Late gadolinium enhancement (%)	4.5 ± 3.3	5.0 ± 2.6	0.363
Global longitudinal strain (%)	−13.5 ± 4.8	−19.8 ± 5.8	<b>0.039</b>
Global circumferential strain (%)	−15.6 ± 8.1	−18.7 ± 9.5	<b>0.009</b>
Global radial strain (%)	30.1 ± 21.9	30.5 ± 17.6	0.935

Continuous variables are given as mean ± standard deviation. Dichotomous variables are given as absolute frequency with percentages in parentheses. *p*-Values were obtained using paired Student's *t*-test or McNemar's test. Values in bold denote statistical significance.

### 3.4. Association between Imaging Parameters and LVEF Recovery

LVEF recovery was defined by an LVEF of  $\geq 50\%$  on TTE follow-up. The mean TTE follow-up time was 563 days (median: 320 days). A total of 13/17 patients (76%) recovered by the end of follow-up (mean time to recovery: 45 days; maximum time to recovery: 40 months). No patient deceased during follow-up time (all-cause mortality: 0%). Univariable Cox regression analysis showed an association between LVEF recovery and visual myocardial edema (HR = 10.17 (95% CI: 1.17, 88.65),  $p = 0.036$ ), initial LVEF (HR = 1.13 (95% CI: 1.02, 1.25),  $p = 0.023$ ), GLS (HR = 0.53 (95% CI: 0.34, 0.84),  $p = 0.007$ ), GCS (HR = 0.81 (95% CI: 0.70, 0.95),  $p = 0.010$ ), and GRS (HR = 1.10 (95% CI: 1.02, 1.18),  $p = 0.010$ ). On multivariable Cox regression analysis, only GLS (HR = 0.51 (95% CI: 0.30, 0.85),  $p = 0.010$ ) remained as an independent predictive variable for LVEF recovery (Table 3). According to Kaplan–Meier analysis, significantly prolonged LVEF recovery time was observed in patients without visual myocardial edema at initial presentation (840 ± 235 days vs. 145 ± 69 days, log rank  $p = 0.014$ ), in patients with initially highly reduced GLS (663 ± 192 days vs. 51 ± 33 days, log rank  $p < 0.001$ ), and in patients with initially highly reduced GCS (647 ± 197 days vs. 73 ± 35 days, log rank  $p = 0.010$ ) (Figure 4), but not in patients with highly reduced LVEF at initial presentation (230 ± 181 days vs. 549 ± 166 days, log rank  $p = 0.125$ ), in patients with bromocriptine added to standard heart failure therapy (315 ± 149 days vs. 432 ± 272 days, log rank  $p = 0.487$ ), or in patients with concomitant preeclampsia (388 ± 270 days vs. 422 ± 178 days, log rank  $p = 0.874$ ).

**Table 3.** Influence of cardiac magnetic resonance imaging data for the prediction of left ventricular ejection fraction recovery in patients with acute peripartum cardiomyopathy.

Variable	Univariable Analysis		Multivariable Analysis	
	Hazard Ratio	p-Value	Hazard Ratio	p-Value
Age (per year)	0.89 (0.77–1.03)	0.116		
Body mass index (per kg/m <sup>2</sup> )	0.99 (0.90–1.09)	0.841		
LVEF (per %)	1.13 (1.02–1.25)	<b>0.023</b>		
LVEDVI (per mL/m <sup>2</sup> )	0.99 (0.96–1.01)	0.228		
LVMI (per g/m <sup>2</sup> )	1.01 (0.96–1.05)	0.790		
LAI (per mL/m <sup>2</sup> )	0.99 (0.96–1.02)	0.585		
RVEF (per %)	1.07 (1.00–1.14)	<b>0.036</b>		
RVEDVI (per mL/m <sup>2</sup> )	1.01 (0.98–1.04)	0.422		
LV GLS (per %)	0.53 (0.34–0.84)	<b>0.007</b>	0.51 (0.30–0.85)	<b>0.010</b>
LV GCS (per %)	0.81 (0.70–0.95)	<b>0.010</b>		
LV GRS (per %)	1.10 (1.02–1.18)	<b>0.010</b>		
LGE (per %)	1.05 (0.92–1.21)	0.475		
T2 signal intensity ratio	1.77 (0.25–12.30)	0.565		
Visual myocardial edema (yes/no)	10.17 (1.17–88.65)	<b>0.036</b>		

Cox regression analysis was used. Data in parentheses are 95% confidence intervals. LVEF = left ventricular ejection fraction, LVEDVI = left ventricular end-diastolic volume index, LVMI = left ventricular mass index, LAI = left atrium index, RVEF = right ventricular ejection fraction, RVEDVI = right ventricular end-diastolic volume index, GLS = global longitudinal strain, GCS = global circumferential strain, GRS = global radial strain, LGE = late gadolinium enhancement. Values in bold denote statistical significance.

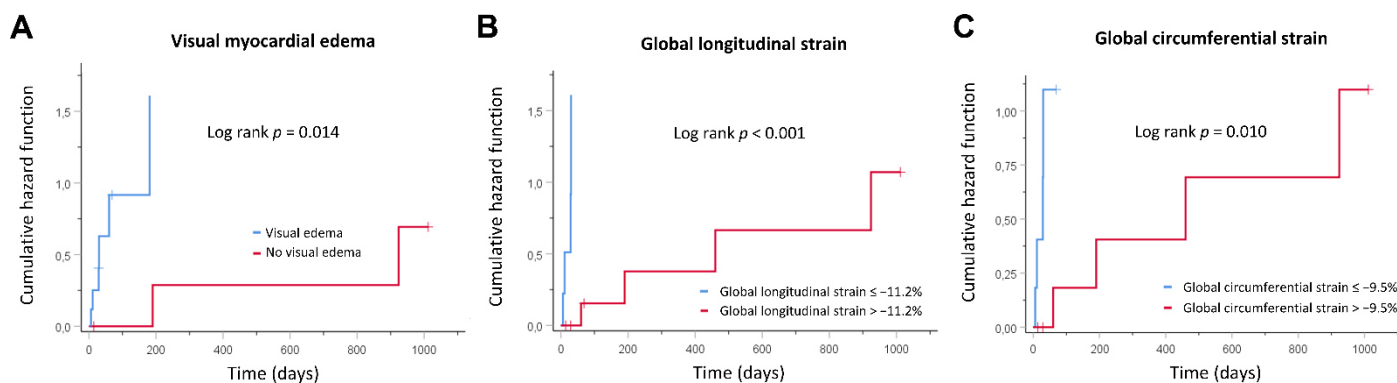


**Figure 4.** Kaplan–Meier curves showing cumulative hazard functions for left ventricular function recovery over time. Curves are given for (A) visual myocardial edema, (B) global longitudinal strain, and (C) global circumferential strain at initial presentation.

**4. Discussion**

This case-control CMR study revealed biventricular systolic dysfunction and signs of diffuse myocardial edema in the acute stage of PPCM. Prolonged myocardial T1 and T2 relaxation times in the predominant absence of LGE lesions indicate a mainly diffuse pattern of myocardial edema and emphasize the diagnostic benefit of quantitative myocardial parameters in patients with PPCM. Furthermore, the absence of myocardial edema was associated with delayed LVEF recovery. At long-term follow-up, 76% of the patients showed LVEF recovery (median time to LVEF recovery: 45 days). However, some patients showed prolonged recovery times (up to 40 months). RVEF reduction and RV dilatation were present in our PPCM cohort, indicating the presence of right ventricular involvement in the acute stage of PPCM. Furthermore, LV strain parameters, especially GLS and GCS, were markedly reduced and associated with LVEF recovery in our cohort. Impaired baseline GLS ( $\geq -11.2\%$ ) and GCS ( $\geq -9.5\%$ ) were associated with delayed recovery times, while no significant difference was observed for impaired baseline LVEF ( $\leq 27\%$ ). Multivariable analysis revealed GLS as an independent prognostic factor for LVEF recovery.

Recovery times in the present literature vary depending on the patient cohort and the definition of recovery. High recovery rates were described by Ersbøll et al. (85% recovered to an LVEF of  $\geq 55\%$  at 12 months after diagnosis) and McNamara et al. (72% recovered to an LVEF of  $\geq 50\%$  at 12 months), and relatively low recovery rates were observed by Mahowald et al. (37% recovered to an LVEF of  $\geq 55\%$  by 12 months) [12,22,23]. Various prognostic factors for long-term recovery of PPCM have been investigated in the past years. Severe LV dysfunction at initial presentation was associated with prolonged recovery times of LVEF in different studies [7,22]. However, the prognostic value of baseline LVEF alone is insufficient for differentiation between early and delayed recovery times and for indication of advanced therapies [5]. Our findings are in line with several speckle tracking echocardiography studies [13,14] and indicate a comprehensive evaluation of LV systolic dysfunction including strain parameters in addition to the assessment of LVEF only in patients with suggested PPCM. According to Haghikia et al. [24], RV dysfunction was present in our cohort of acute PPCM. Our findings support the need for a careful assessment of biventricular function and dimension at the initial presentation of patients with suspected PPCM. Since evaluation of RV parameters by echocardiography may be inaccurate, further evaluation by CMR should be considered for a comprehensive and precise assessment of right ventricular parameters in patients with suggested PPCM. The presence and role of preeclampsia in PPCM is variously described in previous studies, and there is evidence that hypertensive crisis in the presence of preeclampsia can promote LV dysfunction [12,25]. Preeclampsia was present in about a fourth of the patients in our cohort; however, no prognostic impact on LVEF recovery was found in our study.

The etiology of PPCM is still not fully understood and is suggested to be multifactorial. However, noninfectious inflammatory pathways and oxidative stress could play an important role [26]. Renz et al. described an increased T2 ratio in a small case series of acute PPCM, and Liang et al. showed increased T2 mapping values [27,28]. Other CMR studies did not detect a presence of focal or diffuse myocardial edema in PPCM patients [11]; however, imaging was partly performed beyond the acute stage of disease. In the present cohort of patients with acute PPCM, an elevation of T2 signal intensity ratio and T1 and T2 relaxation times were seen, which indicates the presence of diffuse myocardial edema. Furthermore, higher values of the interventricular septum thickness and LV mass index, which decreased on follow-up, may also be a result of myocardial edema/inflammation due to myocyte swelling and fluid accumulation [29]. However, this effect may also be contributed by physiological changes during pregnancy, which may not be completely reversed directly after birth [30]. Our findings of higher myocardial T1 and T2 relaxation times, which decreased on follow-up, are in line with the findings of Liang et al. [28] and indicate acute myocardial injury and myocardial edema, which seem to play an important role in the acute phase of PPCM [31]. Interestingly, prolonged LVEF recovery times were observed in patients without visual myocardial edema, indicating that the presence of visual myocardial edema may be a sign of a potentially reversible myocardial injury. These findings are in line with a study of inflammatory cardiomyopathies [32]. In contrast to the study of Liang et al., ECV values in our study were not significantly different from those in the healthy control group. ECV reflects the volume of cell-free heart tissue. This includes the intracapillary plasma volume (which is increased in inflammatory changes), but also the space, which is occupied by the extracellular matrix, being therefore also a surrogate for myocardial fibrosis [33]. The absence of higher ECV values in conjunction with prolonged T1 and T2 relaxation times in our study could be explained by the mainly acute stage of disease in our cohort, indicating the presence of acute myocardial injury and edema without irreversible myocardial fibrosis. LGE is a well-established marker for the assessment of myocardial fibrosis. Although some studies did report higher rates of LGE in PPCM [24], our observations of a low prevalence of focal LGE lesions in acute PPCM (prevalence of 12% with a mainly patchy LGE pattern) are in line with recent multicenter studies [11,12].

Our study has several limitations. Because of the retrospective design, clinical data assessment was limited. The single-center cohort is small due to the extremely low incidence of PPCM. Thus, the generalizability of regression models is limited, and this study should be considered to be hypothesis generating. There was no histopathological reference standard available; however, clinical use of endomyocardial biopsy has generally become very rare due to “sampling error” and periprocedural risks, and performance is especially avoided during pregnancy or the peripartum period. Due to ethical reasons, the control group consists of nonpregnant women. However, a previous study of myocardial mapping and strain analysis in healthy women during pregnancy showed LV remodeling with mild to moderate LV hypertrophy, but no evidence of functional impairment, dilatation, edema, or fibrosis of the ventricles [30].

**Supplementary Materials:** The following supporting information (Technical parameters, Appendix S1 and Table S1) can be downloaded at: <https://www.mdpi.com/article/10.3390/diagnostics12020378/s1>.

**Author Contributions:** Conceptualization, A.I., T.H.A., A.F., C.E., A.M.S., C.C.P., D.K., D.D., S.Z., U.M.B. and J.A.L.; Data curation, A.I.; Formal analysis, A.I. and J.A.L.; Funding acquisition, A.I.; Investigation, A.I., T.H.A. and W.M.M.; Methodology, A.I., T.H.A., A.F., C.E., S.Z. and J.A.L.; Project administration, A.I., W.M.M., U.A. and J.A.L.; Resources, A.I., U.A. and J.A.L.; Software, A.I. and J.A.L.; Supervision, W.M.M., D.K., D.D., U.A., S.Z., U.M.B. and J.A.L.; Validation, U.A. and J.A.L.; Visualization, A.I. and A.M.S.; Writing—original draft, A.I.; Writing—review & editing, T.H.A., W.M.M., A.F., C.E., A.M.S., C.C.P., D.K., D.D., U.A., S.Z., U.M.B. and J.A.L. All authors have read and agreed to the published version of the manuscript.

**Funding:** A.I. was funded by BONFOR-Forschungskommission der Medizinischen Fakultät Bonn and by the Deutsche Forschungsgemeinschaft (DFG, German Research Foundation) under Germany’s Excellence Strategy—EXC215-1390873048.

**Institutional Review Board Statement:** Not applicable.

**Informed Consent Statement:** Not applicable.

**Data Availability Statement:** The data presented in this study are available on request from the corresponding author. The data are not publicly available due to privacy and ethical restrictions.

**Conflicts of Interest:** U.A. disclosed speaker fees received from Siemens Healthineers in 2018. J.A.L. disclosed speaker fees from Bayer HealthCare and Philips Healthcare.

## References

1. Bauersachs, J.; König, T.; van der Meer, P.; Petrie, M.C.; Hilfiker-Kleiner, D.; Mbakwem, A.; Hamdan, R.; Jackson, A.M.; Forsyth, P.; de Boer, R.A.; et al. Pathophysiology, diagnosis and management of peripartum cardiomyopathy: A position statement from the Heart Failure Association of the European Society of Cardiology Study Group on peripartum cardiomyopathy. *Eur. J. Heart Fail.* **2019**, *21*, 827–843. [[CrossRef](#)] [[PubMed](#)]
2. Arany, Z.; Elkayam, U. Peripartum Cardiomyopathy. *Circulation* **2016**, *133*, 1397–1409. [[CrossRef](#)] [[PubMed](#)]
3. Isogai, T.; Kamiya, C.A. Worldwide Incidence of Peripartum Cardiomyopathy and Overall Maternal Mortality. *Int. Heart J.* **2019**, *60*, 503–511. [[CrossRef](#)] [[PubMed](#)]
4. Hilfiker-Kleiner, D.; Sliwa, K. Pathophysiology and epidemiology of peripartum cardiomyopathy. *Nat. Rev. Cardiol.* **2014**, *11*, 364–370. [[CrossRef](#)] [[PubMed](#)]
5. Davis, M.B.; Arany, Z.; McNamara, D.M.; Golland, S.; Elkayam, U. Peripartum Cardiomyopathy: JACC State-of-the-Art Review. *J. Am. Coll. Cardiol.* **2020**, *75*, 207–221. [[CrossRef](#)]
6. Biteker, M.; Ilhan, E.; Biteker, G.; Duman, D.; Bozkurt, B. Delayed recovery in peripartum cardiomyopathy: An indication for long-term follow-up and sustained therapy. *Eur. J. Heart Fail.* **2012**, *14*, 895–901. [[CrossRef](#)]
7. Golland, S.; Bitar, F.; Modi, K.; Safirstein, J.; Ro, A.; Mirocha, J.; Khatri, N.; Elkayam, U. Evaluation of the clinical relevance of baseline left ventricular ejection fraction as a predictor of recovery or persistence of severe dysfunction in women in the United States with peripartum cardiomyopathy. *J. Card. Fail.* **2011**, *17*, 426–430. [[CrossRef](#)]
8. Luetkens, J.A.; Faron, A.; Isaak, A.; Dabir, D.; Kuetting, D.; Feisst, A.; Schmeel, F.C.; Sprinkart, A.M.; Thomas, D. Comparison of Original and 2018 Lake Louise Criteria for Diagnosis of Acute Myocarditis: Results of a Validation Cohort. *Radiol. Cardiothorac. Imaging* **2019**, *1*, e190010. [[CrossRef](#)]

9. Luetkens, J.A.; Homs, R.; Sprinkart, A.M.; Doerner, J.; Dabir, D.; Kuetting, D.L.; Block, W.; Andrié, R.; Stehning, C.; Fimmers, R.; et al. Incremental value of quantitative CMR including parametric mapping for the diagnosis of acute myocarditis. *Eur. Heart J. Cardiovasc. Imaging* **2016**, *17*, 154–161. [[CrossRef](#)]
10. Luetkens, J.A.; Schlesinger-Irsch, U.; Kuetting, D.L.; Dabir, D.; Homs, R.; Doerner, J.; Schmeel, F.C.; Fimmers, R.; Sprinkart, A.M.; Naehle, C.P.; et al. Feature-tracking myocardial strain analysis in acute myocarditis: Diagnostic value and association with myocardial oedema. *Eur. Radiol.* **2017**, *27*, 4661–4671. [[CrossRef](#)]
11. Schelbert, E.B.; Elkayam, U.; Cooper, L.T.; Givertz, M.M.; Alexis, J.D.; Briller, J.; Felker, G.M.; Chaparro, S.; Kealey, A.; Pisarcik, J.; et al. Myocardial Damage Detected by Late Gadolinium Enhancement Cardiac Magnetic Resonance Is Uncommon in Peripartum Cardiomyopathy. *J. Am. Heart Assoc.* **2017**, *6*, e005472. [[CrossRef](#)] [[PubMed](#)]
12. Ersbøll, A.S.; Bojer, A.S.; Hauge, M.G.; Johansen, M.; Damm, P.; Gustafsson, F.; Vejstrup, N.G. Long-Term Cardiac Function After Peripartum Cardiomyopathy and Preeclampsia: A Danish Nationwide, Clinical Follow-Up Study Using Maximal Exercise Testing and Cardiac Magnetic Resonance Imaging. *J. Am. Heart Assoc.* **2018**, *7*, e008991. [[CrossRef](#)]
13. Briasoulis, A.; Mocanu, M.; Marinescu, K.; Qaqi, O.; Palla, M.; Telila, T.; Afonso, L. Longitudinal systolic strain profiles and outcomes in peripartum cardiomyopathy. *Echocardiography* **2016**, *33*, 1354–1360. [[CrossRef](#)]
14. Sugahara, M.; Kagiya, N.; Hasselberg, N.E.; Blauwet, L.A.; Briller, J.; Cooper, L.; Fett, J.D.; Hsich, E.; Wells, G.; McNamara, D.; et al. Global Left Ventricular Strain at Presentation Is Associated with Subsequent Recovery in Patients with Peripartum Cardiomyopathy. *J. Am. Soc. Echocardiogr.* **2019**, *32*, 1565–1573. [[CrossRef](#)] [[PubMed](#)]
15. Cannan, C.; Weeks, S.; Friedrich, M. CMR features of peri-partum cardiomyopathy. *J. Cardiovasc. Magn. Reson.* **2010**, *12*, P185. [[CrossRef](#)]
16. Arora, N.P.; Mohamad, T.; Mahajan, N.; Danrad, R.; Kottam, A.; Li, T.; Afonso, L.C. Cardiac magnetic resonance imaging in peripartum cardiomyopathy. *Am. J. Med. Sci.* **2014**, *347*, 112–117. [[CrossRef](#)]
17. Sprinkart, A.M.; Luetkens, J.A.; Träber, F.; Doerner, J.; Gieseke, J.; Schnackenburg, B.; Schmitz, G.; Thomas, D.; Homs, R.; Block, W.; et al. Gradient Spin Echo (GraSE) imaging for fast myocardial T2 mapping. *J. Cardiovasc. Magn. Reson.* **2015**, *17*, 12. [[CrossRef](#)]
18. Messroghli, D.R.; Radjenovic, A.; Kozerke, S.; Higgins, D.M.; Sivananthan, M.U.; Ridgway, J.P. Modified Look-Locker inversion recovery (MOLLI) for high-resolution T1 mapping of the heart. *Magn. Reson. Med.* **2004**, *52*, 141–146. [[CrossRef](#)]
19. Schulz-Menger, J.; Bluemke, D.A.; Bremerich, J.; Flamm, S.D.; Fogel, M.A.; Friedrich, M.G.; Kim, R.J.; von Knobelsdorff-Brenkenhoff, F.; Kramer, C.M.; Pennell, D.J.; et al. Standardized image interpretation and post-processing in cardiovascular magnetic resonance-2020 update: Society for Cardiovascular Magnetic Resonance (SCMR): Board of Trustees Task Force on Standardized Post-Processing. *J. Cardiovasc. Magn. Reson.* **2020**, *22*, 19. [[CrossRef](#)]
20. Luetkens, J.A.; Doerner, J.; Thomas, D.K.; Dabir, D.; Gieseke, J.; Sprinkart, A.M.; Fimmers, R.; Stehning, C.; Homs, R.; Schwab, J.O.; et al. Acute myocarditis: Multiparametric cardiac MR imaging. *Radiology* **2014**, *273*, 383–392. [[CrossRef](#)] [[PubMed](#)]
21. Rothman, K.J. No adjustments are needed for multiple comparisons. *Epidemiology* **1990**, *1*, 43–46. [[CrossRef](#)] [[PubMed](#)]
22. McNamara, D.M.; Elkayam, U.; Alharethi, R.; Damp, J.; Hsich, E.; Ewald, G.; Modi, K.; Alexis, J.D.; Ramani, G.V.; Semigran, M.J.; et al. Clinical Outcomes for Peripartum Cardiomyopathy in North America: Results of the IPAC Study (Investigations of Pregnancy-Associated Cardiomyopathy). *J. Am. Coll. Cardiol.* **2015**, *66*, 905–914. [[CrossRef](#)] [[PubMed](#)]
23. Mahowald, M.K.; Basu, N.; Subramaniam, L.; Scott, R.; Davis, M.B. Long-term Outcomes in Peripartum Cardiomyopathy. *Open Cardiovasc. Med. J.* **2019**, *13*, 13–23. [[CrossRef](#)]
24. Haghikia, A.; Röntgen, P.; Vogel-Claussen, J.; Schwab, J.; Westenfeld, R.; Ehlermann, P.; Berliner, D.; Podewski, E.; Hilfiker-Kleiner, D.; Bauersachs, J. Prognostic implication of right ventricular involvement in peripartum cardiomyopathy: A cardiovascular magnetic resonance study. *ESC Heart Fail.* **2015**, *2*, 139–149. [[CrossRef](#)] [[PubMed](#)]
25. Lindley, K.J.; Conner, S.N.; Cahill, A.G.; Novak, E.; Mann, D.L. Impact of Preeclampsia on Clinical and Functional Outcomes in Women with Peripartum Cardiomyopathy. *Circ. Heart Fail.* **2017**, *10*, e003797. [[CrossRef](#)]
26. Ricke-Hoch, M.; Pfeffer, T.J.; Hilfiker-Kleiner, D. Peripartum cardiomyopathy: Basic mechanisms and hope for new therapies. *Cardiovasc. Res.* **2020**, *116*, 520–531. [[CrossRef](#)] [[PubMed](#)]
27. Renz, D.M.; Röttgen, R.; Habedank, D.; Wagner, M.; Böttcher, J.; Pfeil, A.; Dietz, R.; Hamm, B.; de Kivelitz, E.; Elgeti, T. Kardiale Bildgebung bei peripartaler Kardiomyopathie: Evaluation eines umfassenden MR-Untersuchungsprotokolls. *RöFo* **2011**, *183*, VO316\_4. [[CrossRef](#)]
28. Liang, Y.-D.; Xu, Y.-W.; Li, W.-H.; Wan, K.; Sun, J.-Y.; Lin, J.-Y.; Zhang, Q.; Zhou, X.-Y.; Chen, Y.-C. Left ventricular function recovery in peripartum cardiomyopathy: A cardiovascular magnetic resonance study by myocardial T1 and T2 mapping. *J. Cardiovasc. Magn. Reson.* **2020**, *22*, 2. [[CrossRef](#)]
29. Zagrosek, A.; Wassmuth, R.; Abdel-Aty, H.; Rudolph, A.; Dietz, R.; Schulz-Menger, J. Relation between myocardial edema and myocardial mass during the acute and convalescent phase of myocarditis—A CMR study. *J. Cardiovasc. Magn. Reson.* **2008**, *10*, 19. [[CrossRef](#)]
30. Nii, M.; Ishida, M.; Dohi, K.; Tanaka, H.; Kondo, E.; Ito, M.; Sakuma, H.; Ikeda, T. Myocardial tissue characterization and strain analysis in healthy pregnant women using cardiovascular magnetic resonance native T1 mapping and feature tracking technique. *J. Cardiovasc. Magn. Reson.* **2018**, *20*, 52. [[CrossRef](#)]



31. Azibani, F.; Pfeffer, T.J.; Ricke-Hoch, M.; Dowling, W.; Pietzsch, S.; Briton, O.; Baard, J.; Abou Moulig, V.; König, T.; Berliner, D.; et al. Outcome in German and South African peripartum cardiomyopathy cohorts associates with medical therapy and fibrosis markers. *ESC Heart Fail.* **2020**, *7*, 512–522. [[CrossRef](#)] [[PubMed](#)]
32. Vermes, E.; Childs, H.; Faris, P.; Friedrich, M.G. Predictive value of CMR criteria for LV functional improvement in patients with acute myocarditis. *Eur. Heart J. Cardiovasc. Imaging* **2014**, *15*, 1140–1144. [[CrossRef](#)] [[PubMed](#)]
33. Moon, J.C.; Messroghli, D.R.; Kellman, P.; Piechnik, S.K.; Robson, M.D.; Ugander, M.; Gatehouse, P.D.; Arai, A.E.; Friedrich, M.G.; Neubauer, S.; et al. Myocardial T1 mapping and extracellular volume quantification: A Society for Cardiovascular Magnetic Resonance (SCMR) and CMR Working Group of the European Society of Cardiology consensus statement. *J. Cardiovasc. Magn. Reson.* **2013**, *15*, 92. [[CrossRef](#)] [[PubMed](#)]

### 3.3 Quantitative kardiale MRT bei Immun-Checkpoint-Inhibitor-induzierter Myokarditis

“Cardiac MRI Depicts Immune Checkpoint Inhibitor-induced Myocarditis: A Prospective Study”

Faron A\*, Isaak A\*, Mesropyan N, Reinert M, Schwab K, Sirokay J, Sprinkart AM, Bauernfeind FG, Dabir D, Pieper CC, Heine A, Kuetting D, Attenberger U, Landsberg J, Luetkens JA.

Erschienen in *Radiology*. 2021 Dec;301(3):602-609. \*geteilte Erstautorenschaft

**Zielsetzung und Methoden** – Immun-Checkpoint-Inhibitoren (ICI) zur Krebstherapie sind mit einem Spektrum immunbedingter Nebenwirkungen verbunden. Das Ausmaß subklinischer kardialer Veränderungen im Zusammenhang mit der ICI-Therapie ist jedoch unzureichend untersucht. Ziel dieser prospektiven intraindividuellen kardialen MRT-Studie war es eine potenzielle Myokardschädigung im Zusammenhang mit der ICI-Therapie zu untersuchen. Von November 2019 bis April 2021 wurde bei onkologischen Studienteilnehmer/-innen ohne bekannte Herzerkrankung unmittelbar vor sowie 3 Monate nach Beginn der ICI-Therapie eine quantitative kardiale MRT durchgeführt.

**Ergebnisse** – Insgesamt 22 Studienteilnehmer/-innen ( $65 \pm 14$  Jahre; 13 Männer), die eine ICI-Therapie erhielten (im Median vier Infusionen), wurden prospektiv eingeschlossen. Studienteilnehmer/-innen zeigten bei der Nachuntersuchung signifikante Erhöhungen der myokardialen T1- und T2-Relaxationszeiten sowie der T2-SI-Ratio (siehe *Figure 2* und *Figure 3* (Faron, Isaak et al., 2021)), die mit der Entwicklung eines diffusen Myokardödems vereinbar sind. Der linksventrikuläre longitudinale Strain zeigte sich als Zeichen einer zunehmenden systolischen Dysfunktion signifikant verringert (siehe *Figure 2* (Faron, Isaak et al., 2021)). 22 Studienteilnehmer/-innen (9 %) wiesen neue LGE-Läsionen in nicht-ischämischer Lokalisation auf. Geringe Perikardergüsse wurden bei der Nachuntersuchung häufiger beobachtet (5 % vs. 45 %). Eine Studienteilnehmerin (5 %) zeigte bei der MRT-Folgeuntersuchung das Bild einer akuten Myokarditis, wurde daraufhin stationär aufgenommen und entwickelte im stationären Verlauf eine fulminante, immunvermittelte Multiorganreaktion mit letalem Ausgang. *Figure 4* (Faron, Isaak et al., 2021) zeigt eine Zusammenfassung der MRT-Ergebnisse und die angenommene, vereinfachte Theorie zur ICI-vermittelten Herzmuskelschädigung.

**Schlussfolgerungen** – Studienteilnehmer/-innen unter Immun-Checkpoint-Inhibitor-Therapie zeigten in der kardialen MRT-Nachuntersuchung Zeichen einer systolischen Dysfunktion und eines diffusen Myokardödems hinweisend für eine subklinische myokardiale Inflammation. Die quantitative kardiale MRT kann inflammatorische Myokardveränderungen der ICI-Therapie frühzeitig detektieren.

# Cardiac MRI Depicts Immune Checkpoint Inhibitor–induced Myocarditis: A Prospective Study



Anton Faron, MD\* • Alexander Isaak, MD\* • Narine Mesropyan, MD • Matthäus Reinert, MD • Katjana Schwab, MD • Judith Sirokay, MD • Alois M. Sprinkart, MD • Franz-Georg Bauernfeind, MD • Darius Dabir, MD • Claus C. Pieper, MD • Annkristin Heine, MD • Daniel Kuetting, MD • Ulrike Attenberger, MD • Jennifer Landsberg, MD • Julian A. Luetkens, MD

From the Department of Diagnostic and Interventional Radiology (A.F., A.I., N.M., M.R., A.M.S., D.D., C.C.P., D.K., U.A., J.A.L.), Quantitative Imaging Laboratory Bonn (QILaB) (A.F., A.I., N.M., A.M.S., D.K., J.A.L.), Department of Oncology, Hematology, and Rheumatology (K.S., F.G.B., A.H.), and Department of Dermatology and Allergy (J.S., J.L.), University Hospital Bonn, Venusberg-Campus 1, 53127 Bonn, Germany. Received March 30, 2021; revision requested May 20; revision received July 12; accepted July 28. **Address correspondence to** J.A.L. (e-mail: [julian.luetkens@ukbonn.de](mailto:julian.luetkens@ukbonn.de)).

A.F. and A.I. supported by grants from the BONFOR research program (grants 2020-2A-04 [A.F.] and 2021-1A-05 [A.I.]).

\* A.F. and A.I. contributed equally to this work.

Conflicts of interest are listed at the end of this article.

Radiology 2021; 000:1–8 • <https://doi.org/10.1148/radiol.2021210814> • Content codes:  

**Background:** Immune checkpoint inhibitors (ICIs) for cancer treatment are associated with a spectrum of immune-related adverse events, including ICI-induced myocarditis; however, the extent of subclinical acute cardiac effects related to ICI treatment is unclear.

**Purpose:** To explore the extent of cardiac injury and inflammation related to ICI therapy that can be detected with use of cardiac MRI.

**Materials and Methods:** In this prospective study from November 2019 to April 2021, oncologic participants, without known underlying structural heart disease or cardiac symptoms, underwent multiparametric cardiac MRI before planned ICI therapy (baseline) and 3 months after starting ICI therapy (follow-up). The cardiac MRI protocol incorporated assessment of cardiac function, including systolic myocardial strain, myocardial edema, late gadolinium enhancement (LGE), T1 and T2 relaxation times, and extracellular volume fraction. The paired *t* test, Wilcoxon signed-rank test, and McNemar test were used for intraindividual comparisons.

**Results:** Twenty-two participants (mean age  $\pm$  standard deviation, 65 years  $\pm$  14; 13 men) were evaluated, receiving a median of four infusions of ICI therapy (interquartile range, four to six infusions). Compared with baseline MRI, participants displayed increased markers of diffuse myocardial edema at follow-up (T1 relaxation time, 972 msec  $\pm$  26 vs 1006 msec  $\pm$  36 [ $P < .001$ ]; T2 relaxation time, 54 msec  $\pm$  3 vs 58 msec  $\pm$  4 [ $P < .001$ ]; T2 signal intensity ratio, 1.5  $\pm$  0.3 vs 1.7  $\pm$  0.3 [ $P = .03$ ]). Left ventricular average systolic longitudinal strain had decreased at follow-up MRI ( $-23.4\% \pm 4.8$  vs  $-19.6\% \pm 5.1$ , respectively;  $P = .005$ ). New nonischemic LGE lesions were prevalent in two of 22 participants (9%). Compared with baseline, small pericardial effusions were more evident at follow-up (one of 22 participants [5%] vs 10 of 22 [45%];  $P = .004$ ).

**Conclusion:** In participants who received immune checkpoint inhibitor therapy for cancer treatment, follow-up cardiac MRI scans showed signs of systolic dysfunction and increased parameters of myocardial edema and inflammation.

©RSNA, 2021

Online supplemental material is available for this article.

Immune checkpoint inhibitor (ICI) therapy improves treatment and survival in various cancers (1). In ICI therapy, the administration of inhibitory monoclonal antibodies targets negative regulatory pathways within the host immune system that leads to T-cell activation and promotion of immune-mediated tumor cell elimination (2). To date, seven ICIs have been approved by the U.S. Food and Drug Administration, targeting either the cytotoxic T-lymphocyte antigen 4 (CTLA-4) (ipilimumab) or the programmed death 1 (PD-1) pathway (eg, nivolumab, pembrolizumab). Despite their advantages in cancer therapy, ICI-specific side effects (commonly termed immune-related adverse events) are a potentially severe drawback of this therapy, which may also affect the cardiovascular system (3–5). ICI-related myocarditis is considered a rare but potentially fatal event (6,7) that seems to most likely occur within the first 3 months after treatment initiation (8).

The exact pathogenic mechanism of ICI-related myocarditis is not fully understood. Distinct myocardial T-cell

infiltration is present at histopathologic analysis, possibly provoked by T-cell receptors targeting a shared, homologous, or dissimilar antigen between the myocardium and the tumor (3,6). Increasing reporting rates and awareness of ICI-related myocarditis (4,9) have led to expert groups demanding further evaluation of this side effect, including less severe or even subclinical courses of ICI-related myocarditis (10). For this purpose, cardiac MRI is the imaging modality of choice, particularly due to its inherent capabilities of advanced tissue characterization (10). Multiparametric cardiac MRI can be used to detect and quantify diffuse myocardial tissue alterations, such as myocardial edema and fibrosis (11,12). Furthermore, alterations in myocardial function can be detected with high sensitivity by using myocardial strain analysis (13).

In this prospective study, oncologic participants with planned ICI treatment underwent multiparametric cardiac MRI immediately prior to treatment initiation as well as 3 months after the start of treatment. The purpose of our



## Abbreviations

CTLA-4 = cytotoxic T-lymphocyte antigen 4, ICI = immune checkpoint inhibitor, LGE = late gadolinium enhancement, PD-1 = programmed death 1

## Summary

Immune checkpoint inhibitor therapy induced a high burden of sub-clinical cardiac disease, including myocardial inflammation and systolic dysfunction detected at cardiac MRI.

## Key Results

- In a prospective study of 22 participants with cancer evaluated before and 3 months after immune checkpoint inhibitor (ICI) therapy, mean myocardial T1 (972 msec vs 1006 msec;  $P < .001$ ) and T2 (54 msec vs 58 msec;  $P < .001$ ) relaxation times were increased and myocardial longitudinal strain ( $-23.4\%$  vs  $-19.6\%$ ;  $P = .005$ ) was reduced compared with baseline cardiac MRI.
- ICIs were associated with small pericardial effusions at 3-month follow-up versus baseline MRI examinations (10 of 22 participants [45%] vs one of 22 [5%];  $P = .004$ ).

explorative study was to investigate to what extent ICI treatment leads to acute cardiac effects in terms of inflammation, fibrosis, and systolic dysfunction that can be detected with cardiac MRI.

## Materials and Methods

This prospective study was approved by our institutional review board (application number 314/19), and all participants provided written informed consent before undergoing baseline cardiac MRI.

### Study Participants

Oncologic patients scheduled for ICI therapy were randomly enrolled during the recruitment period between November 2019 and April 2021. Participants were included irrespective of the planned treatment regimen (anti-CTLA-4, anti-PD-1, anti-programmed death ligand 1, or anti-CTLA-4 and anti-PD-1). Only participants without known underlying structural heart disease (eg, dilated cardiomyopathy, medical history of myocardial infarction) or cardiac symptoms were included. ICI therapy was the only cancer treatment administered during the study period. Exclusion criteria were refusal to participate in the study, contraindications to contrast-enhanced cardiac MRI, and preexisting cardiac disease. Each participant underwent two multiparametric cardiac MRI examinations. The first cardiac MRI examination (baseline) was performed directly before ICI treatment initiation. The second cardiac MRI examination (follow-up) was scheduled for 3 months after initiation of ICI treatment. Only participants who completed the entire study protocol were included in the final analysis. Blood samples were drawn before every cardiac MRI scan.

### Cardiac MRI Protocol

Each participant underwent two cardiac MRI examinations (baseline and follow-up) on the same clinical whole-body MRI system (Ingenia 1.5 T, Philips Healthcare). For signal reception, a 32-channel torso coil with digital interface was used. A signal intensity correction algorithm (constant level appear-

ance, Philips Medical Systems) was used to correct for torso coil–related signal inhomogeneities. Electrocardiogram-gated steady-state free precession cine images were obtained in short-axis, two-chamber, and four-chamber views for functional analysis. For visualization of myocardial edema and calculation of T2 signal intensity ratio, T2-weighted short tau inversion-recovery sequences in short-axis (covering the whole left ventricle) and transverse views were performed. Segmented inversion-recovery gradient-echo sequences were used for late gadolinium enhancement (LGE) imaging and were obtained in short-axis, two-chamber, and four-chamber views. The Look-Locker method was applied to determine the optimal inversion time for LGE image acquisition (14). Myocardial T1 and T2 mapping was performed in end-diastolic short-axis views with acquisition of apical, midventricular, and basal sections. For myocardial T1 mapping, a standard 3(3)3(3)5 modified Look-Locker inversion-recovery, or MOLLI, acquisition scheme was applied (15). Postcontrast T1 maps using the same acquisition scheme were obtained 10 minutes after contrast material administration. For myocardial T2 mapping, a six-echo gradient spin-echo sequence, or GraSE, was applied (16). Blood hematocrit levels were measured from blood samples to calculate extracellular volume fraction. For contrast enhancement, a bolus of 0.2 mmol per kilogram of body weight of gadoterate meglumine (Clariscan, GE Healthcare) was administered. The sequence parameters are provided in Table E1 (online).

### Image Analysis

Image analysis of baseline and follow-up scans was performed by two board-certified radiologists (J.A.L. and D.K., with 8 and 7 years of experience, respectively, in cardiac MRI) using dedicated software (IntelliSpace Portal, version 10.1; Philips Healthcare). Both readers were blinded to the clinical information, and imaging studies were presented in a random order. The presence of focal areas of regional high signal intensities in a nonischemic distribution pattern on T2 short tau inversion-recovery images and LGE images was visually assessed by consensus agreement of the two readers. Semiquantitative markers of myocardial edema (T2 signal intensity ratio) and myocardial injury and fibrosis (enhanced volume percentage on short-axis LGE images using full width at half maximum technique) were calculated as previously reported (11,17). Myocardial T1 and T2 relaxation maps were motion corrected using a software-implemented algorithm (fast elastic image registration, IntelliSpace Portal, version 10.1). Global T1 and T2 relaxation times and global extracellular volumes were calculated using a segmental approach as previously described (11,12,18). For feature-tracking strain measurements, cine images in short-axis and four-chamber orientation were used. Left ventricular average systolic longitudinal, circumferential, and radial strain were calculated using dedicated software (Image-Arena 4.6, TOMTEC Imaging Systems) (13,19). Because specific recommendations for the diagnosis of ICI-induced myocarditis are missing, MRI criteria developed for acute myocarditis (eg, viral myocarditis) were adapted for use in this study (12).

Inter- and intrareader reproducibility measurements are provided in Appendix E1, Table E2, and Figure E1 (online). An

interscan reproducibility analysis of T1 and T2 relaxation times is provided in Appendix E1 (online).

### Statistical Analysis

Prism (version 8.4.1, GraphPad Software) was used for statistical analysis. Data were checked for normal distribution using the Shapiro-Wilk test. Participant characteristics are given as means  $\pm$  standard deviations, absolute frequencies with percentages, or medians with interquartile ranges, as appropriate. For intraindividual comparison of continuous variables between baseline and follow-up MRI examinations, the paired *t* test or Wilcoxon signed-rank test was used, as appropriate. For intraindividual comparison of dichotomous data, the McNemar test was applied. For post hoc subgroup analyses, oncologic participants were grouped according to troponin T values, ICI-related side effects, and treatment regimen, and the unpaired *t* test or Mann-Whitney *U* test was used, as appropriate. *P* < .05 was considered indicative of statistically significant difference.

## Results

### Participant Characteristics

After exclusion of 22 patients, a total of 22 participants were included (mean age  $\pm$  standard deviation, 65 years  $\pm$  14; 13 men) (Fig 1). The mean time  $\pm$  standard deviation between baseline and follow-up MRI was 109 days  $\pm$  30, during which a median of four infusions of ICI therapy (interquartile range, four to six infusions) were administered. ICI combination therapy, consisting of an anti-CTLA-4 antibody (ipilimumab) and an anti-PD-1 antibody (nivolumab) was administered to four of the 22 study participants (18%), while the remainder received ICI monotherapy, consisting of either an anti-PD-1 antibody (nivolumab, pembrolizumab, or cemiplimab) (17 of 22 [77%]) or an anti-programmed death ligand 1 antibody (durvalumab) (one of 22 [5%]). In nine of 22 participants (41%), ICI antibodies were administered as an adjuvant therapy. Clinical characteristics of and distribution of ICI therapy among study participants are provided in Tables 1 and 2.

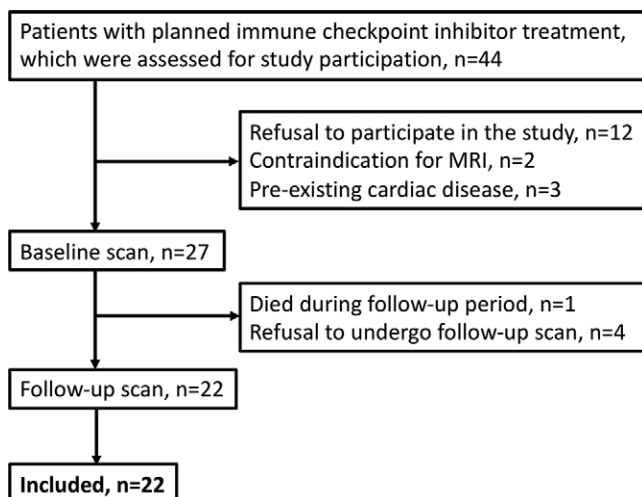


**Figure 1:** Study flow diagram.

### Cardiac MRI Results

We found a decrease in mean left ventricular ejection fraction ( $62\% \pm 7$  vs  $59\% \pm 7$ ; *P* = .048) between baseline and follow-up MRI examinations.

**Table 1: Clinical Characteristics of the Study Sample**

Variable	Value
No. of participants	22
Age (y)	65 $\pm$ 14
Sex*	
M	13 (59)
F	9 (41)
Weight (kg)	79 $\pm$ 17
Height (cm)	174 $\pm$ 9
Body surface area (m <sup>2</sup> )	1.9 $\pm$ 0.3
Body mass index (kg/m <sup>2</sup> )	26 $\pm$ 5
ECOG performance status*	
0	19 (86)
1	2 (9)
2	0 (0)
3	1 (5)
4	0 (0)
5	0 (0)
Cardiovascular risk factors*	
Arterial hypertension	9 (41)
Hyperlipidemia	2 (9)
Tobacco use	3 (14)
Diabetes mellitus	0 (0)
Chronic kidney disease	0 (0)
No cardiovascular risk factors	8 (36)

Note.—Unless otherwise specified, data are means  $\pm$  standard deviations. ECOG = Eastern Cooperative Oncology Group.

\* Data are numbers of participants, with percentages in parentheses.

**Table 2: Distribution of Immune Checkpoint Inhibitor Therapy according to Tumor Entity within the Study Sample**

Tumor Entity, Substance, and Molecular Target	No. of Participants ( <i>n</i> = 22)
<b>Melanoma</b>	
Pembrolizumab (PD-1)	8 (36)
Nivolumab (PD-1)	5 (23)
Nivolumab and ipilimumab (PD-1 and CTLA-4)	4 (18)
<b>Non-small cell lung cancer</b>	
Durvalumab (PD-L1)	1 (5)
<b>Head and neck squamous cell carcinoma</b>	
Cemiplimab (PD-1)	2 (9)
Pembrolizumab (PD-1)	1 (5)
Nivolumab (PD-1)	1 (5)

Note.—Data in parentheses are percentages. CTLA-4 = cytotoxic T-lymphocyte antigen 4, PD-1 = programmed death 1, PD-L1 = programmed death ligand 1.

**Table 3: Cardiac MRI Results at Baseline and Follow-up Examinations**

Variable	Baseline (n = 22)	Follow-up (n = 22)	P Value
Left ventricular ejection fraction (%)	62 ± 7	59 ± 7	.048*
Left ventricular end-diastolic volume index (mL/m <sup>2</sup> )	73 ± 14	71 ± 13	.32
Left ventricular mass index (g/m <sup>2</sup> )	47 ± 11	47 ± 15	.80
Visible myocardial edema <sup>†</sup>	0 (0)	2 (9)	.48
Visible myocardial LGE <sup>†</sup>	7 (32)	9 (41)	.48
Visible pericardial LGE <sup>†</sup>	0 (0)	1 (5)	>.99
Pericardial effusion <sup>†</sup>	1 (5)	10 (45)	.004*
Pleural effusion <sup>†</sup>	0 (0)	2 (9)	.48
T2 signal intensity ratio	1.5 ± 0.3	1.7 ± 0.3	.03*
LGE (%)	10.1 ± 5.5	12.0 ± 7.2	.21
Average systolic longitudinal strain (%)	−23.4 ± 4.8	−19.6 ± 5.1	.005*
Average systolic circumferential strain (%)	−23.8 ± 5.1	−23.2 ± 5.4	.56
Average systolic radial strain (%)	31.9 ± 8.0	29.3 ± 8.9	.13
T1 relaxation time, native (msec)	972 ± 26	1006 ± 36	<.001*
Extracellular volume fraction (%)	25.6 ± 4.5	26.0 ± 3.8	.86
T2 relaxation time (msec)	54 ± 3	58 ± 4	<.001*

Note.—Unless otherwise specified, data are means ± standard deviations. *P* values were obtained by using the paired *t* test, Wilcoxon signed-rank test, or McNemar test, as appropriate. LGE = late gadolinium enhancement.

\* Denotes statistically significant difference.

<sup>†</sup> Data are numbers of participants, with percentages in parentheses.

Mean T2 signal intensity ratio was higher at follow-up compared with baseline MRI (1.5 ± 0.3 vs 1.7 ± 0.3; *P* = .03), and in two participants (9%), visible diffuse myocardial edema was present at follow-up. In nine of 22 participants (41%), slight pericardial effusions were newly visible at follow-up MRI examination (Table 3).

Visible focal LGE lesions were present in seven of 22 participants (32%) at baseline MRI examination, with striatal (five of seven [71%]) or patchy (two of seven [29%]) LGE in the inferolateral midwall (four of seven [57%]) or subepicardium (three of seven [43%]). In two of 22 participants (9%), new focal nonischemic LGE lesions were detected at follow-up (patchy focal enhancement of the basal inferolateral subepicardium and a striatal focal enhancement of the midventricular lateral subepicardium with associated pericardial enhancement). We found no evidence of differences between baseline and follow-up MRI examinations in terms of mean quantitative LGE (10.1% ± 5.5 vs 12.0% ± 7.2; *P* = .21).

Mean myocardial T1 relaxation times (972 msec ± 26 at baseline vs 1006 msec ± 36 at follow-up; *P* < .001) and T2 relaxation times (54 msec ± 3 vs 58 msec ± 4; *P* < .001) were higher at follow-up compared with baseline MRI examination (Figs 2, 3).

Regarding myocardial strain analysis, lower average systolic longitudinal strain was observed at follow-up (−23.4% ± 4.8 vs −19.6% ± 5.1; *P* = .005). We found no evidence of differences between baseline and follow-up MRI examinations regarding average systolic circumferential (−23.8% ± 5.1 vs −23.2% ± 5.4; *P* = .56) and radial strain values (31.9% ± 8.0 vs 29.3% ± 8.9; *P* = .13).

We found no differences regarding T1 relaxation times (1005 msec ± 25 vs 1008 msec ± 38; *P* = .89), T2 relaxation

times (59 msec ± 5 vs 57 msec ± 4; *P* = .54), quantitative LGE (15.5% ± 5 vs 11.2% ± 8; *P* = .30), and left ventricular ejection fraction (57% ± 8 vs 59% ± 7; *P* = .64) between participants who received ICI combination therapy and those who were administered ICI monotherapy.

#### ICI-related Side Effects

In six of 22 participants (27%), mild to moderate noncardiovascular ICI-specific side effects were documented between baseline and follow-up MRI examinations. Those side effects were dermatitis (four of 22 [18%]), thyroiditis (two of 22 [9%]), hypophysitis (one of 22 [5%]), colitis (one of 22 [5%]), and myositis (one of 22 [5%]). ICI-related myocarditis was not suspected in any participant at the time of follow-up MRI examination. In two of 22 participants (9%), ICI treatment was discontinued between baseline and follow-up MRI examinations due to noncardiovascular ICI-specific side effects. Between participants with and without ICI-related side effects, we found no evidence of differences regarding T1 relaxation times (998 msec ± 24 vs 1012 msec ± 40; *P* = .41), T2 relaxation times (58 msec ± 4 vs 58 msec ± 4; *P* = .38), quantitative LGE (13.7% ± 8 vs 11.2% ± 7; *P* = .46), and left ventricular ejection fraction (58% ± 7 vs 59% ± 7; *P* = .67). At follow-up, *N*-terminal pro-B-type natriuretic peptide values were normal (normal value, <450 pg/L; mean, 130 pg/mL; interquartile range, 46–193 pg/mL). Baseline troponin T values were unremarkable in all participants (normal value, <14 ng/L). In three of 22 participants (14%), elevated troponin T values (>14 ng/L; mean, 26 ng/L ± 8) were observed at follow-up. We found no differences in these three participants with regard to T1 relaxation times (1025 msec ± 48 vs 1003 msec ± 35; *P* = .35), T2 relaxation times (61 msec ± 5 vs

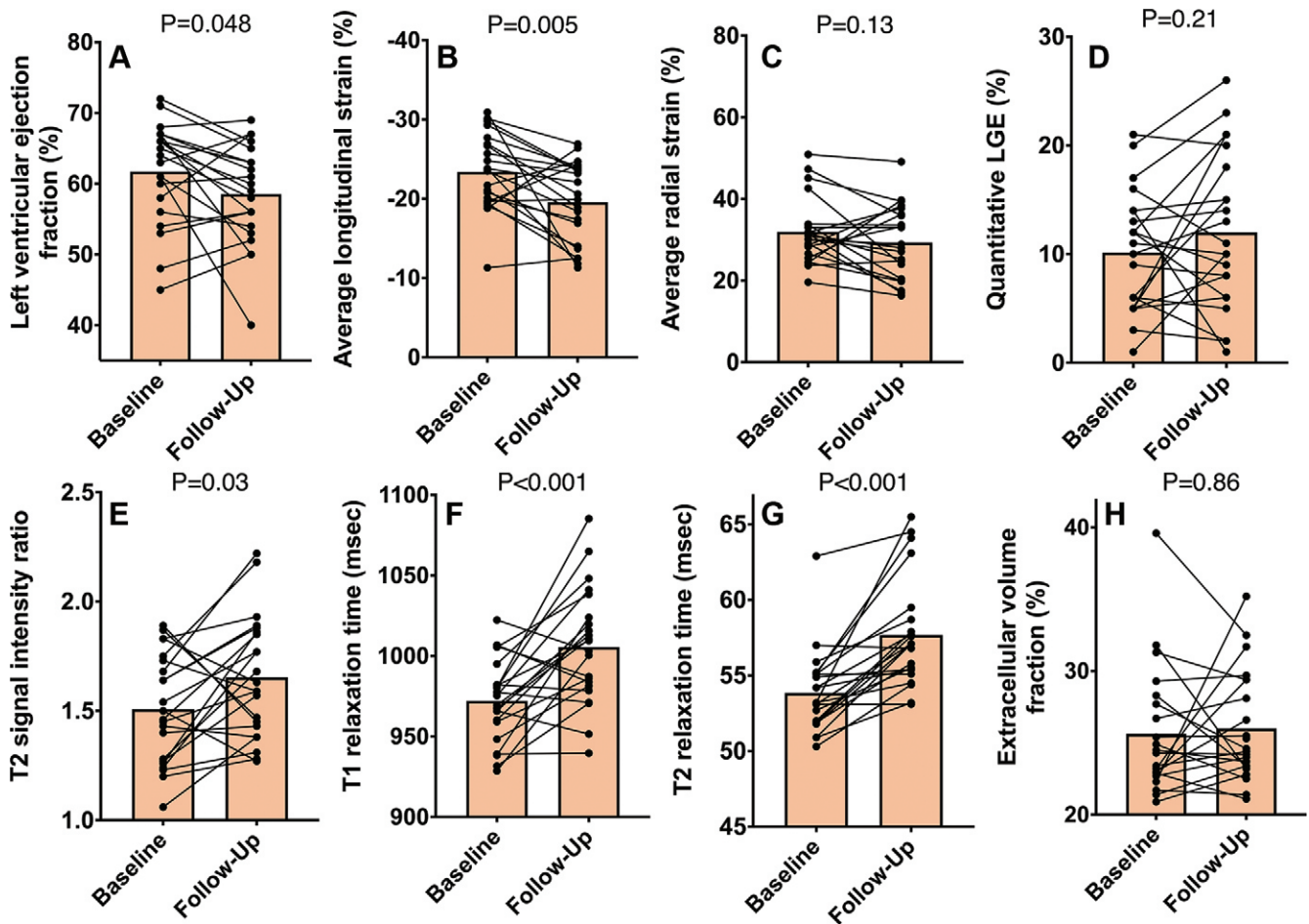


**Figure 2:** Bar graphs show changes in cardiac MRI parameters between baseline and follow-up MRI examinations. Bars represent mean data. Intraindividual values are plotted between baseline and follow-up MRI examinations for (A) left ventricular ejection fraction, (B) average longitudinal strain, (C) average radial strain, (D) quantitative late gadolinium enhancement (LGE), (E) T2 signal intensity ratio, (F) T1 relaxation time, (G) T2 relaxation time, and (H) extracellular volume fraction. For intraindividual comparison, paired *t* test or Wilcoxon signed-rank test was used.

57 msec  $\pm$  3;  $P = .30$ ), and quantitative LGE ( $16.3\% \pm 7$  vs  $11.3\% \pm 7$ ;  $P = .27$ ) compared with participants with unremarkable troponin T levels at follow-up, but they did display decreased left ventricular ejection fraction ( $50\% \pm 10$  vs  $60\% \pm 6$ ;  $P = .02$ ). In one participant with increased troponin T (29 ng/L), follow-up cardiac MRI scans displayed signs of acute ICI-related myocarditis with visible diffuse myocardial edema and a distinct increase in T1 relaxation time ( $\Delta T1 = 33$  msec, where  $\Delta$  = change in relaxation time) and T2 relaxation time ( $\Delta T2 = 13$  msec) compared with the baseline MRI examination. In addition, pericardial and pleural effusions were present. The participant had received four infusions of combination ICI therapy. After undergoing MRI, the participant was immediately admitted to the oncology department for further diagnostic work-up. A fulminant multiorgan immune-related adverse reaction was diagnosed, including signs of myocarditis, hepatitis, pneumonitis, and colitis. The participant died 32 days after follow-up MRI examination.

## Discussion

The extent of subclinical acute cardiac effects related to immune checkpoint inhibitor (ICI) treatment is unclear. This intraindivi-

vidual comparison study revealed a high burden of acute cardiac effects in patients with cancer undergoing ICI treatment, indicating that subclinical ICI cardiotoxicity may be more common than previously assumed. After treatment initiation, participants showed increased markers of diffuse myocardial edema (T1 relaxation times, 972 msec  $\pm$  26 vs 1006 msec  $\pm$  36 [ $P < .001$ ]; T2 relaxation times, 54 msec  $\pm$  3 vs 58 msec  $\pm$  4 [ $P < .001$ ]) and decreased left ventricular average systolic longitudinal strain values ( $-23.4\% \pm 4.8$  vs  $-19.6\% \pm 5.1$ ;  $P = .005$ ), supporting evidence of subclinical myocardial inflammation as an early treatment effect. In addition, small pericardial effusions were evident in more participants at follow-up than baseline examination (one of 22 [5%] vs 10 of 22 [45%];  $P = .004$ ), indicating immune-related serositis.

Following an initial report of fulminant myocarditis in two patients with melanoma treated with combination ICI therapy in 2016, ICI-related myocarditis was identified as a rare but potentially life-threatening immune-related adverse event (5,6). Thereafter, it was assumed that potentially due to a lack of awareness, only severe cases were reported, leading to a distortion in the perception of this clinical syndrome (10). Thus, an expert panel defined criteria to subclassify



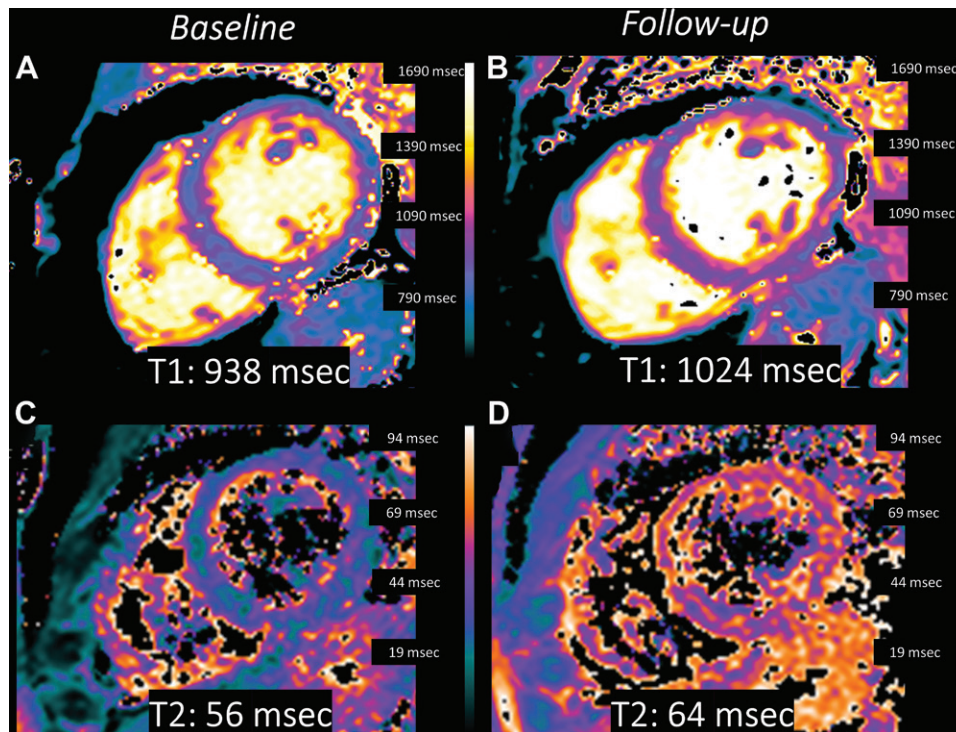


**Figure 3:** MRI scans in a 66-year-old man with history of head and neck squamous cell carcinoma, before (baseline) and 3 months after (follow-up) treatment with a programmed death 1 inhibitor (pembrolizumab). **(A, B)** Native T1 mapping images in short-axis view show increased myocardial T1 relaxation time at follow-up examination, indicating acute myocardial injury. **(C, D)** T2 mapping images in short-axis view show increased myocardial T2 relaxation time at follow-up examination, indicating myocardial edema.

ICI-related myocarditis according to its clinical course as fulminant (acute myocarditis with fast evolution and hemodynamic compromise), clinically significant nonfulminant, or subclinical (10). Following this classification, one of the 22 participants in our study presented with fulminant ICI-related myocarditis at follow-up. Notably, as with all the other study participants, myocarditis was not suspected at the time of follow-up in this participant. In the remaining study participants without cardiac symptoms, we also observed a high burden of diffuse myocardial edema and a subclinical decrease in left ventricular systolic function. In another report, histopathologic analysis of ICI-related myocarditis revealed lymphocytic infiltrates within the cardiac muscle cells, consisting of T cells and macrophages (6). Accordingly, we observed increased T1 and T2 relaxation times at follow-up examination, indicating diffuse myocardial edema as a possible correlate for an ICI-induced immune cell infiltration (3,6). Both T1 and T2 mapping are very sensitive in the detection of extra- and intracellular edema in acute myocarditis (12,16,20). For the detection of diffuse myocardial injury with mapping techniques, site-specific reference values must be obtained. Compared with previously published reference values for our group ( $966 \text{ msec} \pm 25$  for myocardial T1 and  $53 \text{ msec} \pm 2$  for myocardial T2 [12]), which were obtained using the same imaging techniques as in this study, the T1 and T2 relaxation times at follow-up MRI examination exceeded the normal range of mapping parameters. Therefore,

myocardial mapping might be very important for the detection of diffuse inflammatory myocardial injury induced by ICI therapy.

We observed no changes regarding quantitative markers of myocardial fibrosis (quantitative LGE and extracellular volume) between baseline and follow-up MRI examinations, possibly because myocardial fibrosis is more a long-term consequence of ongoing myocardial inflammation. In two study participants, slightly new visible focal LGE lesions in a nonischemic distribution pattern were found, possibly caused by acute inflammatory necrotic lesions. This observation is consistent with findings from a pooled analysis of ICI-related cardiotoxicity cases, in which a minority of patients (three of 13) with ICI-related myocarditis displayed positive LGE findings (21). In another large retrospective analysis of an international registry conducted by Zhang et al (22), less than half of the patients hospitalized due to ICI-related myocarditis had positive LGE.

A proposed pathogenic mechanism for ICI-induced myocardial injury and inflammation and clinical examples are provided in Figure 4. With the specific pathomechanism of ICI-related myocardial injury in mind (6), our findings support evidence of a specific imaging pattern of ICI-related myocarditis, which is mainly driven by the presence of a diffuse myocardial edema (as a substrate of immune infiltration) and is not characterized by the expansive presence of LGE lesions, as observed in viral myocarditis (11). We also

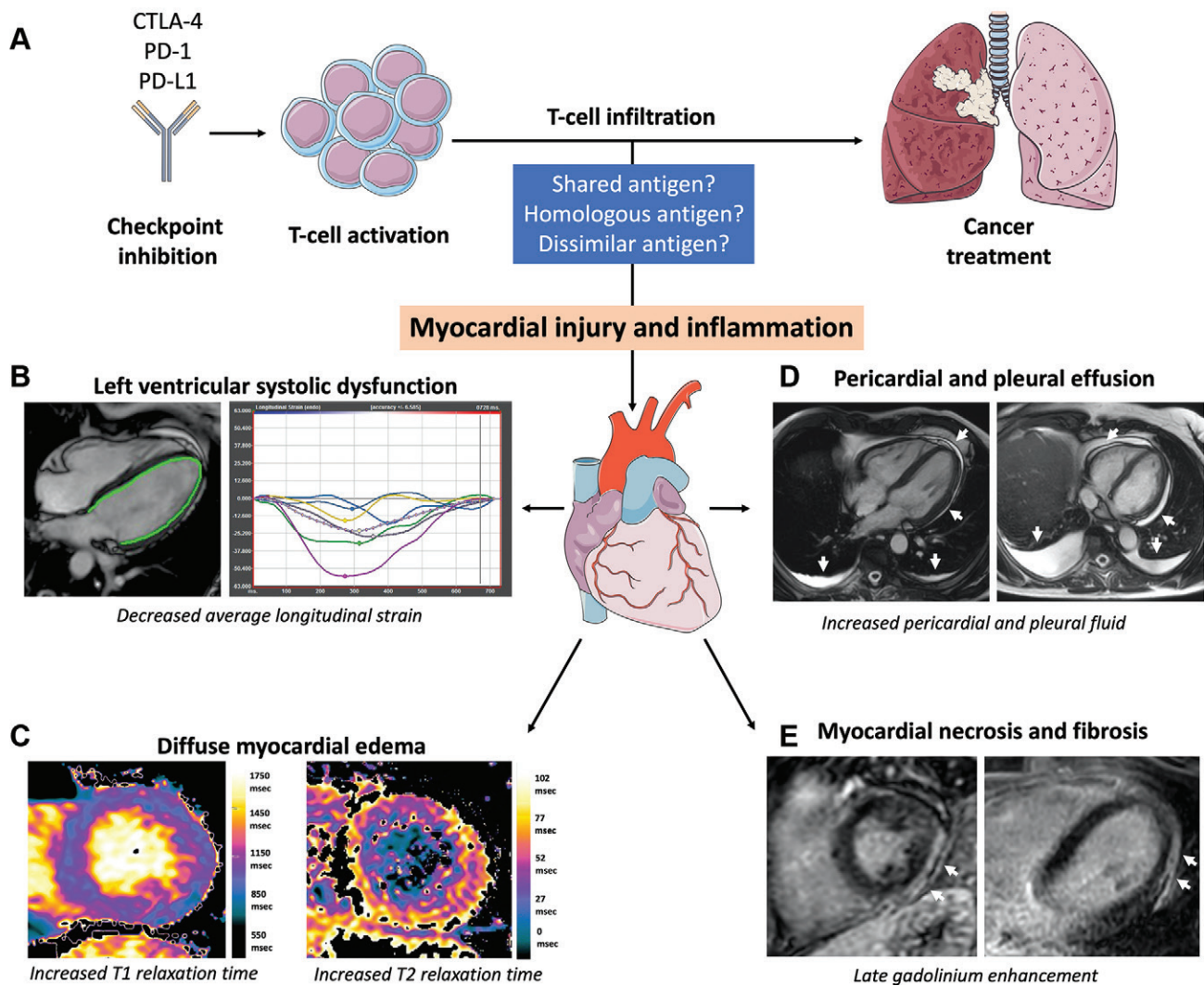


**Figure 4:** Diagram shows proposed pathogenic mechanism of immune checkpoint inhibitor (ICI)-induced myocardial injury and inflammation and a summary of results. **(A)** ICIs are monoclonal antibodies targeting negative regulatory pathways (called checkpoints)—such as cytotoxic T-lymphocyte antigen 4 (CTLA-4), programmed death 1 (PD-1), or programmed death ligand 1 (PD-L1)—within the host immune system, leading to T-cell activation. Histopathologic analysis of patients with ICI-related myocarditis revealed that besides infiltrating the tumor site, T cells also infiltrate the myocardium, possibly through a shared, homologous, or dissimilar antigen. T-cell infiltration may generate myocardial injury and inflammation (6). **(B)** In our study, participants displayed signs of left ventricular systolic dysfunction, with decreased average longitudinal strain values on follow-up cardiac MRI scans. The green outline represents the subendocardial contour of strain analysis. **(C)** Participants had a diffuse myocardial edema with increased T1 and T2 relaxation times as the key imaging finding. **(D)** Pericardial and pleural effusions (arrows) were more frequently observed at follow-up examination compared with baseline. **(E)** New focal late gadolinium enhancement lesions were observed in two participants on follow-up MRI scans, with patchy focal enhancement in the basal inferolateral subepicardium or striatal focal enhancement of the midventricular lateral subepicardium with associated pericardial enhancement (arrows). All image examples are derived from the described study cohort. The figure contains free medical images from Servier (<https://smart.servier.com>) used under a CC BY 3.0 license (23).

observed lower average longitudinal strain at follow-up MRI examinations, which is consistent with a previous speckle-tracking echocardiographic study (24). Differences in strain were more pronounced than those in left ventricular ejection fraction, indicating mainly subclinical systolic dysfunction.

Although participants with known structural heart disease were specifically excluded in our study, 32% had focal LGE lesions at baseline MRI examination, indicating unrecognized cardiac disease with focal myocardial scarring. However, non-ischemic LGE lesions per se can be caused by various medical conditions or previous unperceived myocarditis (12,25). Furthermore, several risk factors are shared between oncologic

and cardiovascular diseases (7). Although it is unclear to what extent myocardial disease may contribute to ICI-related cardiotoxicity, this observation may be of particular relevance for the interpretation of future cross-sectional cardio-oncologic MRI studies, in which LGE prevalence should not be generally interpreted as treatment effects.

Our study has limitations. One limitation is the small study size. In addition, no histopathologic reference standard (endomyocardial biopsy) was used for quantification of myocardial inflammation and fibrosis. Therefore, the pathophysiologic conclusions discussed in our study cannot be correlated with histopathologic results. However, the applied measurements



were validated against histologic data in previous studies (26–28) and are recommended for noninvasive diagnosis of inflammatory cardiomyopathies (29).

In conclusion, multiparametric cardiac MRI showed a high burden of subclinical acute myocardial disease with elevated markers of inflammation and signs of systolic dysfunction in participants receiving immune checkpoint inhibitor (ICI) therapy for cancer treatment. Because ICI-related myocarditis may take a potentially fatal course (6,9), our findings have three major implications for clinical practice and future research. First, they prompt the need for closer cardiologic monitoring during ICI therapy, which may potentially help forestall fulminant courses of ICI-related cardiotoxicity. Additionally, cardiac MRI that includes quantitative techniques represents a highly sensitive noninvasive diagnostic tool that should play a central role in the diagnostic work-up of these patients. Second, the long-term effects of ICI therapy on cardiac health must be investigated. Third, the observed high burden of subclinical cardiotoxicity may have important implications for appropriate treatment decisions, for instance, with regard to cost and benefit of adjuvant ICI therapy. Larger studies are warranted to ultimately determine the clinical implications of our findings.

**Author contributions:** Guarantors of integrity of entire study, A.F., N.M., J.A.L.; study concepts/study design or data acquisition or data analysis/interpretation, all authors; manuscript drafting or manuscript revision for important intellectual content, all authors; approval of final version of submitted manuscript, all authors; agrees to ensure any questions related to the work are appropriately resolved, all authors; literature research, A.F., A.L., N.M., K.S., J.S., A.H., U.A., J.L., J.A.L.; clinical studies, A.F., N.M., M.R., K.S., J.S., F.G.B., D.D., C.C.P., A.H., D.K., J.L., J.A.L.; statistical analysis, A.F., A.L., N.M., K.S., J.A.L.; and manuscript editing, A.F., A.L., N.M., K.S., A.M.S., D.D., C.C.P., A.H., D.K., U.A., J.L., J.A.L.

**Disclosures of Conflicts of Interest:** A.F. disclosed no relevant relationships. A.I. disclosed no relevant relationships. N.M. disclosed no relevant relationships. M.R. disclosed no relevant relationships. K.S. disclosed no relevant relationships. J.S. disclosed a clinician science grant from Deutsche Dermatologische Gesellschaft. A.M.S. disclosed no relevant relationships. F.G.B. disclosed no relevant relationships. D.D. disclosed no relevant relationships. C.C.P. disclosed grant from Guerbet; disclosed speaker fees from Guerbet, Bayer Vital, and Philips Healthcare. A.H. disclosed no relevant relationships. D.K. disclosed no relevant relationships. U.A. disclosed speaker fees received from Siemens Healthineers in 2018. J.L. disclosed compensation received for board membership from Bristol Myers Squibb, MSD, and Novartis. J.A.L. disclosed speaker fees from Philips Healthcare.

**Data sharing:** Data generated or analyzed during the study are available from the corresponding author by request.

## References

- Postow MA, Callahan MK, Wolchok JD. Immune checkpoint blockade in cancer therapy. *J Clin Oncol* 2015;33(17):1974–1982.
- Darvin P, Toor SM, Sasidharan Nair V, Elkord E. Immune checkpoint inhibitors: recent progress and potential biomarkers. *Exp Mol Med* 2018;50(12):1–11.
- Postow MA, Sidlow R, Hellmann MD. Immune-related adverse events associated with immune checkpoint blockade. *N Engl J Med* 2018;378(2):158–168.
- Lyon AR, Yousaf N, Battisti NML, Moslehi J, Larkin J. Immune checkpoint inhibitors and cardiovascular toxicity. *Lancet Oncol* 2018;19(9):e447–e458.
- Amiri-Kordestani L, Moslehi J, Cheng J, et al. Cardiovascular adverse events in immune checkpoint inhibitor clinical trials: a U.S. Food and Drug Administration pooled analysis. *J Clin Oncol* 2018;36(15\_suppl):3009.
- Johnson DB, Balko JM, Compton ML, et al. Fulminant myocarditis with combination immune checkpoint blockade. *N Engl J Med* 2016;375(18):1749–1755.
- Palaskas N, Lopez-Mattei J, Durand JB, Iliescu C, Deswal A. Immune checkpoint inhibitor myocarditis: pathophysiological characteristics, diagnosis, and treatment. *J Am Heart Assoc* 2020;9(2):e013757.
- Mahmood SS, Fradley MG, Cohen JV, et al. Myocarditis in patients treated with immune checkpoint inhibitors. *J Am Coll Cardiol* 2018;71(16):1755–1764.
- Moslehi JJ, Salem JE, Sosman JA, Lebrun-Vignes B, Johnson DB. Increased reporting of fatal immune checkpoint inhibitor-associated myocarditis. *Lancet* 2018;391(10124):933.
- Bonaca MP, Olenchock BA, Salem JE, et al. Myocarditis in the setting of cancer therapeutics: proposed case definitions for emerging clinical syndromes in cardio-oncology. *Circulation* 2019;140(2):80–91.
- Luetkens JA, Doerner J, Thomas DK, et al. Acute myocarditis: multiparametric cardiac MR imaging. *Radiology* 2014;273(2):383–392.
- Luetkens JA, Faron A, Isaak A, et al. Comparison of original and 2018 Lake Louise Criteria for diagnosis of acute myocarditis: results of a validation cohort. *Radiol Cardiothorac Imaging* 2019;1(3):e190010.
- Luetkens JA, Schlesinger-Irsch U, Kuetting DLR, et al. Feature-tracking myocardial strain analysis in acute myocarditis: diagnostic value and association with myocardial oedema. *Eur Radiol* 2017;27(11):4661–4671.
- Look D, Locker D. Time saving in measurement of NMR and EPR relaxation times. *Rev Sci Instrum* 1970;41(2):250–251.
- Messroghli DR, Radjenovic A, Kozzerke S, Higgins DM, Sivananthan MU, Ridgway JP. Modified Look-Locker inversion recovery (MOLLI) for high-resolution T1 mapping of the heart. *Magn Reson Med* 2004;52(1):141–146.
- Sprinkart AM, Luetkens JA, Träber F, et al. Gradient spin echo (GraSE) imaging for fast myocardial T2 mapping. *J Cardiovasc Magn Reson* 2015;17(1):12.
- Schulz-Menger J, Bluemke DA, Bremerich J, et al. Standardized image interpretation and post processing in cardiovascular magnetic resonance: Society for Cardiovascular Magnetic Resonance (SCMR) board of trustees task force on standardized post processing. *J Cardiovasc Magn Reson* 2013;15(1):35.
- Luetkens JA, Klein S, Träber F, et al. Quantification of liver fibrosis at T1 and T2 mapping with extracellular volume fraction MRI: preclinical results. *Radiology* 2018;288(3):748–754.
- Luetkens JA, Petry P, Kuetting D, et al. Left and right ventricular strain in the course of acute myocarditis: a cardiovascular magnetic resonance study. *RöFo* 2018;190(8):722–732.
- Ferreira VM, Piechnik SK, Dall'Armellina E, et al. Non-contrast T1-mapping detects acute myocardial edema with high diagnostic accuracy: a comparison to T2-weighted cardiovascular magnetic resonance. *J Cardiovasc Magn Reson* 2012;14(1):42.
- Escudier M, Cautela J, Malissen N, et al. Clinical features, management, and outcomes of immune checkpoint inhibitor-related cardiotoxicity. *Circulation* 2017;136(21):2085–2087.
- Zhang L, Awadalla M, Mahmood SS, et al. Cardiovascular magnetic resonance in immune checkpoint inhibitor-associated myocarditis. *Eur Heart J* 2020;41(18):1733–1743.
- Les Laboratoires Servier. *Servier Medical Art*. <https://smart.servier.com>. Accessed February 14, 2021.
- Awadalla M, Mahmood SS, Groarke JD, et al. Global longitudinal strain and cardiac events in patients with immune checkpoint inhibitor-related myocarditis. *J Am Coll Cardiol* 2020;75(5):467–478.
- Isaak A, Praktijnjo M, Jansen C, et al. Myocardial fibrosis and inflammation in liver cirrhosis: MRI study of the liver-heart axis. *Radiology* 2020;297(1):51–61.
- Jeuthe S, Wassilew K, O H-Ici D, et al. Myocardial T1 maps reflect histological findings in acute and chronic stages of myocarditis in a rat model. *J Cardiovasc Magn Reson* 2016;18:19.
- Böner F, Spieker M, Haberkorn S, et al. Myocardial T2 mapping increases noninvasive diagnostic accuracy for biopsy-proven myocarditis. *JACC Cardiovasc Imaging* 2016;9(12):1467–1469.
- Bohnen S, Radunski U, Lund G, et al. Performance of t1 and t2 mapping cardiovascular magnetic resonance to detect active myocarditis in patients with recent-onset heart failure. 2015. 2015;8(6):e003073.
- Ferreira VM, Schulz-Menger J, Holmvang G, et al. Cardiovascular magnetic resonance in nonischemic myocardial inflammation: expert recommendations. *J Am Coll Cardiol* 2018;72(24):3158–3176.

### 3.4 Quantitative kardiale und hepatische MRT bei der Leberzirrhose

*“Myocardial Fibrosis and Inflammation in Liver Cirrhosis: MRI Study of the Liver-Heart Axis”*

Isaak A\*, Praktiknjo M\*, Jansen C, Faron A, Sprinkart AM, Pieper CC, Chang J, Fimmers R, Meyer C, Dabir D, Thomas D, Trebicka J, Attenberger U, Kuetting D, Luetkens JA.

Erschienen in *Radiology*. 2020 Oct;297(1):51-61. \*geteilte Erstautorenschaft

**Zielsetzung und Methoden** – Bei der Leberzirrhose wird die Konstellation verschiedener Symptome, die auf strukturelle und funktionelle Herzmuskelveränderungen hinweisen, als zirrhotische Kardiomyopathie bezeichnet. Die Pathophysiologie dieser Erkrankung ist noch nicht ausreichend geklärt, aber eine multifaktorielle Entstehung durch Effekte der veränderten Hämodynamik sowie der systemischen Inflammation und Fibrogenese werden vermutet (siehe *Figure 2* (Isaak et al., 2020)). Ziel dieser prospektiven Studie war die Evaluation subklinisch vorliegender fibrotischer und inflammatorischer Myokardveränderungen bei Studienteilnehmer/-innen mit Leberzirrhose in Bezug auf den Schweregrad der Lebererkrankung. Ein kombiniertes multiparametrisches MRT-Protokoll des Herzens (Funktion, LGE, T2-gewichtete Ödembildgebung, T1/T2-Mapping und ECV) und der Leber (Morphologie, MR-Elastographie, T1/T2-Mapping und ECV) wurde etabliert.

**Ergebnisse** – Von November 2018 bis Dezember 2019 wurden insgesamt 42 Studienteilnehmer/-innen mit Leberzirrhose ( $57 \pm 11$  Jahre; 23 Männer) und 18 gesunde Studienteilnehmer/-innen ( $54 \pm 19$  Jahre; 11 Männer) mittels kombinierter Herz-Leber-MRT untersucht. Im Vergleich zu der Kontrollgruppe wiesen Teilnehmer/-innen mit Leberzirrhose eingeschränkte longitudinale Strainparameter sowie eine Erhöhung der myokardialen T1- und T2-Relaxationszeiten und ECV-Werte sowie des qualitativen und quantitativen LGE auf (siehe *Figure 3* und *Figure 4* (Isaak et al., 2020)). Mit höherem Child-Pugh Score wurde eine Zunahme der myokardialen T1- und T2-Relaxationszeiten, der ECV-Werte (siehe *Figure 5* (Isaak et al., 2020)) und der fokalen LGE-Läsionen beobachtet (z.B. Vorhandensein von fokalem LGE: 27 % vs. 53 % vs. 82 %; Child A vs. B vs. C). Die MR-Elastographie-basierte Lebersteifigkeit korrelierte mit den quantitativen Myokardparametern (insbesondere mit dem quantifizierten LGE, den myokardialen T1-Relaxationszeiten und den ECV-Werten) und war ein unabhängiger Prädiktor für das Vorhandensein von fokalem LGE (siehe *Table 4* (Isaak et al., 2020)). Ein Grenzwert von 9,2 kPa für die Lebersteifigkeit in der MR-Elastographie war mit dem Vorliegen nicht-ischämischer LGE-Läsionen assoziiert (Sensitivität: ca. 77 %, Spezifität: ca. 75 %).



**Schlussfolgerungen** – Studienteilnehmer/-innen mit Leberzirrhose zeigten in der kombinierten quantitativen Herz-Leber-MRT Zeichen der systolischen Dysfunktion, der diffusen myokardialen Inflammation und der fokalen und diffusen Myokardfibrose, welche mit dem klinischen und bildgebenden Schweregrad der Lebererkrankung zunahmen.

# Myocardial Fibrosis and Inflammation in Liver Cirrhosis: MRI Study of the Liver-Heart Axis



Alexander Isaak, MD\* • Michael Praktikno, MD\* • Christian Jansen, MD • Anton Faron, MD • Alois M. Sprinkart, PhD • Claus C. Pieper, MD • Johannes Chang, MD • Rolf Fimmers, PhD • Carsten Meyer, MD • Darius Dabir, MD • Daniel Thomas, MD • Jonel Trebicka, MD • Ulrike Attenberger, MD • Daniel Kuetting, MD • Julian A. Luetkens, MD

From the Departments of Radiology (A.I., A.F., A.M.S., C.C.P., C.M., D.D., D.T., U.A., D.K., J.A.L.) and Internal Medicine I (M.P., C.J., J.C.), University Hospital Bonn, Venusberg-Campus 1, 53127 Bonn, Germany; Quantitative Imaging Laboratory Bonn (QILaB), Bonn, Germany (A.I., A.F., A.M.S., D.D., D.T., D.K., J.A.L.); Institute for Medical Biometry, Informatics and Epidemiology (IMBIE), University of Bonn, Bonn, Germany (R.F.); Department of Internal Medicine 1, University Hospital Frankfurt, Frankfurt am Main, Germany (J.T.). Received March 19, 2020; revision requested April 28; revision received June 11; accepted June 23. **Address correspondence** to J.A.L. (e-mail: [julian.luetkens@ukbonn.de](mailto:julian.luetkens@ukbonn.de)).

\*A.I. and M.P. contributed equally to this work.

Conflicts of interest are listed at the end of this article.

See also the editorial by de Roos and Lamb in this issue.

Radiology 2020; 297:51–61 • <https://doi.org/10.1148/radiol.20201057> • Content codes:  

**Background:** Cardiac involvement in liver cirrhosis in the absence of underlying cardiac disease is termed *cirrhotic cardiomyopathy*. The pathophysiology of this condition is still poorly understood.

**Purpose:** To investigate the extent of subclinical imaging changes in terms of fibrosis and inflammation and to explore the relationship between the severity of liver disease and the degree of myocardial involvement.

**Materials and Methods:** In this prospective study from November 2018 to December 2019, participants with liver cirrhosis and healthy control participants underwent hepatic and cardiac MRI. The multiparametric scan protocol assessed hepatic (T1 and T2 relaxation times, extracellular volume [ECV], and MR elastography–based liver stiffness) and cardiac (T1 and T2 relaxation times, ECV, myocardial edema, late gadolinium enhancement [LGE], and myocardial strain) parameters. Student *t* tests, one-way analysis of variance, Pearson correlation, and multivariable binary regression analysis were used for statistical analyses.

**Results:** A total of 42 participants with liver cirrhosis (mean age  $\pm$  standard deviation, 57 years  $\pm$  11; 23 men) and 18 control participants (mean age, 54 years  $\pm$  19; 11 men) were evaluated. Compared with control participants, the participants with liver cirrhosis displayed reduced longitudinal strain and elevated markers of myocardial disease (T1 and T2 relaxation times, ECV, and qualitative and quantitative LGE). Myocardial T1 (978 msec  $\pm$  23 vs 1006 msec  $\pm$  29 vs 1044 msec  $\pm$  14;  $P < .001$ ) and T2 relaxation times (56 msec  $\pm$  4 vs 59 msec  $\pm$  3 vs 62 msec  $\pm$  8;  $P = .04$ ) and ECV (30%  $\pm$  5 vs 33%  $\pm$  5 vs 38%  $\pm$  7;  $P = .009$ ) were higher depending on Child-Pugh class (A vs B vs C). Positive LGE lesions (three of 11 [27%] vs 10 of 19 [53%] vs nine of 11 [82%];  $P = .04$ ) were more prevalent in advanced Child-Pugh classes. MR elastography–based liver stiffness was an independent predictor for LGE (odds ratio, 1.6; 95% confidence interval: 1.2%, 2.1%;  $P = .004$ ) and correlated with quantitative LGE ( $r = 0.67$ ;  $P < .001$ ), myocardial T1 relaxation times ( $r = 0.55$ ;  $P < .001$ ), and ECV ( $r = 0.39$ ;  $P = .01$ ).

**Conclusion:** In participants with liver cirrhosis, systolic dysfunction and elevated parameters of myocardial edema and fibrosis were observed at MRI, which were more abnormal with greater severity of liver disease.

© RSNA, 2020

Online supplemental material is available for this article.

In chronic liver disease, the development of liver fibrosis and finally liver cirrhosis results in complications such as portal hypertension or liver failure (1). Although patients with nonalcoholic steatohepatitis or alcoholic liver disease have an increased risk for the development of cardiomyopathy and cardiovascular events (2), a specific type of cardiac dysfunction, termed *cirrhotic cardiomyopathy* (CCM), occurs in up to 50% of patients with advanced liver disease (3). This specific entity is independent of the underlying etiology of liver disease and is different from alcoholic cardiomyopathy (4). Although theories exist, the pathophysiology of CCM is still poorly understood (5,6). One of the proposed pathologic mechanisms in cirrhosis with portal hypertension is based on an increased release of vasodilators leading to a reduced

systemic vascular resistance, central hypovolemia, and a hyperdynamic cardiac state (7). Inflammatory pathways also seem to play an important role (8,9). In the absence of other known cardiac disease, echo- and electrocardiographic parameters are the basis of CCM diagnostic criteria (10). First defined in 2005, the recently redefined diagnostic criteria for CCM (11) include MRI as a suggested area for future research due to methods of quantitative imaging. Parametric MRI techniques such as T1 mapping quantify myocardial fibrosis in diffuse tissue pathologies (eg, in nonischemic cardiomyopathies [12]). T2 mapping can detect edema and inflammatory myocardial disease with high sensitivity (13,14). Also, myocardial strain analysis can quantify myocardial functional alterations (15). Myocardial T1 mapping techniques translated

## Abbreviations

CCM = cirrhotic cardiomyopathy, ECV = extracellular volume, LGE = late gadolinium enhancement

## Summary

Study participants with liver cirrhosis showed a high burden of cardiac disease at MRI including myocardial inflammation, myocardial fibrosis, and systolic dysfunction.

## Key Results

- Per Child-Pugh class (A vs B vs C), there were higher mean values of myocardial T1 relaxation times (978 msec vs 1006 msec vs 1044 msec;  $P < .001$ ), extracellular volume (ECV) (30% vs 33% vs 38%;  $P = .009$ ), and the presence of late gadolinium enhancement (LGE) lesions (27% vs 53% vs 82%;  $P = .04$ ).
- MR elastography–based liver stiffness was an independent predictor for LGE (odds ratio, 1.6;  $P = .004$ ) and correlated with myocardial T1 relaxation times ( $r = 0.55$ ;  $P < .001$ ) and ECV ( $r = 0.39$ ;  $P = .01$ ).

into liver MRI seem to be a promising tool for liver fibrosis quantification (16). MR elastography provides measurement of liver tissue stiffness and has a strong correlation with the stage of liver fibrosis (17).

In this prospective study, a comprehensive multiparametric hepatic and cardiac MRI was performed in participants with liver cirrhosis without known cardiac disease. The purpose of our explorative multiparametric MRI study was to investigate the extent of subclinical imaging changes in terms of fibrosis and inflammation in participants with advanced liver disease and to explore the relationship between the severity of liver disease and the degree of myocardial involvement.

## Materials and Methods

The institutional ethics commission approved this prospective case-control study, and all participants gave written informed consent prior to MRI.

### Study Participants

Participants with clinically defined cirrhosis and healthy control participants were included consecutively during the recruitment period from November 2018 to December 2019. Participants with liver cirrhosis had manifestation of portal hypertension and were clinically evaluated for transjugular intrahepatic portosystemic shunt insertion. In this context, a structured cardiologic examination was performed including 12-lead electrocardiogram, transthoracic echocardiogram, and a detailed evaluation regarding prior cardiac disease and coronary artery disease symptoms. Only participants without known underlying cardiac disease or symptoms were included. Exclusion criteria were contraindications for contrast material–enhanced MRI and known malignant disease. The control group consisted of healthy volunteers and outpatients referred for nonspecific cardiac symptoms (eg, nonspecific chest pain) or exclusion of structural heart disease (eg, due to family disposition for sudden cardiac death or cardiomyopathies). All control participants had an unremarkable past medical history of hepatic and

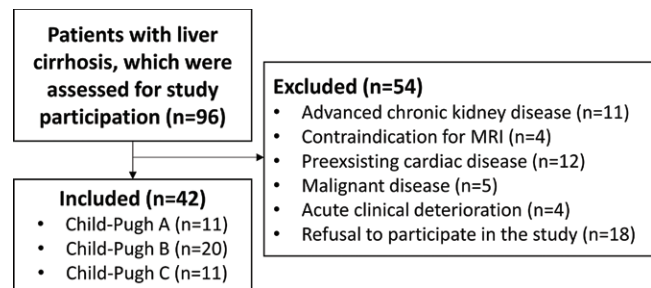


**Figure 1:** Flowchart shows included participants with liver cirrhosis and patients who were excluded due to prior defined exclusion criteria.

cardiac disease and showed normal cardiac and hepatic MRI results without structural abnormalities.

### MRI Protocol

Combined cardiac and hepatic examinations were performed during a single scan for each participant with a clinical whole-body MRI system (Ingenia 1.5 T; Philips Healthcare, Best, the Netherlands). A 32-channel torso coil (coverage, 60 cm) with digital interface was used for signal reception. Cardiac scan protocol included electrocardiogram-gated steady-state free-precession cine images (short-axis, four-chamber, and two-chamber views). For visualization of myocardial edema and calculation of T2 signal intensity ratio, T2-weighted short-tau inversion-recovery sequences were performed (short-axis, two-chamber, and transversal views). Late gadolinium enhancement (LGE) imaging was based on segmented inversion-recovery gradient-echo sequences (short-axis, two-chamber, and four-chamber views). Myocardial T1 and T2 mapping were obtained in end-diastole in apical, midventricular, and basal short-axis orientation (18,19). For contrast enhancement, a single bolus of 0.2 mmol/kg body weight of gadobutrol (Gadovist; Bayer Healthcare, Leverkusen, Germany) was given. Myocardial and hepatic T1 maps were acquired 10 and 12 minutes after contrast material injection, respectively. For ECV calculation, blood hematocrit levels were assessed directly prior to the MRI scan.

Hepatic scan protocol included a six-echo gradient-echo sequence to calculate proton density fat fraction and T2\* maps. Liver MR elastography was implemented to acquire a quantitative elastogram for liver stiffness assessment. Additionally, non–electrocardiogram-gated hepatic T1 and T2 mapping sequences of the liver were performed. All hepatic maps were acquired in transversal orientation, covering the liver parenchyma slightly above the liver hilum (16). A detailed description of the MRI protocol and sequence parameters is provided in Appendix E1 and Table E1 (online).

### Cardiac MRI Analysis

Image analysis was performed by two board-certified radiologists (D.T. and J.A.L., with 20 and 8 years of experience, respectively, in hepatic and cardiac MRI) using dedicated software (IntelliSpace Portal, version 10.1; Philips Healthcare). Readers were blinded to the clinical information. The presence of focal-regional high-signal intensities on T2 short-

**Table 1: Clinical and MRI Characteristics of Participants with Liver Cirrhosis and Healthy Control Participants**

Variable	Participants with Liver Cirrhosis (n = 42)	Healthy Control Participants (n = 18)	P Value
<b>Clinical parameters</b>			
Age (y)	57 ± 11	54 ± 19	.56
Men*	23 (55)	13 (72)	.21
Weight (kg)	74 ± 19	77 ± 16	.56
Body mass index (kg/m <sup>2</sup> )	24.7 ± 5.3	24.0 ± 4.8	.62
Body surface area (m <sup>2</sup> )	1.9 ± 0.3	1.9 ± 0.2	.62
Heart frequency (bpm)	79 ± 13	66 ± 12	.001 <sup>†</sup>
<b>Cardiac MRI parameters</b>			
Left ventricular ejection fraction (%)	63 ± 8	61 ± 4	.15
Left ventricular end-diastolic volume index (mL/m <sup>2</sup> )	75 ± 18	77 ± 16	.66
Right ventricular ejection fraction (%)	56 ± 10	54 ± 6	.42
Right ventricular end-diastolic volume index (mL/m <sup>2</sup> )	81 ± 19	85 ± 16	.43
Cardiac index (L/min/m <sup>2</sup> )	3.7 ± 0.9	2.9 ± 0.5	<.001 <sup>†</sup>
Left atrium volume index (mL/m <sup>2</sup> )	53 ± 13	34 ± 9	<.001 <sup>†</sup>
Left ventricular mass index (g/m <sup>2</sup> )	45 ± 10	43 ± 7	.38
Interventricular septal thickness (mm)	8.2 ± 1.8	8.1 ± 1.6	.89
T2 signal intensity ratio	1.7 ± 0.3	1.6 ± 0.2	.06
Visual myocardial edema*	0 (0)	0 (0)	>.99
Visual late gadolinium enhancement*	22 (52)	0 (0)	<.001 <sup>†</sup>
Late gadolinium enhancement (%)	6.0 ± 5.6	1.6 ± 1.0	<.001 <sup>†</sup>
Longitudinal strain (%)	-18.5 ± 4.0	-22.5 ± 3.6	<.001 <sup>†</sup>
Circumferential strain (%)	-22.1 ± 5.4	-24.0 ± 2.8	.08
Radial strain (%)	35.6 ± 11.2	34.2 ± 10.2	.64
T1 relaxation time, native (msec)	1008 ± 34	958 ± 17	<.001 <sup>†</sup>
Extracellular volume fraction (%)	34 ± 6	26 ± 3	<.001 <sup>†</sup>
T2 relaxation time (msec)	59 ± 5	53 ± 2	<.001 <sup>†</sup>
<b>Hepatic MRI parameters</b>			
Proton density fat fraction (%)	3.3 ± 2.5	4.8 ± 2.7	.12
T2* relaxation time (msec)	35 ± 7	33 ± 9	.55
MR elastography–based liver stiffness (kPa)	9.7 ± 3.4	2.0 ± 0.5	<.001 <sup>†</sup>
T1 relaxation time, native (msec)	715 ± 73	526 ± 55	<.001 <sup>†</sup>
Extracellular volume fraction (%)	42 ± 8	27 ± 5	<.001 <sup>†</sup>
T2 relaxation time (msec)	57 ± 8	47 ± 5	<.001 <sup>†</sup>

Note.—Unless otherwise specified, data are means ± standard deviation. P values were obtained by using Student *t* test,  $\chi^2$  test (cell count greater than five), or Fisher exact test (cell count less than or equal to five).

\* Data are absolute frequencies, with percentages in parentheses.

<sup>†</sup> Denotes significant values.

tau inversion-recovery and on LGE images in a nonischemic distribution pattern was assessed visually by consensus agreement of the two readers. Semiquantitative T2 signal intensity ratio (13) and semiquantitative enhanced volume percentage (performed in short-axis LGE images) using the full width at half maximum technique (20) were calculated. Myocardial relaxation maps were motion corrected by using fast elastic image registration software (IntelliSpace Portal, version 10.1). T1 and T2 relaxation times were calculated as previously described (13). Hematocrit-corrected ECV values were determined by using T1 values before and after contrast material administration (13). Feature tracking strain measurements were derived from cine images in four-chamber and short-axis views by using dedicated software (Image-Arena 4.6; TomTec Imaging Systems, Unterschleissheim, Germany)

(15,21). Average left ventricular longitudinal, circumferential, and radial strain values were assessed.

### Hepatic MRI Analysis

Hepatic images were evaluated by one radiologist (J.A.L.) blinded to the cardiac findings and clinical information in a separate reading session. For the assessment of T1 and T2 relaxation times, three representative regions of interest were drawn centrally in three hepatic segments (segments 2, 4a, and 7), and mean relaxation times were calculated. Hematocrit-corrected extracellular volume fraction values were calculated from T1 values before and after contrast material administration (16). Liver tissue stiffness mean values were derived from stiffness confidence map by drawing the largest possible regions of interest (minimum of 1 cm<sup>2</sup>) in three different representative regions of the liver.

**Table 2: Clinical and MRI Analysis of Cirrhosis Subgroups according to Child-Pugh Class**

Variable	Class A (n = 11)	Class B (n = 20)	Class C (n = 11)	P Value
<b>Clinical parameters</b>				
Age (y)	60 ± 11	54 ± 12	59 ± 11	.24
Men*	5 (46)	13 (65)	5 (46)	.45
Weight (kg)	73 ± 13	77 ± 23	70 ± 16	.63
Body mass index (kg/m <sup>2</sup> )	25.4 ± 4.3	25.0 ± 6.2	23.4 ± 4.6	.66
Body surface area (m <sup>2</sup> )	1.9 ± 0.2	1.9 ± 0.3	1.8 ± 0.2	.64
MELD score	10 ± 2 <sup>†</sup>	12 ± 5	15 ± 5 <sup>‡</sup>	.03 <sup>§</sup>
TTE-based diastolic dysfunction*	6 (55)	12 (60)	7 (64)	.91
<b>Biochemical parameters</b>				
International normalized ratio	1.3 ± 0.1	1.3 ± 0.5	1.3 ± 0.4	.89
Serum albumin (g/L)	37 ± 5 <sup>∥</sup>	30 ± 9 <sup>†‡</sup>	23 ± 6 <sup>‡∥</sup>	<.001 <sup>§</sup>
Total bilirubin (mg/dL)	0.9 ± 0.3 <sup>†</sup>	1.1 ± 0.7 <sup>†</sup>	2.6 ± 1.4 <sup>‡∥</sup>	<.001 <sup>§</sup>
GGT (U/L)	164 ± 233	184 ± 194	219 ± 306	.86
ALT (U/L)	23 ± 7	26 ± 12	33 ± 17	.17
AST (U/L)	42 ± 24	58 ± 39	61 ± 31	.34
Leukocytes (G/L)	6.1 ± 2.9	7.9 ± 5.4	7.1 ± 3.9	.55
CRP (mg/L)	13 ± 23	14 ± 9	22 ± 23	.42
<b>Cardiac MRI parameters</b>				
Left ventricular ejection fraction (%)	65 ± 5	63 ± 8	62 ± 12	.61
Left ventricular end-diastolic volume index (mL/m <sup>2</sup> )	70 ± 18	78 ± 20	76 ± 14	.48
Right ventricular ejection fraction (%)	57 ± 7	55 ± 10	57 ± 14	.71
Right ventricular end-diastolic volume index (mL/m <sup>2</sup> )	72 ± 21	83 ± 18	85 ± 15	.19
Cardiac index (L/min/m <sup>2</sup> )	3.6 ± 1.1	3.7 ± 1.0	3.7 ± 0.8	.94
Left atrium volume index (mL/m <sup>2</sup> )	49 ± 11	50 ± 13	59 ± 15	.19
Left ventricular mass index (g/m <sup>2</sup> )	42 ± 11	46 ± 12	46 ± 6	.52
T2 signal intensity ratio	1.7 ± 0.3	1.8 ± 0.3	1.7 ± 0.4	.70
Visual myocardial edema*	0 (0)	0 (0)	0 (0)	>.99
Visual late gadolinium enhancement*	3 (27)	10 (53)	9 (82)	.04 <sup>§</sup>
Late gadolinium enhancement (%)	1.6 ± 1.7 <sup>†</sup>	4.3 ± 2.7 <sup>†</sup>	13.1 ± 5.3 <sup>‡∥</sup>	<.001 <sup>§</sup>
Longitudinal strain (%)	-18.7 ± 4.9	-18.2 ± 3.9	-18.7 ± 3.3	.94
Circumferential strain (%)	-23.0 ± 4.3	-21.5 ± 6.1	-22.1 ± 5.3	.76
Radial strain (%)	42.2 ± 13.0	33.1 ± 9.6	33.1 ± 10.3	.09
T1 relaxation time, native (msec)	978 ± 23 <sup>†∥</sup>	1006 ± 29 <sup>†‡</sup>	1044 ± 14 <sup>‡∥</sup>	<.001 <sup>§</sup>
Extracellular volume fraction (%)	30 ± 5 <sup>†</sup>	33 ± 5	38 ± 7 <sup>‡</sup>	.009 <sup>§</sup>
T2 relaxation time (msec)	56 ± 4 <sup>†</sup>	59 ± 3	62 ± 8 <sup>‡</sup>	.04 <sup>§</sup>
<b>Hepatic MRI parameters</b>				
Ratio of caudate to right lobe	0.5 ± 0.2	0.5 ± 0.2	0.4 ± 0.1	.49
Right hepatic vein diameter (mm)	3.7 ± 1.9	3.7 ± 1.6	3.7 ± 0.9	.99
Proton density fat fraction (%)	4.4 ± 3.2	3.0 ± 2.4	2.7 ± 1.9	.26
T2* relaxation time (msec)	33 ± 8	36 ± 5	34 ± 7	.39
MR elastography-based liver stiffness (kPa)	6.1 ± 1.7 <sup>∥</sup>	9.5 ± 2.3 <sup>†‡</sup>	13.5 ± 1.7 <sup>‡∥</sup>	<.001 <sup>§</sup>
T1 relaxation time, native (msec)	639 ± 46 <sup>†∥</sup>	719 ± 46 <sup>†‡</sup>	782 ± 63 <sup>‡∥</sup>	<.001 <sup>§</sup>
Extracellular volume fraction (%)	35 ± 6 <sup>†∥</sup>	42 ± 6 <sup>†‡</sup>	50 ± 7 <sup>‡∥</sup>	<.001 <sup>§</sup>
T2 relaxation time (msec)	52 ± 6 <sup>†</sup>	56 ± 9	62 ± 5 <sup>‡</sup>	.008 <sup>§</sup>

Note.—Unless otherwise specified, data are means ± standard deviation. P values were obtained using one-way analysis of variance followed by Tukey multiple comparison tests. ALT = alanine transaminase, AST = aspartate transaminase, CRP = C-reactive protein, GGT =  $\gamma$ -glutamyl transferase, MELD = model for end-stage liver disease, TTE = transthoracic echocardiography.

\* Data are absolute frequencies, with percentages in parentheses.

<sup>†</sup> P < .05 versus Child class C.

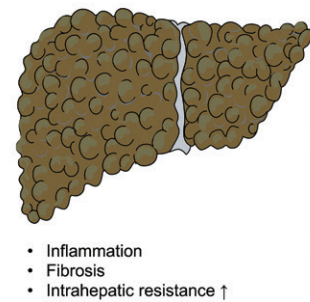
<sup>‡</sup> P < .05 versus Child class A.

<sup>§</sup> Denotes significant values.

<sup>∥</sup> P < .05 versus Child class B.



## LIVER CIRRHOSIS WITH PORTAL HYPERTENSION



Splanchnic and peripheral arterial vasodilation

↑ release of vasodilators

Bacterial translocation and systemic inflammation

Central hypovolemia with hyperdynamic circulation

↓ SVR

↑ RAAS

↑ SNS

↑ inflammatory mediators (cytokines, chemokines)

↑ HR

↑ CO

## CIRRHOTIC CARDIOMYOPATHY

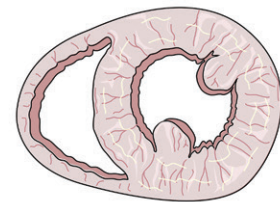


**Figure 2:** Diagram shows proposed pathogenic mechanism of cirrhotic cardiomyopathy in patients with advanced liver disease. Chronic liver injury may induce hepatic fibrosis, which finally distorts normal liver architecture by expansion of extracellular space and impairs hepatic function. Loss of normal liver architecture favors increased intrahepatic vascular resistance leading to portal hypertension. Combined with liver dysfunction, portal hypertension with consecutive portosystemic shunting leads to higher systemic concentration of circulating vasodilators, which favors splanchnic and peripheral arterial vasodilation. These processes lead to decreased systemic vascular resistance (SVR) and redistribution of blood volume that results in central hypovolemia. Therefore, vasodilatation in cirrhosis leads to development of hyperdynamic syndrome with reduced central blood volume followed by baroreceptor-induced activation of potent vasoconstricting systems, such as renin–angiotensin–aldosterone system (RAAS) and sympathetic nervous system (SNS). Hyperdynamic circulation and activation of potent vasoconstrictor systems stress the heart and lead to development of cardiac dysfunction and fibrosis, resulting in development of cirrhotic cardiomyopathy. Recent studies proposed theories of increased activation of inflammatory pathways. These hypotheses build on bacterial translocation and systemic inflammation with increased release of pathogen-associated molecular patterns and several cytokines (eg, tumor necrosis factor- $\alpha$ ), which also lead to increased vasodilatation processes and, apart from that, seem to have direct effects on the heart by inducing cardiac inflammation and oxidative stress. CO = cardiac output, HR = heart rate. Figure 2 contains modified free medical images from Servier Medical Art, licensed under a Creative Commons Attribution 3.0 Unported license (<https://smart.servier.com/>).

### Statistical Analysis

Prism (version 8.0.0; GraphPad Software, San Diego, Calif) and SPSS Statistics (version 26; IBM, Armonk, NY) were used for statistical analysis. Participant characteristics are presented as means  $\pm$  standard deviation or as percent to absolute frequency. Continuous variables between two groups were compared by using Student *t* test. Because of the exploratory study design, no adjustments for multiple comparisons were made (22). Dichotomous variables were compared by using the  $\chi^2$  test (with a cell count greater than five) or Fisher exact test (with a cell count less than or equal to five). One-way analysis of variance followed by Tukey multiple comparison tests were used to compare MRI parameters in different stages of liver cirrhosis. Pearson correlation coefficients were used to test correlations between continuous variables. A univariable and multivariable binary logistic regression analysis was applied to test the impact of clinical and liver imaging variables for the prediction of positive LGE. After a forward selection of relevant covariates with  $P < .1$  at univariable analysis, covariates were added in a multivariable model to further fit the impact of variables. To find a liver imaging–based cutoff for the presence of LGE, the area under the receiver operating characteristic curve was calculated for MR elastography–based liver stiffness. Youden index was used to determine the optimal cutoff. The level of statistical significance was set to  $P < .05$ .

## Results

### Participant Characteristics

A total of 60 participants were included in this prospective study (42 participants with liver cirrhosis [mean age  $\pm$  standard deviation, 57 years  $\pm$  11; 23 men] and 18 control participants [mean age, 54 years  $\pm$  19; 11 men]) (Fig 1). There was

no difference between participants with cirrhosis and healthy control participants in age ( $P = .12$ ), sex ( $P = .24$ ), weight ( $P = .61$ ), or body mass index ( $P = .60$ ) (Table 1). The origin of liver cirrhosis was alcohol consumption (24 of 42, 57%), viral hepatitis (four of 42, 12%), autoimmune hepatitis (three of 42, 7%), nonalcoholic steatohepatitis (three of 42, 7%), hemochromatosis (one of 42, 2%), congenital anomalies (one of 42, 2%), or cryptogenic (five of 42, 12%).

Cirrhosis groups were subdivided into three classes by using the clinically established Child-Pugh score (class A: 11 of 42, 26%; B: 20 of 42, 48%; C: 11 of 42, 26%) (Table 2). Model for end-stage liver disease score was different between Child-Pugh A and C ( $10 \pm 2$  vs  $15 \pm 5$ ;  $P = .03$ ).

### Cardiac MRI Results

No differences in left ventricular ejection fraction ( $63\% \pm 8$  vs  $61\% \pm 4$ ;  $P = .15$ ) or left ventricular end-diastolic volume index ( $75 \text{ mL/m}^2 \pm 18$  vs  $77 \text{ mL/m}^2 \pm 16$ ;  $P = .66$ ) were found between the cirrhosis and the control group. A high-normal left ventricular ejection fraction ( $>70\%$ ) was detected in nine of 42 (21%) participants with liver cirrhosis. Three of eleven (27%) participants with Child-Pugh class C had a lower left ventricular ejection fraction ( $<55\%$ ). Evaluation of hemodynamic parameters showed a higher heart rate (79 beats per minute  $\pm 13$  vs 66 beats per minute  $\pm 12$ ;  $P = .001$ ) and a higher cardiac index ( $3.7 \text{ L/min/m}^2 \pm 0.9$  vs  $2.9 \text{ L/min/m}^2 \pm 0.5$ ;  $P < .001$ ) in participants with liver cirrhosis compared with healthy control participants. Compared with the control group, left atrium volume index was greater in the cirrhosis group ( $53 \text{ mL/m}^2 \pm 13$  vs  $34 \text{ mL/m}^2 \pm 9$ ;  $P < .001$ ).

Myocardial T1 relaxation times (1008 msec  $\pm 34$  vs 958 msec  $\pm 17$ ;  $P < .001$ ) and ECV ( $34\% \pm 6$  vs  $26\% \pm 3$ ;  $P < .001$ )

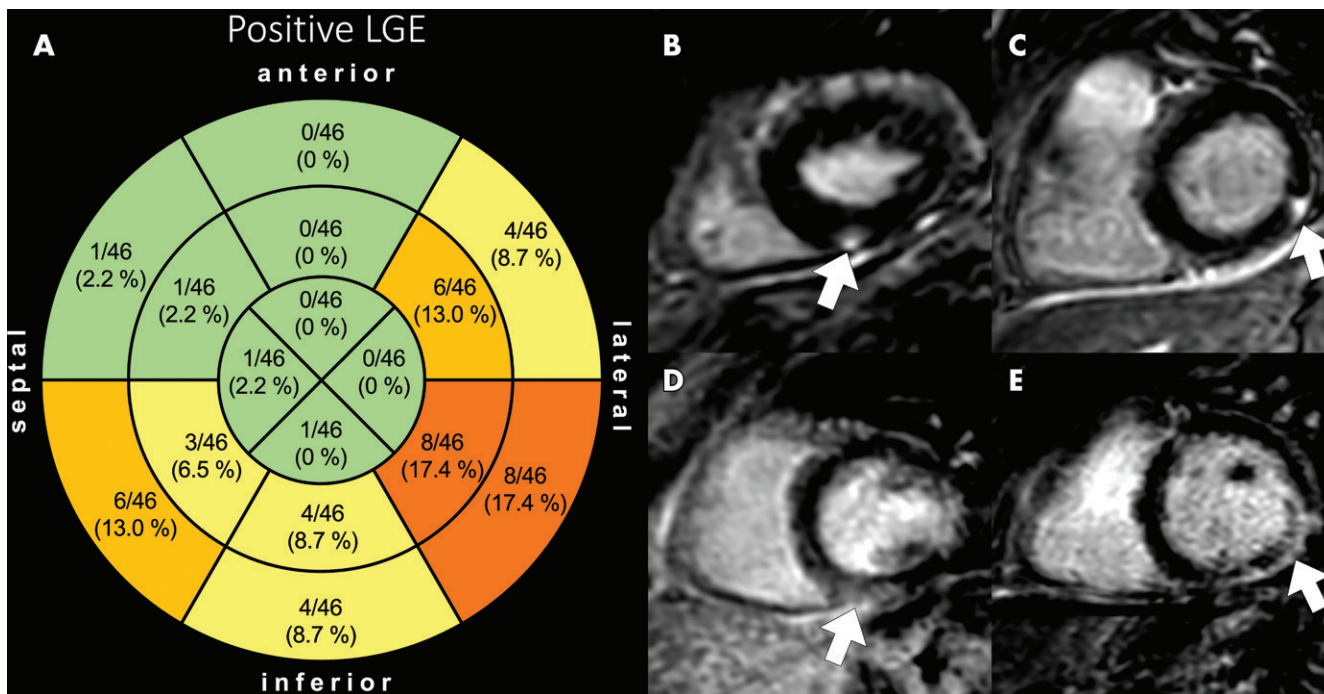


**Figure 3:** Images show representative examples of participants with liver cirrhosis with positive late gadolinium enhancement (LGE). A, Distribution of positive LGE according to segments of myocardium indicate preferable involvement of inferolateral and inferoseptal segments. Exemplary contrast material-enhanced segmented inversion-recovery gradient-echo sequences in short-axis view show positive LGE with B, C, focal and D, E, diffuse pattern (arrows).

.001) as well as T2 relaxation times ( $59 \text{ msec} \pm 5$  vs  $53 \text{ msec} \pm 2$ ;  $P < .001$ ) were elevated in participants with liver cirrhosis compared with healthy control participants. T2 signal intensity ratio was within normal range in both groups, with no difference in the cirrhosis group compared with healthy volunteers ( $1.7 \pm 0.3$  vs  $1.6 \pm 0.2$ ;  $P = .06$ ). No visual focal myocardial edema was observed.

Participants with liver cirrhosis had lower mean longitudinal strain values ( $-18.5\% \pm 4.0$  vs  $-22.5\% \pm 3.6$ ;  $P < .001$ ). No differences were found for circumferential ( $-22.1\% \pm 5.4$  vs  $-24.0\% \pm 2.8$ ;  $P = .08$ ) or radial strain ( $35.6\% \pm 11.2$  vs  $34.2\% \pm 10.2$ ;  $P = .64$ ). An updated CCM concept is provided in Figure 2.

In 22 participants with liver cirrhosis, focal LGE lesions were present, whereas no visual LGE could be detected in the control group (22 of 42, 52% vs 0 of 18, 0%;  $P < .001$ ). Patchy or striatal LGE was preferably located at the inferolateral and inferoseptal midwall and subepicardium (Fig 3). Quantitative LGE analysis showed elevated values in participants with liver cirrhosis compared with control participants ( $6.0\% \pm 5.6$  vs  $1.6\% \pm 1.0$ ;  $P < .001$ ). Participants with liver cirrhosis and positive LGE had higher myocardial T1 ( $1014 \text{ msec} \pm 36$  vs  $981 \text{ msec} \pm 36$ ;  $P = .002$ ) and T2 relaxation times ( $60 \text{ msec} \pm 6$  vs  $56 \text{ msec} \pm 3$ ;  $P = .01$ ) and ECV values ( $36\% \pm 6$  vs  $30\% \pm 7$ ;  $P = .02$ ), and they had lower longitudinal strain values ( $-17.4\% \pm 4.0$  vs  $-21.0\% \pm 3.8$ ;  $P = .048$ ) compared with LGE-negative participants. There was no difference in quantitative cardiac parameters between alcohol- and nonalcohol-caused cirrhosis (T1 relaxation time:  $1016 \text{ msec} \pm 30$  vs  $998 \text{ msec} \pm 37$ ;  $P = .12$ ; T2

relaxation time:  $59 \text{ msec} \pm 4$  vs  $59 \text{ msec} \pm 6$ ;  $P = .70$ ; ECV:  $35\% \pm 6$  vs  $32\% \pm 5$ ;  $P = .60$ ).

**Hepatic MRI Results**

MR elastography-based liver stiffness ( $9.7 \text{ kPa} \pm 3.4$  vs  $2.0 \text{ kPa} \pm 0.5$ ;  $P < .001$ ), hepatic T1 relaxation times ( $715 \text{ msec} \pm 73$  vs  $526 \text{ msec} \pm 55$ ;  $P < .001$ ), ECV ( $42\% \pm 8$  vs  $27\% \pm 5$ ;  $P < .001$ ), and T2 relaxation times ( $57 \text{ msec} \pm 8$  vs  $47 \text{ msec} \pm 5$ ;  $P < .001$ ) were higher in participants with liver cirrhosis compared with control participants and were more pronounced across the Child-Pugh classes (Table 2). There were correlations between MR elastography-based liver stiffness and other quantitative hepatic parameters, especially between hepatic T1 relaxation times ( $r = 0.81$ ;  $P < .001$ ) and hepatic ECV ( $r = 0.65$ ;  $P < .001$ ).

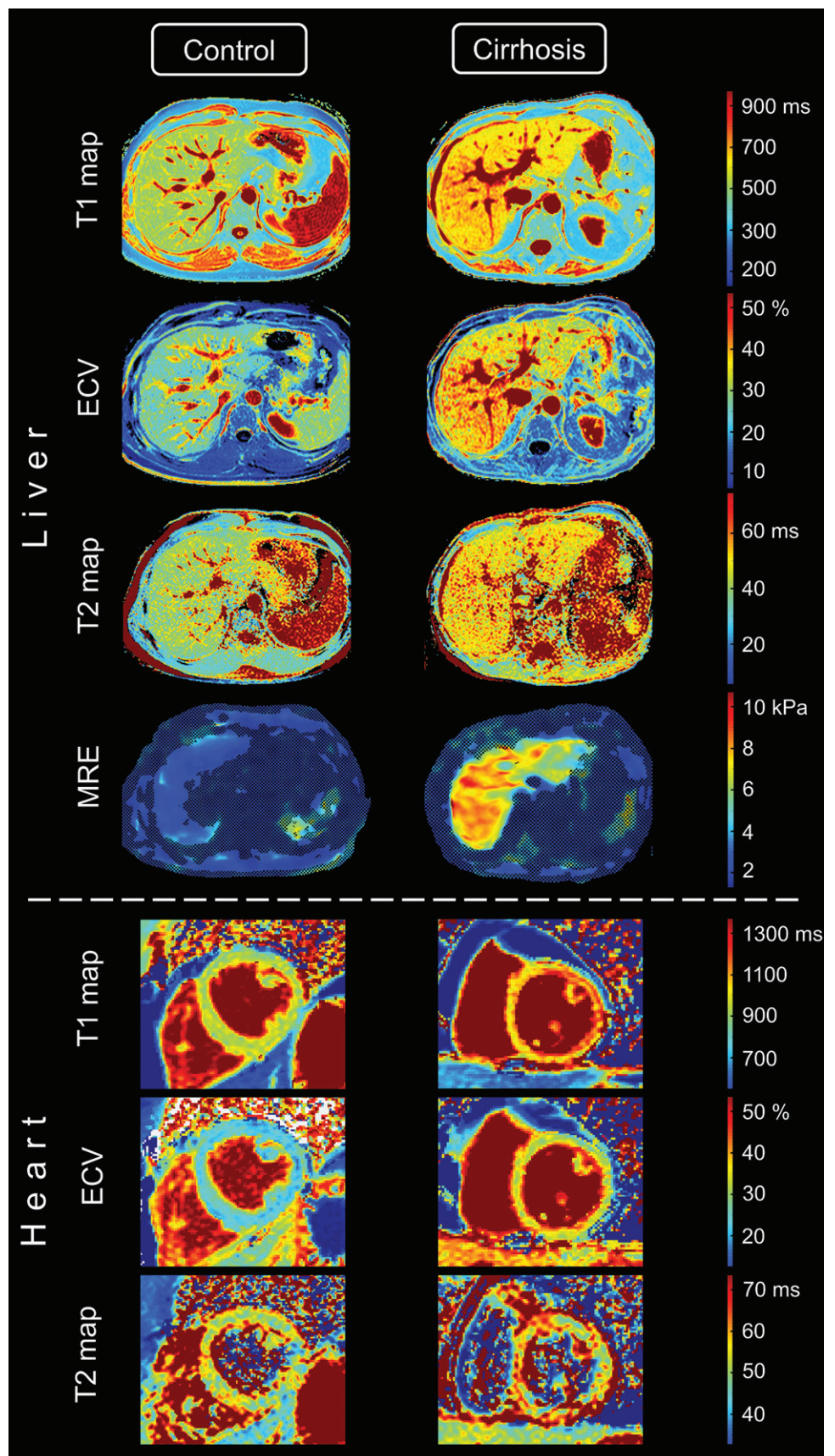
**Evaluation of the Heart-Liver Axis**

Myocardial T1 relaxation times (A:  $978 \text{ msec} \pm 23$  vs B:  $1006 \text{ msec} \pm 29$  vs C:  $1044 \text{ msec} \pm 14$ ;  $P < .001$ ), ECV (A:  $30\% \pm 5$  vs B:  $33\% \pm 5$  vs C:  $38\% \pm 7$ ;  $P = .009$ ), and T2 relaxation times (A:  $56 \text{ msec} \pm 4$  vs B:  $59 \text{ msec} \pm 3$  vs C:  $62 \text{ msec} \pm 8$ ;  $P = .04$ ) were higher across the Child-Pugh classes (Figs 4, 5). Furthermore, quantitative myocardial parameters were greater in participants with a model for end-stage liver disease score of 15 or greater when compared with participants with a model for end-stage liver disease score of less than 15 (T1 relaxation time:  $1031 \text{ msec} \pm 31$  vs  $1001 \text{ msec} \pm 32$ ,  $P = .02$ ; ECV:  $38\% \pm 7$  vs  $32\% \pm 5$ ,  $P = .03$ ). Relative frequency of visually observed LGE was greater depending on the Child-Pugh class (A: three of 11, 27% vs B: 10 of 20, 53% vs C: nine of 11,



**Figure 4:** Images show clinical examples of comprehensive multiparametric hepatic and cardiac MRI parameters in a healthy control participant (30-year-old man) and participant (59-year-old woman) with Child-Pugh class B cirrhosis. Quantitative maps are given for hepatic and cardiac T1 relaxation times (T1 map), extracellular volume fraction (ECV), T2 relaxation time (T2 map), and MR elastography (MRE)-based liver stiffness. Quantitative parameters are considerably higher in participant with cirrhosis. Figure exemplarily illustrates alterations in quantitative hepatic and cardiac parameters found in our study.

82%;  $P = .04$ ). Significant correlations were observed between MR elastography-based liver stiffness and quantitative LGE ( $r = 0.67$ ;  $P < .001$ ), myocardial T1 relaxation times ( $r = 0.55$ ;  $P < .001$ ), and myocardial ECV ( $r = 0.39$ ;  $P = .01$ ) (Fig 6, Table 3). Functional longitudinal strain correlated with MR elastography ( $r = 0.37$ ;  $P = .005$ ), hepatic T1 ( $r = 0.34$ ;  $P = .009$ ), and hepatic T2 relaxation times ( $r = 0.29$ ;  $P = .03$ ) as well as ECV ( $r = 0.42$ ;  $P = .001$ ) (Table 3). In the cirrhosis group, univariable binary logistic regression analysis revealed an association between the presence of LGE and Child-Pugh-Score (odds ratio [OR], 5.9; 95% confidence interval [CI]: 1.1%, 32%;  $P = .04$ ) and imaging markers of liver fibrosis such as MR elastography (OR, 1.5; 95% CI: 1.1%, 2.0%;  $P = .004$ ), hepatic T1 relaxation times (OR, 1.01; 95% CI: 1.00%, 1.02%;  $P = .03$ ), and hepatic ECV (OR, 1.2; 95% CI: 1.1%, 1.3%;  $P = .006$ ) (Table 4). In the multivariable binary logistic regression model, MR elastography-based liver stiffness remained the only variable significantly associated with the presence of positive LGE in participants with liver cirrhosis (OR: 1.6; CI: 1.2%, 2.1%;  $P = .004$ ) (Table 4). A cut-off of more than 9.2 kPa for MR elastography-based liver stiffness achieved a sensitivity of 17 of 22 (77.3%; CI: 54.6%, 92.1%) and a specificity of 15 of 20 (75.0%;





CI: 50.9%, 91.2%) for the presence of nonischemic LGE.

## Discussion

This combined cardiac and liver MRI study reveals a high burden of cardiac disease with signs of focal and diffuse myocardial fibrosis and diffuse myocardial edema, supporting evidence of subclinical myocardial inflammation in advanced liver disease. Myocardial T1 (978 msec  $\pm$  23 vs 1006 msec  $\pm$  29 vs 1044 msec  $\pm$  14;  $P < .001$ ) and T2 relaxation times (56 msec  $\pm$  4 vs 59 msec  $\pm$  3 vs 62 msec  $\pm$  8;  $P = .04$ ), extracellular volume (ECV) (30%  $\pm$  5 vs 33%  $\pm$  5 vs 38%  $\pm$  7;  $P = .009$ ), and the presence of late gadolinium enhancement (LGE) (27% vs 53% vs 82%;  $P = .04$ ) were higher depending on Child-Pugh class (A vs B vs C), indicating a link between the clinical

grade of liver disease and cardiac fibrosis and inflammation. Simultaneous acquisition of imaging-based liver and cardiac parameters revealed correlations between the severity of liver cirrhosis and myocardial disease, indicating that myocardial fibrosis in liver cirrhosis might not only be induced by a high cardiac workload but might also be caused by liver-associated mechanisms. MR elastography-based liver stiffness was an independent predictor for LGE (odds ratio, 1.6;  $P = .004$ ) and correlated with quantitative LGE ( $r = 0.67$ ;  $P < .001$ ), myocardial T1 relaxation times ( $r = 0.55$ ;  $P < .001$ ), and ECV ( $r = 0.39$ ;  $P = .01$ ). Higher cardiac indexes, as a sign of a hyperdynamic circulation, and correlations between subclinical myocardial dysfunction and imaging-based hepatic and cardiac parameters of fibrosis indicate that fibrotic myocardial remodeling may be a structural element in cirrhosis.

Our results are in line with previous cardiac MRI studies proposing that myocardial fibrosis could play an important role for the development of CCM. The particularly high amount of positive LGE in our study is supported by the study of Lossnitzer et al (23) who also found a high and variable extent of patchy LGE in patients with advanced liver disease. Wiese et al (24) described elevated ECV values in liver cirrhosis as a sign of

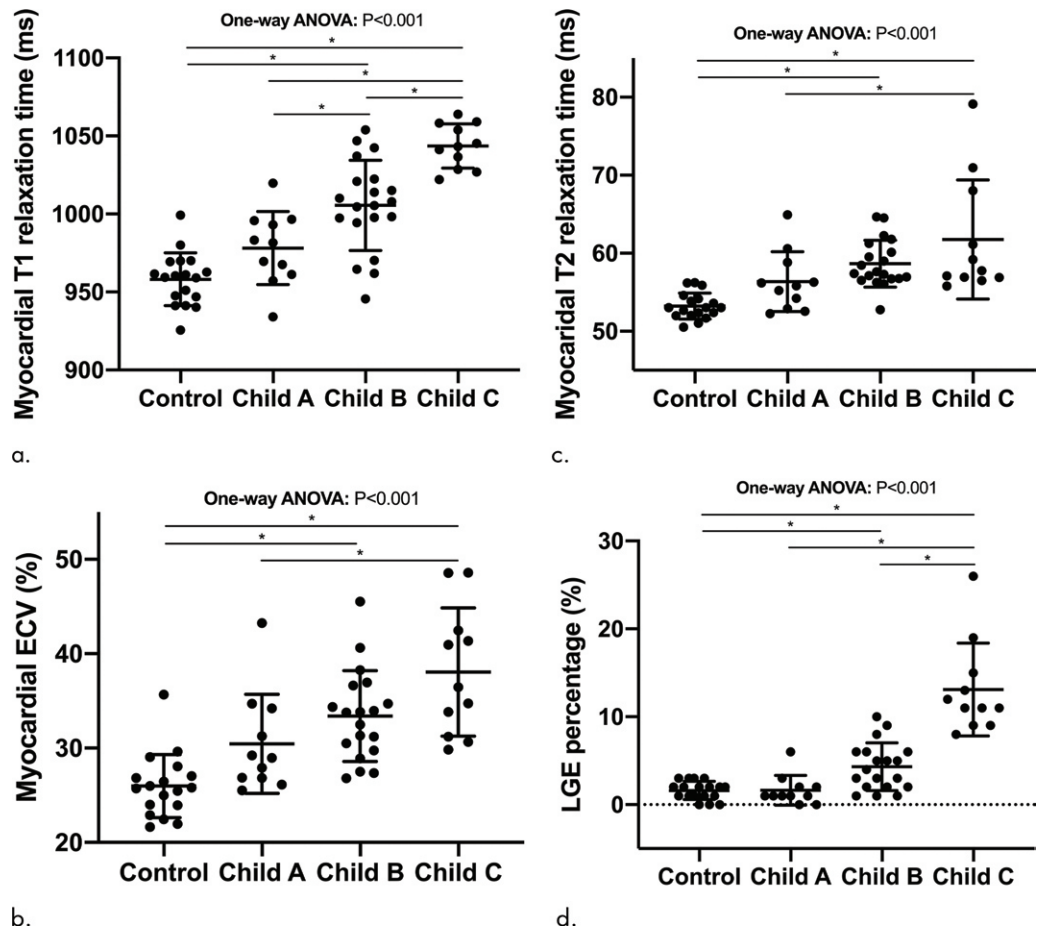


**Figure 5:** Column graphs with individual plotted values show distribution of quantitative myocardial MRI parameters in control group and in clinically subclassified cirrhosis group (Child-Pugh classes A, B, and C). Mean of data is represented by horizontal line. Whiskers represent standard deviation. \* indicates significant pairwise comparison ( $P < .05$ ). ANOVA = analysis of variance, ECV = extracellular volume fraction, LGE = late gadolinium enhancement.

subclinical diffuse myocardial fibrosis, which likely represents a structural element of CCM, and showed an association of ECV values with disease severity and transplant-free survival. Lee et al (25) also reported a pattern of greater myocardial ECV in 32 patients with liver cirrhosis that decreased 1 year after transplantation, suggesting a positive remodeling of diffuse myocardial alterations in normalized liver function. None of the mentioned cardiac MRI studies investigated imaging-based liver markers. However, other preliminary study results described correlations between myocardial ECV and markers of collagen formation, indicating an active process of fibrogenesis in liver cirrhosis (26), supporting our correlations between the severity of clinical and imaging-based grade of liver cirrhosis and myocardial fibrosis.

T2 mapping plays an important role in the diagnostic evaluation of inflammatory myocardial disease (27) but was poorly investigated in the context of CCM so far. In accordance with established hypotheses of systemic inflammatory conditions and recently propagated myocardial inflammatory pathways in liver cirrhosis (8,28), our findings of diffuse myocardial edema indicate the presence of subclinical myocardial inflammation in liver cirrhosis. The absence of visual edema in our study

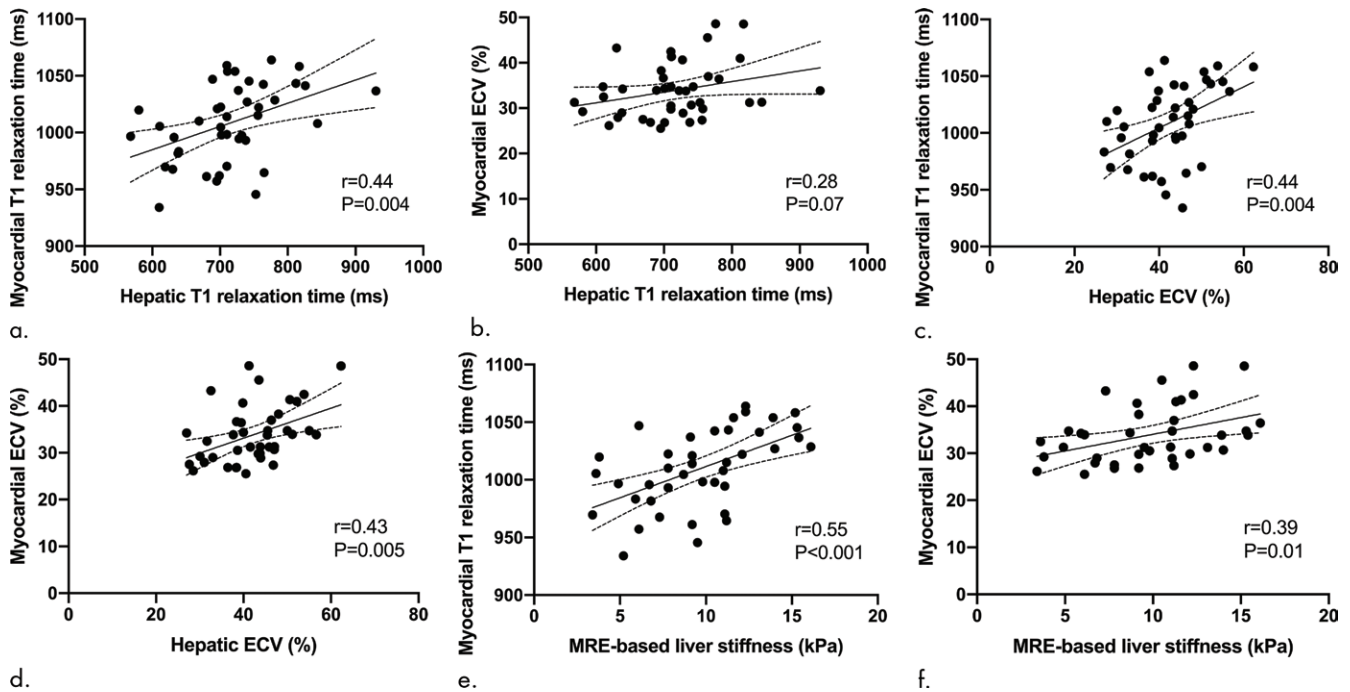


**Figure 6:** Scatterplots show correlation between myocardial and hepatic MRI parameters within cirrhosis group ( $n = 42$ ; exclusion of healthy control participants). Pearson correlation coefficients are provided. ECV = extracellular volume fraction, MRE = MR elastography.

**Table 3: Correlation Matrix of Different Hepatic and Cardiac MRI Parameters within the Cirrhosis Group ( $n = 42$ ) under Exclusion of Healthy Control Participants**

Cardiac MRI Parameters	MR Elastography		T1 Native		ECV		T2	
	<i>r</i> Value	<i>P</i> Value	<i>r</i> Value	<i>P</i> Value	<i>r</i> Value	<i>P</i> Value	<i>r</i> Value	<i>P</i> Value
T1 native	0.55	<.001*	0.44	.004*	0.44	.004*	0.27	.09
ECV	0.39	.01*	0.28	.07	0.43	.005*	0.11	.51
T2	0.27	.10	0.05	.77	0.42	.006*	0.21	.18
Quantitative LGE	0.67	<.001*	0.51	.001*	0.70	<.001*	0.25	.11
Longitudinal strain	0.37	.005*	0.34	.009*	0.42	.001*	0.29	.03*

Note.—Pearson correlation coefficients are provided. ECV = extracellular volume fraction, LGE = late gadolinium enhancement, T1 native = native T1 relaxation time, T2 = T2 relaxation time.

\* Denotes significant values.

can be explained by the higher sensitivity of quantitative techniques in case of a diffuse pattern of inflammation (14). In this context, the high amount of visible LGE might also be part of a healing response of subclinical myocardial inflammation (eg, myocarditis).

We observed higher cardiac indexes as a sign of a hyperdynamic circulation in participants with liver cirrhosis. This hyperdynamic circulation has been proposed as an important element for the development of CCM. Although left ventricular ejection fraction was high normal in some participants (also with greater longitudinal myocardial strain), the mean longitudinal strain was reduced in participants with liver cirrhosis, indicating a subclinical systolic dysfunction, which is in line with different speckle tracking echocardiography studies (11,29,30). Our findings promote the concept that a greater cardiac work, which stresses the heart, may lead to the development of cardiac dysfunction over time (3).

Our study had several limitations because of its observational form. We did not use a histopathologic reference standard (endomyocardial biopsy) for fibrosis and inflammation quantification. Yet, several studies have validated these applied parameters against histologic analysis (16,31). For cardiac image analysis, the presence of cirrhosis or normal liver parenchyma could possibly be seen in short-axis views. Therefore, image analysis was not totally blinded. Liver steatosis and siderosis may lead to an underestimation of hepatic relaxation times (32), but there was no need for a correction because of the lack of fatty liver disease or siderosis in our cohort. Alcoholic effects might be confounders. However, in accordance with other studies, cardiac involvement in cirrhosis was independent from the general etiology of liver disease and was observed in alcohol-related as well as in nonalcohol-related cirrhosis (4,33,34). Inflammation and portal hypertension may increase quantitative liver parameters leading to an overestimation of fibrosis (35). Finally, our sample

**Table 4: Influence of Clinical and Liver MRI Data for the Prediction of the Presence of Late Gadolinium Enhancement in Participants with Liver Cirrhosis**

Variable	Univariable Analysis		Multivariable Analysis	
	Odds Ratio	<i>P</i> Value	Odds Ratio	<i>P</i> Value
Age (per year)	1.02 (0.96, 1.1)	.52	...	...
Sex (men vs women)	0.93 (0.27, 3.2)	.90	...	...
Child-Pugh score (A and B vs C)	5.9 (1.1, 32)	.04*	...	...
MELD (per point)	1.04 (0.91, 1.9)	.55	...	...
Serum albumin (per g/L)	0.92 (0.85, 1.00)	.04*	0.92 (0.84, 1.00)	.06
Total bilirubin (per mg/dL)	1.5 (0.65, 3.5)	.34	...	...
International normalized ratio	2.6 (0.24, 27)	.43	...	...
GGT (per U/L)	1.00 (1.00, 1.00)	.23	...	...
AST (per U/L)	1.01 (0.99, 1.04)	.21	...	...
ALT (per U/L)	1.01 (0.96, 1.1)	.86	...	...
Ratio of caudate to right lobe	0.70 (0.02, 26)	.85	...	...
Right hepatic vein diameter	1.2 (0.79, 1.9)	.38	...	...
MR elastography–based liver stiffness (per kPa)	1.5 (1.1, 2.0)	.004*	1.6 (1.2, 2.1)	.004*
Hepatic native T1 relaxation time (per msec)	1.01 (1.00, 1.02)	.03*	...	...
Hepatic extracellular volume fraction (per %)	1.2 (1.1, 1.3)	.006*	...	...

Note.—Data in parentheses are 95% confidence intervals. *P* values were obtained by using a binary logistic regression analysis. ALT = alanine transaminase, AST = aspartate transaminase, GGT =  $\gamma$ -glutamyl transferase, MELD = model for end-stage liver disease.

\* Denotes significant values.

size was small, so additional confirmatory analyses are needed before the results of this exploratory study can be generalized.

In conclusion, comprehensive MRI showed a high burden of myocardial disease in participants with liver cirrhosis with signs of systolic dysfunction as well as elevated parameters of myocardial edema and fibrosis, which intensify with severity of liver disease. Myocardial fibrosis and subclinical myocardial inflammation seem to be a structural component of cirrhotic cardiomyopathy. MR elastography–based liver stiffness was identified as an independent predictor for the presence of late gadolinium enhancement (LGE) in participants with cirrhosis. Because nonischemic LGE lesions are considered to be an arrhythmogenic substrate and are related to major adverse cardiac events and poor outcome in patients with structural heart disease (eg, in nonischemic cardiomyopathies) (36–38), our findings prompt the need for closer cardiologic check-ups (eg, for cardiac medication adjustment or optimization of individual cardiovascular risk profile), especially in patients with clinically advanced liver disease or if imaging-based fibrosis markers are particularly high (MR elastography–based liver stiffness >9.2 kPa). MRI provides noninvasive, sensitive tissue characterization and shows a diffuse pattern of myocardial fibrosis and inflammation in individuals with cirrhosis. Thus, MRI should play a greater role in cardiac evaluation of individuals with advanced liver disease. We recommend further follow-up MRI studies with larger sample sizes of these individuals.

**Acknowledgment:** We thank Burkhard Madler, PhD (Philips Medical Systems, Hamburg, Germany) for his excellent technical assistance.

**Author contributions:** Guarantors of integrity of entire study, A.I., C.J., C.M., J.A.L.; study concepts/study design or data acquisition or data analysis/interpretation, all authors; manuscript drafting or manuscript revision for important intellectual content, all authors; approval of final version of submitted manuscript,

all authors; agrees to ensure any questions related to the work are appropriately resolved, all authors; literature research, A.I., M.P., C.J., A.F., A.M.S., J.C., D.T., J.T., U.A., D.K., J.A.L.; clinical studies, A.I., M.P., C.J., C.C.P., C.M., D.D., D.T., J.T., D.K., J.A.L.; experimental studies, C.J., A.M.S., J.A.L.; statistical analysis, A.I., M.P., C.J., A.F., J.C., R.F., J.A.L.; and manuscript editing, A.I., M.P., C.J., A.F., A.M.S., C.C.P., J.C., C.M., D.D., D.T., J.T., U.A., D.K., J.A.L.

**Disclosures of Conflicts of Interest:** A.I. disclosed no relevant relationships. M.P. disclosed no relevant relationships. C.J. disclosed no relevant relationships. A.F. disclosed no relevant relationships. A.M.S. disclosed no relevant relationships. C.C.P. Activities related to the present article: disclosed no relevant relationships. Activities not related to the present article: is a consultant for and has grants/grants pending with Guerbet; received payment for lectures including service on speakers bureaus from Philips Healthcare, Bayer Vital, and Guerbet. Other relationships: disclosed no relevant relationships. J.C. disclosed no relevant relationships. R.F. disclosed no relevant relationships. C.M. disclosed no relevant relationships. D.D. disclosed no relevant relationships. D.T. disclosed no relevant relationships. J.T. Activities related to the present article: disclosed no relevant relationships. Activities not related to the present article: is a consultant for Gore, CSL Behring, Grifols, and Versantis; has grants/grants pending with Gore and Falk; received payment for lectures including service on speakers bureaus from Gore, Grifols, Sequena, MSD, and Falk; received payment for manuscript preparation from Falk. Other relationships: disclosed no relevant relationships. U.A. Activities related to the present article: disclosed no relevant relationships. Activities not related to the present article: received payment for lectures including service on speakers bureaus from Siemens Healthineers. Other relationships: disclosed no relevant relationships. D.K. disclosed no relevant relationships. J.A.L. disclosed no relevant relationships.

## References

- Nusrat S, Khan MS, Fazili J, Madhoun MF. Cirrhosis and its complications: evidence based treatment. *World J Gastroenterol* 2014;20(18):5442–5460.
- Franque SM, van der Graaff D, Kwanten WJ. Non-alcoholic fatty liver disease and cardiovascular risk: pathophysiological mechanisms and implications. *J Hepatol* 2016;65(2):425–443.
- Zardi EM, Abbate A, Zardi DM, et al. Cirrhotic cardiomyopathy. *J Am Coll Cardiol* 2010;56(7):539–549.
- Ma Z, Lee SS. Cirrhotic cardiomyopathy: getting to the heart of the matter. *Hepatology* 1996;24(2):451–459.
- Moller S, Bendtsen F. The pathophysiology of arterial vasodilatation and hyperdynamic circulation in cirrhosis. *Liver Int* 2018;38(4):570–580.
- Bernardi M, Moreau R, Angeli P, Schnabl B, Arroyo V. Mechanisms of decompensation and organ failure in cirrhosis: from peripheral arterial vasodilation to systemic inflammation hypothesis. *J Hepatol* 2015;63(5):1272–1284.

7. Wiese S, Hove JD, Bendtsen F, Møller S. Cirrhotic cardiomyopathy: pathogenesis and clinical relevance. *Nat Rev Gastroenterol Hepatol* 2014;11(3):177–186.
8. Matyas C, Erdelyi K, Trojnar E, et al. Interplay of liver-heart inflammatory axis and cannabinoid 2 receptor signaling in an experimental model of hepatic cardiomyopathy. *Hepatology* 2020;71(4):1391–1407.
9. Praktijnjo M, Monteiro S, Grandt J, et al. Cardiodynamic state is associated with systemic inflammation and fatal acute-on-chronic liver failure. *Liver Int* 2020;40(6):1457–1466.
10. Møller S, Bernardi M. Interactions of the heart and the liver. *Eur Heart J* 2013;34(36):2804–2811.
11. Izzy M, VanWagner LB, Lin G, et al. Redefining cirrhotic cardiomyopathy for the modern era. *Hepatology* 2020;71(1):334–345.
12. Haaf P, Garg P, Messroghli DR, Broadbent DA, Greenwood JP, Plein S. Cardiac T1 mapping and extracellular volume (ECV) in clinical practice: a comprehensive review. *J Cardiovasc Magn Reson* 2016;18(1):89.
13. Luetkens JA, Doerner J, Thomas DK, et al. Acute myocarditis: multiparametric cardiac MR imaging. *Radiology* 2014;273(2):383–392.
14. Luetkens JA, Faron A, Isaak A, et al. Comparison of original and 2018 Lake Louise Criteria for diagnosis of acute myocarditis: results of a validation cohort. *Radiol Cardiothorac Imaging* 2019;1(3):e190010.
15. Luetkens JA, Schlesinger-Irsch U, Kuetting DL, et al. Feature-tracking myocardial strain analysis in acute myocarditis: diagnostic value and association with myocardial oedema. *Eur Radiol* 2017;27(11):4661–4671.
16. Luetkens JA, Klein S, Träber F, et al. Quantification of liver fibrosis at T1 and T2 mapping with extracellular volume fraction MRI: preclinical results. *Radiology* 2018;288(3):748–754.
17. Kennedy P, Wagner M, Castéra L, et al. Quantitative elastography methods in liver disease: current evidence and future directions. *Radiology* 2018;286(3):738–763.
18. Messroghli DR, Radjenovic A, Kozerke S, Higgins DM, Sivananthan MU, Ridgway JP. Modified look-locker inversion recovery (MOLLI) for high-resolution T1 mapping of the heart. *Magn Reson Med* 2004;52(1):141–146.
19. Sprinkart AM, Luetkens JA, Träber F, et al. Gradient spin echo (GraSE) imaging for fast myocardial T2 mapping. *J Cardiovasc Magn Reson* 2015;17(1):12.
20. Schulz-Menger J, Bluemke DA, Bremerich J, et al. Standardized image interpretation and post processing in cardiovascular magnetic resonance: Society for Cardiovascular Magnetic Resonance (SCMR) board of trustees task force on standardized post processing. *J Cardiovasc Magn Reson* 2013;15(1):35.
21. Luetkens JA, Petry P, Kuetting D, et al. Left and right ventricular strain in the course of acute myocarditis: a cardiovascular magnetic resonance study. *Rofo* 2018;190(8):722–732.
22. Rothman KJ. No adjustments are needed for multiple comparisons. *Epidemiology* 1990;1(1):43–46.
23. Lossnitzer D, Steen H, Zahn A, et al. Myocardial late gadolinium enhancement cardiovascular magnetic resonance in patients with cirrhosis. *J Cardiovasc Magn Reson* 2010;12(1):47.
24. Wiese S, Hove J, Mo S, et al. Myocardial extracellular volume quantified by magnetic resonance is increased in cirrhosis and related to poor outcome. *Liver Int* 2018;38(9):1614–1623.
25. Lee YB, Lee J-H. Cirrhotic cardiomyopathy: an independent prognostic factor for cirrhotic patients. *Clin Mol Hepatol* 2018;24(4):372–373.
26. Reese-Petersen AL, Wiese S, Moeller S, Genovese S. Myocardial fibrosis is reflected by two novel biomarkers of collagen formation in patients with cirrhosis: results from a prospective study with advanced cardiac MRI. *Eur Heart J* 2018;39(suppl\_1):.
27. Luetkens JA, Homs R, Sprinkart AM, et al. Incremental value of quantitative CMR including parametric mapping for the diagnosis of acute myocarditis. *Eur Heart J Cardiovasc Imaging* 2016;17(2):154–161.
28. Yang YY, Liu H, Nam SW, Kunos G, Lee SS. Mechanisms of TNFalpha-induced cardiac dysfunction in cholestatic bile duct-ligated mice: interaction between TNFalpha and endocannabinoids. *J Hepatol* 2010;53(2):298–306.
29. Sampaio F, Pimenta J, Bettencourt N, et al. Systolic and diastolic dysfunction in cirrhosis: a tissue-Doppler and speckle tracking echocardiography study. *Liver Int* 2013;33(8):1158–1165.
30. Hammami R, Boudabbous M, Jdidi J, et al. Cirrhotic cardiomyopathy: is there any correlation between the stage of cardiac impairment and the severity of liver disease? *Libyan J Med* 2017;12(1):1283162.
31. Banerjee R, Pavlides M, Tunnicliffe EM, et al. Multiparametric magnetic resonance for the non-invasive diagnosis of liver disease. *J Hepatol* 2014;60(1):69–77.
32. Tunnicliffe EM, Banerjee R, Pavlides M, Neubauer S, Robson MD. A model for hepatic fibrosis: the competing effects of cell loss and iron on shortened modified Look-Locker inversion recovery T<sub>1</sub> (shMOLLI-T<sub>1</sub>) in the liver. *J Magn Reson Imaging* 2017;45(2):450–462.
33. Bernardi M, Rubboli A, Trevisani F, et al. Reduced cardiovascular responsiveness to exercise-induced sympathoadrenergic stimulation in patients with cirrhosis. *J Hepatol* 1991;12(2):207–216.
34. Lee SS, Marty J, Mantz J, Samain E, Braillon A, Lebrec D. Desensitization of myocardial beta-adrenergic receptors in cirrhotic rats. *Hepatology* 1990;12(3 Pt 1):481–485.
35. Srinivasa Babu A, Wells ML, Teytelboym OM, et al. Elastography in chronic liver disease: modalities, techniques, limitations, and future directions. *RadioGraphics* 2016;36(7):1987–2006.
36. Weng Z, Yao J, Chan RH, et al. Prognostic value of LGE-CMR in HCM: a meta-analysis. *JACC Cardiovasc Imaging* 2016;9(12):1392–1402.
37. Becker MAJ, Cornel JH, van de Ven PM, van Rossum AC, Allaart CP, Germans T. The prognostic value of late gadolinium-enhanced cardiac magnetic resonance imaging in nonischemic dilated cardiomyopathy: a review and meta-analysis. *JACC Cardiovasc Imaging* 2018;11(9):1274–1284.
38. Kuruvilla S, Adenaw N, Katwal AB, Lipinski MJ, Kramer CM, Salerno M. Late gadolinium enhancement on cardiac magnetic resonance predicts adverse cardiovascular outcomes in nonischemic cardiomyopathy: a systematic review and meta-analysis. *Circ Cardiovasc Imaging* 2014;7(2):250–258.

## 4. Diskussion

In den Arbeiten dieser kumulativen Habilitationsschrift wurde die diagnostische Wertigkeit der quantitativen kardialen MRT bei erworbenen primären Kardiomyopathien sowie bei sekundären Kardiomyopathien herausgearbeitet. Die einzelnen Arbeiten untersuchen insbesondere die klinische Anwendung neuer sensitiver quantitativer MRT-Biomarker und legen den Schwerpunkt auf die Detektion myokardialer Inflammation. Die Ergebnisse dieser Arbeit tragen dazu bei, spezifische erworbene Kardiomyopathien genauer und früher diagnostizieren zu können. Ferner wird die Möglichkeit der frühzeitigen, subklinischen Detektion einer potenziellen sekundären kardialen Beteiligung aufgezeigt, die das zeitnahe Ergreifen präventiver Maßnahmen und therapeutischer Anpassungen ermöglichen kann. Die Arbeiten verdeutlichen den hohen diagnostischen Wert der quantitativen kardialen MRT für Patient/-innen mit dem Risiko einer sekundären Herzbeteiligung und drängen insgesamt auf eine breitere Verfügbarkeit in der klinischen Routine. Vor dem Hintergrund der durch Kardiomyopathien verursachten Komplikationen, wie der Herzinsuffizienz und dem plötzlichen Herztod, könnte die Früherkennung einer kardialen Beteiligung eine prognostisch entscheidende Rolle bei Patient/-innen mit Systemerkrankungen oder Systemtherapien spielen.

Die kardiale MRT hat sich in den letzten Jahrzehnten zum absoluten Goldstandard für die nicht-invasive bildgebende Diagnostik von nicht-ischämischen Kardiomyopathien entwickelt (Bluemke and Teague, 2019; Karamitsos et al., 2020). Die myokardiale Gewebecharakterisierung konnte in den letzten Jahren durch die Neuentwicklung quantitativer MRT-Verfahren (myokardiales Mapping) entscheidend verbessert werden und erlaubt eine sensitivere Detektion pathologischer Myokardveränderungen (Messroghli et al., 2017). Aus diesem Grund wurden Mapping-Techniken vor kurzem in die MRT-Diagnosekriterien der nicht-ischämischen myokardialen Inflammation (Myokarditis) aufgenommen (Ferreira et al., 2018).

Unsere Ergebnisse knüpfen an diese Entwicklungen an und zeigen, dass ein klinischer Einsatz der Mapping-Techniken auch in spezifischen Kohorten wie der pädiatrischen Myokarditis einen zusätzlichen diagnostischen Nutzen hat und eine exzellente Verlaufsbeurteilung erlaubt. Obwohl die akute Myokarditis bei Kindern eher selten ist (geschätzte Inzidenz von ca. 1-2 pro 100.000 Kinder (Arola et al., 2017)) ist diese der Grund für etwa ein Drittel der

dilatativen Kardiomyopathien im Kindesalter und bekanntermaßen mit dem plötzlichen Herztod assoziiert (Canter et al., 2014). Eine hohe Dunkelziffer unerkannter und subklinisch verlaufender Myokarditiden im Kindes- und Jugendalter wird vermutet (Canter et al., 2014). Aus diesem Grund ist eine genaue Diagnose und die Möglichkeit der Verlaufsbeurteilung der entzündlichen Aktivität im Kindesalter besonders wichtig. Der diagnostische Mehrwert der 2018 Lake-Louise-Kriterien gegenüber den Kriterien von 2009 wurde zuvor jedoch nur für erwachsene Kohorten evaluiert (Luetkens et al., 2019a; Li et al., 2021). Eine MRT-Studie zeigte bereits einen prinzipiellen Mehrwert der Mapping-Techniken auch in einer pädiatrischen Kohorte (Cornicelli et al., 2019). Darauf aufbauend bestätigte unsere Studie, dass die Anwendung der 2018 Diagnosekriterien auch in einer pädiatrischen Myokarditis-Kohorte eine höhere diagnostische Performance aufweist als die originalen Lake-Louise-Kriterien. Dies lässt sich in erster Linie durch die zusätzliche Detektion diffuser myokardialer Inflammationsmuster erklären (z.B. bei diffuser lymphozytärer Myokarditis, chronischer Myokarditis oder bereits in Rekonvaleszenz befindlicher Myokarditis). Gleichzeitig erlauben die Mapping-Techniken eine kontrastmittelfreie Beurteilung der myokardialen Entzündungsaktivität und können so prinzipiell zur Bildung eines kontrastmittelfreien diagnostischen Scores genutzt werden, der eine ähnliche diagnostische Genauigkeit wie die 2018 Lake-Louise-Kriterien aufwies (Isaak et al., 2021a). Das T2-Mapping gilt als spezifischster Parameter zur Beurteilung des Myokardödems (Messroghli et al., 2017) und stellte sich in unserer Kohorte als sensitivster Einzelparameter für die Diagnose der pädiatrischen Myokarditis heraus. Darüber hinaus korrelierte dieser mit der Krankheitsschwere (z.B. mit der Notwendigkeit zur intensivmedizinischen Aufnahme sowie der Dauer des intensivstationären Aufenthalts). Da die quantitativen Mapping-Techniken eine exzellente Verlaufsbeurteilung der Entzündungsaktivität bei Patient/-innen mit akuter Myokarditis bieten, eignen sie sich auch für Nachsorgeuntersuchungen (Luetkens et al., 2016b; Aquaro et al., 2017), z.B. von Patient/-innen mit persistierender Symptomatik, initial fulminantem Krankheitsverlauf oder bildgebend ausgedehntem Entzündungsbefund.

Gleichzeitig erlaubt die Kardio-MRT eine Prognoseabschätzung anhand der Lokalisation der myokardialen Nekrose bzw. Fibrose (Aquaro et al., 2019). Hingegen deutet eine aktuelle Studie darauf hin, dass nicht-ischämische LGE-Läsionen in funktionell und morphologisch normalen Herzen nicht zwingend mit einem schlechteren Outcome assoziiert sind (Lota et al., 2021). Zukünftige Studien müssen nun klären, ob die Befunde in der LGE-Bildgebung eine

klinisch relevante Prognoseabschätzung in Abhängigkeit der jeweiligen Kardiomyopathie bzw. der zugrunde liegenden Systemerkrankung bieten, und in wieweit auch Mapping-Parameter durch die Detektion des diffusen Myokardödems und der interstitiellen Fibrose eine langfristige Prognoseabschätzung erlauben (Petersen and Khanji, 2021; Li et al., 2022).

Obwohl die Diagnose der akuten Myokarditis meist anhand der Darstellung von entzündlichen Nekrosen in der LGE-Bildgebung gelingt, ist diese Technik bei der Detektion von diffuser Inflammation ungenau (Lurz et al., 2016; Gräni et al., 2019). So ist die Beurteilung des diffusen Myokardödems mittels T2-gewichteten Sequenzen bzw. der diffusen Inflammation oder Fibrose mittels LGE methodenbedingt nur in qualitativer (visuelle Erhebung) und semi-quantitativer Form (Vergleich mit Referenzgewebe) möglich. Diverse Kardiomyopathien sind jedoch von rein diffusen inflammatorischen Myokardveränderungen geprägt. Bei den primären erworbenen Kardiomyopathien gehören hierzu in erster Linie die Tako-Tsubo Kardiomyopathie und die peripartale Kardiomyopathie. Ergebnisse unserer Gruppe konnten zeigen, dass bei der Myokarditis (Dabir et al., 2019b) und der Tako-Tsubo Kardiomyopathie (Dabir et al., 2019a) selbst Myokardsegmente außerhalb visuell erfassbarer Pathologien eine mittels Mapping nachweisbare diffuse Mitbeteiligung aufwiesen. Die hohe Sensitivität der Techniken erlaubt so auch die Erfassung von in Rekonvaleszenz befindlichen Erkrankungen, bei denen die kardiale MRT erst nach der akuten Phase durchgeführt wird (z.B. bei normalisierter regionaler Wandbewegungsstörung im Rahmen der Tako-Tsubo Kardiomyopathie und noch persistierendem Myokardödem).

Die peripartale Kardiomyopathie ist eine seltene, lebensbedrohliche kardiale Schwangerschaftskomplikation und zeigt sich als dilatativer Kardiomyopathie-Phänotyp (Bauersachs et al., 2019). Für die Diagnose ist der Ausschluss diverser anderweitiger primärer und sekundärer kardialer Pathologien notwendig (v.a. Lungenarterienembolie), weshalb nach der initialen Durchführung der Echokardiographie eine erweiterte Diagnostik mittels kardialer MRT erfolgen sollte (Abklärung weiterer Differentialdiagnosen wie akute Myokarditis, Tako-Tsubo Kardiomyopathie, angeborene primäre Kardiomyopathie oder kongenitaler Herzfehler), sofern die entsprechende Verfügbarkeit und Expertise gegeben ist. Obwohl bei der peripartalen Kardiomyopathie Kontroversen zu Kontrastmittelmehranreicherungen in der LGE-Bildgebung bestehen, zeigten Multicenterstudien, dass derartige Veränderungen in der Gesamtkohorte selten sind (Schelbert et al., 2017; Ersbøll et al., 2018). Ähnliche Kontroversen



bestehen auch bei dem Thema Myokardödem, wobei die Kardio-MRT Untersuchungen in viele Studien außerhalb der akuten Präsentation und ohne quantitative Techniken durchgeführt wurden (Ricci et al., 2020). Einige Kardio-MRT Studien mit Untersuchungen zum Zeitpunkt der akuten Symptomatik fanden Zeichen des diffusen Myokardödems mittels semi-quantitativem Ansatz der T2-Ödembildgebung (Renz et al., 2011) sowie mittels quantitativer Mapping-Techniken (Liang et al., 2020). In unserer Studie konnten wir ebenfalls das Vorliegen eines diffusen Myokardödems in der Mehrzahl der Patientinnen mit peripartaler Kardiomyopathie aufzeigen. Darüber hinaus wiesen Patientinnen mit fehlendem Myokardödem und eingeschränkten linksventrikulären Strain-Parametern eine verzögerte langfristige Erholung der linksventrikulären Ejektionsfraktion auf. Derartige Konstellationen, bei denen das Myokardödem eine prinzipielle funktionelle Reversibilität darstellt und dessen Fehlen mit irreversiblen Funktionseinschränken einhergeht, sind z.B. auch bei der Myokarditis vorbeschrieben (Vermees et al., 2014). Insgesamt konnten wir aufzeigen, dass die diffuse myokardiale Inflammation (in Form eines globalen Myokardödems) in der akuten Phase der peripartalen Kardiomyopathie mittels quantitativer kardialer MRT detektierbar ist und eine derartige Gewebecharakterisierung sowohl diagnostische also auch prognostische Informationen liefern kann. Dies verdeutlicht den besonderen Stellenwert der quantitativen MRT-Techniken bei Myokarderkrankungen mit primär diffuser Manifestation, die mit dem alleinigen Einsatz konventioneller Techniken übersehen werden könnten.

Die Kardiokonkologie ist ein neues Interessengebiet, das sich auf die Erkennung, Überwachung und Behandlung von Herz-Kreislauf-Erkrankungen konzentriert, die als Nebenwirkungen onkologischer Therapien auftreten können. Dabei ist die frühzeitige Detektion kardiotoxischer Myokardpathologien von zentraler Bedeutung. Sind kardiotoxische Effekte bei den konventionellen Chemotherapien wie den Anthrazyklinen und den Alkylantien bereits langjährig bekannt, werden nun auch bei modernen zielgerichteteren und immun-basierten onkologischen Therapien spezifische kardiale Nebenwirkungen beobachtet (Harries et al., 2020). Bei den neuen ICI-Therapien wurde ein erweitertes Spektrum an immun-vermittelter Nebenwirkungen beschrieben, u.a. seltene, aber fulminant verlaufende Myokarditiden (Johnson et al., 2016; Amiri-Kordestani et al., 2018). Nach derzeitigem Wissensstand ist die Immuntherapie-vermittelte Kardiotoxizität zwar eine relativ seltene Nebenwirkung (wobei die tatsächliche Inzidenz derzeit unbekannt ist), jedoch ist diese oft mit einem besonders fulminanten, potenziell tödlichen Verlauf assoziiert (Lyon et al., 2018). Deshalb wurde



vermutet, dass möglicherweise aufgrund des mangelnden Bewusstseins und der unzureichenden Sensitivität der kardialen Primärdiagnostik nur schwere Fälle kardialer Nebenwirkungen gemeldet wurden. In diesem Zusammenhang hat ein Expertengremium eine Klassifikation für die ICI-induzierte Myokarditis vorgeschlagen, in der diese entsprechend ihres klinischen Verlaufs als fulminant, nicht-fulminant aber klinisch-signifikant oder subklinisch eingeteilt werden kann (Bonaca et al., 2019). Das Vorliegen von subklinischer Inflammation unter ICI-Therapie war bis dahin und ist auch noch heute unzureichend untersucht.

Unsere prospektive intra-individuelle Vergleichsstudie zielte darauf ab das Ausmaß der Herzschädigung bzw. -entzündung im Zusammenhang mit der ICI-Therapie mittels quantitativer kardialer MRT zu ermitteln. Nur Studienteilnehmer/-innen ohne vorbekannte Herzerkrankung wurden eingeschlossen. Wir fanden eine deutlich zunehmende Last an subklinischen Herzveränderungen unter ICI-Therapie, einschließlich diffuser myokardialer Inflammation und systolischer Dysfunktion (Faron, Isaak et al., 2021). So zeigten Studienteilnehmer/-innen im Verlaufs-Kardio-MRT nach ICI-Therapieeinleitung eine globale Erhöhung der myokardialen T1- und T2-Relaxationszeiten und wiesen ein vermehrtes Auftreten kleinerer Perikardergüsse auf (Faron, Isaak et al., 2021). Unsere Studie bestätigt die Hypothese, dass eine subklinische ICI-vermittelte Kardiotoxizität häufiger vorliegt als initial vermutet und das Risiko fulminanter Verläufe möglicherweise frühzeitig mittels Kardio-MRT erfasst werden könnte. Obwohl nach der oben aufgeführten Klassifikation alle Studienteilnehmer/-innen mit Zeichen der diffusen myokardialen Inflammation prinzipiell als subklinische ICI-Myokarditis eingestuft wurden (keine kardiale Symptomatik), zeigte sich bei einer Patientin (5 %) im Verlaufs-MRT der Befund einer akuten Myokarditis mit daraufhin eingeleiteter stationärer Aufnahme und fulminantem, letalem Verlauf (Faron et al., 2021). Da fokale Befunde bei der ICI-induzierten Kardiomyopathie oft fehlen können (Escudier et al., 2017; Zhang et al., 2020) und diffuse Veränderungen mit den konventionellen Kardio-MRT Techniken nur schwer und unzuverlässig detektierbar sind und nur eingeschränkt verlaufsbeurteilt werden können, unterstreicht unsere Studie den besonderen Wert der quantitativen Mapping-Techniken bei den toxischen bzw. therapieassoziierten Kardiomyopathien. Eine Kardio-MRT-Studie mit histopathologischen Analysen zeigte, dass die ICI-induzierte Myokarditis sich nahezu ausschließlich (bis zu 98 %) durch eine (diffuse) lymphozytäre Herzmuskelinfiltration auszeichnet, die das Korrelat des diffusen Myokardödems im Kardio-MRT sein kann (Zhang et al., 2020). Gleichzeitig zeigt diese Studie,

dass mehr als 50 % der Patient/-innen mit ICI-Myokarditis ein unauffälliges Kardio-MRT aufwiesen – wobei quantitative Parameter nicht verfügbar waren (Zhang et al., 2020). Die Ergebnisse dieser Studie deuten darauf hin, dass bei klinischem Verdacht auf eine ICI-assoziierte Myokarditis und fehlenden Auffälligkeiten im Kardio-MRT, allein basierend auf LGE und konventioneller T2-gewichteter Ödembildgebung, die Diagnose nicht sicher ausgeschlossen werden kann, sodass bei persistierendem klinischen Verdacht eine endomyokardiale Biopsie in Erwägung gezogen werden sollte (Zhang et al., 2020). Eine aktuelle Multicenterstudie zeigt, dass die zusätzliche Verwendung von Mapping-Techniken und die Anwendung der 2018 Lake-Louise-Kriterien einen hohen diagnostischen Wert bei Patient/-innen mit einer ICI-Myokarditis hat und das T1-Mapping darüber hinaus ein unabhängiger Prädiktor für das Auftreten von schwerwiegenden unerwünschten kardiovaskulären Ereignissen ist (Thavendiranathan et al., 2021). Eine weitere aktuelle Kardio-MRT-Studie zeigt, dass sich die bildgebenden Merkmale der ICI-Myokarditis von denen der typischen viralen Myokarditis unterscheiden scheinen und ein septales LGE ein Prädiktor für schwere kardiovaskuläre Ereignisse sein kann (Cadour et al., 2022).

Darüber hinaus zeigt unsere Studie, dass Befunde im LGE allein ohne weitere begleitende klinische oder bildgebende Zeichen der Inflammation und ohne sichere Beurteilbarkeit ihrer Dynamik (kein MRT-Ausgangsbefund vor Therapieinitiierung) differenziert bewertet werden sollten. So wiesen 32 % der Studienteilnehmer/-innen in unserer Studie trotz anamnestisch nicht vorbekannter Herzerkrankung bereits bei der Erstuntersuchung, also vor ICI-Therapie, nicht-ischämische myokardiale Mehranreicherungen im LGE auf (myokardiale Fibrose) (Faron et al., 2021). Derartige Befunde allein, ohne begleitende klinische oder bildgebende Zeichen der aktiven Inflammation, können in onkologischen Kardio-MRT Querschnittsstudien und in der klinischen Routine somit fälschlicherweise als ICI-vermittelter Effekt gewertet werden (falsch-positive Diagnose, möglicherweise mit Relevanz für die onkologische Therapie).

Das Vorhandensein von nicht-ischämischer Fibrose bei Patient/-innen ohne vorbekannte Herzerkrankung ist also nicht gänzlich ungewöhnlich und kann z.B. auf eine zurückliegende, subklinisch verlaufende Myokarditis oder auf eine kardiale Beteiligung im Rahmen diverser chronischer Systemerkrankungen zurückzuführen sein (sekundäre Kardiomyopathien nach AHA (Maron et al., 2006)). Derartige Herzbeteiligungen verlaufen oft ohne oder mit einer vollkommen unspezifischen kardialen Symptomatik und werden größtenteils erst im

Spätstadium erkannt. Da die Myokardfibrose bei diversen Kardiomyopathien als arrhythmogenes Substrat nachgewiesen wurde und mit dem plötzlichen Herztod in Verbindung gebracht wird, kann ihr Nachweis prognostisch relevant sein (Kuruville et al., 2014; Disertori et al., 2016; Zorzi et al., 2016). So konnte unsere Gruppe bei kardial asymptomatischen Patient/-innen mit myotoner Dystrophie Typ 1 und 2 (Gruppe der neuromuskulären Erkrankungen), eine hohe Last an fokaler und diffuser Myokardfibrose nachweisen (Luetkens et al., 2019b). In vorherigen Studien bei Patient/-innen mit myotoner Dystrophie wurde das Vorhandensein von fokaler Myokardfibrose mit pathologischen EKG-Veränderungen in Verbindung gebracht (Hermans et al., 2012; Schmachl et al., 2016), was auf einen direkten Zusammenhang zwischen einer strukturellen Herzbeteiligung (sekundäre Kardiomyopathie) und der Entwicklung von Herzrhythmusstörungen schließen lässt.

Am Beispiel der zirrhotischen Kardiomyopathie zeigt die letzte Arbeit, dass die quantitative MRT eine wichtige diagnostische und damit möglicherweise auch prognostische Rolle bei sekundären Kardiomyopathien spielen kann. Sie zeigt, dass Systemerkrankungen mit einer erheblichen Last an kardialen Pathologien einhergehen können, die lange subklinisch verlaufen, in körperlichen Stresssituationen (z.B. Dekompensation der Grunderkrankung, Infektion, operativer oder interventioneller Eingriff) jedoch klinisch apparent werden können. Obwohl sich die pathophysiologischen Mechanismen je nach Systemerkrankung unterscheiden und in der absoluten Mehrheit nicht vollständig verstanden sind, werden den Mechanismen der systemischen Inflammation und Fibrogenese eine entscheidende Rolle bei einer derartigen Herzbeteiligung zugesprochen. Die zirrhotische Kardiomyopathie ist eine besondere Form der sekundären Kardiomyopathien. Man vermutet, dass diese vor allem durch funktionelle Veränderungen der Hämodynamik bei der Leberzirrhose entsteht (Zardi et al., 2010; Møller and Bernardi, 2013). Obwohl dieses klinische Syndrom bereits vor Jahrzehnten abgrenzend zur alkoholischen Kardiomyopathie beschrieben wurde (Kowalski and Abelmann, 1953; Ma and Lee, 1996), sind die zugrunde liegenden funktionellen und strukturellen Herzveränderungen unzureichend untersucht.

In unserer prospektiven quantitativen Cardio-MRT-Studie zeigten Studienteilnehmer/-innen mit Leberzirrhose eine hohe Last an subklinischen Herzmuskelpathologien, u.a. Merkmale der myokardialen Inflammation, myokardialen Fibrose und systolischen Dysfunktion bei Zeichen der hyperdynamen Zirkulation. Dabei kam es mit Zunahme des Child-Pugh-Scores auch zu

einer Zunahme dieser Myokardpathologien (insbesondere Erhöhung der myokardialen T1- und T2-Relaxationszeiten und des ECV sowie zunehmende Häufung der fokalen LGE-Läsionen (Isaak et al., 2020)). Die Kombination der verschiedenen kardialen Parameter lässt darauf schließen, dass sowohl die diffuse Fibrose, als auch die diffuse Inflammation, myokardiale Gewebemerkmale der zirrhotischen Kardiomyopathie darstellen könnten und insbesondere in fortgeschrittenen Stadien der Leberzirrhose auftreten. Zudem lag vor allem bei den fortgeschritteneren Leberzirrhose-Stadien eine hohe Last an fokaler, also bereits visuell sichtbarer Fibrose vor. Dabei fanden wir keinen Gruppenunterschied zwischen Studienteilnehmer/-innen mit alkoholtoxischer und nicht-alkoholtoxischer Leberzirrhose. Unsere Ergebnisse werden von vorherigen Studien gestützt, die bei Patient/-innen mit Leberzirrhose ebenfalls eine Häufung nicht-ischämischer myokardialer LGE-Läsionen (Lossnitzer et al., 2010) sowie eine Erhöhung der myokardialen ECV-Werte (Wiese et al., 2018) beschreiben. Gründe für diese strukturellen Myokardveränderungen im Rahmen der Leberzirrhose können neben der sogenannten hyperdynamen Zirkulation und der damit verbundenen höheren Arbeitsbelastung des Herzens (höherer Herzindex) (Zardi et al., 2010), auch systemische Mechanismen der Fibrogenese sein (Wiese et al., 2020).

Wie bereits ausgeführt, spielt das T2-Mapping eine wesentliche Rolle bei der Diagnose von diffus-entzündlichen Herzmuskelerkrankungen. Dies wurde im Zusammenhang mit der zirrhotischen Kardiomyopathie bislang jedoch unzureichend untersucht. Unsere Ergebnisse zeigen Zeichen des diffusen Myokardödems (global erhöhte myokardiale T2-Relaxationszeiten), die mit einer subklinischen myokardialen Inflammation vereinbar sind (Isaak et al., 2020). Damit unterstützt unsere Studie die zunehmend etablierte Hypothese der systemischen Inflammation im Rahmen der Leberzirrhose (Bernardi et al., 2015; Matyas et al., 2020; Praktiknjo et al., 2020).

Überdies konnten wir durch die erstmalige Etablierung einer kombinierten multiparametrischen Herz-Leber-MRT direkte Korrelationen zwischen kardialen und hepatischen MRT-Biomarkern aufzeigen, die auf einen Zusammenhang zwischen dem Grad der Leber- und Herzerkrankung hinweisen. So korrelierte die MR-Elastographie-basierte Lebersteifigkeit (etablierter nicht-invasiver Fibroseparameter) mit den quantitativen Herzparametern und zeigte sich als unabhängiger Prädiktor für das Vorliegen von nicht-ischämischem LGE (Myokardfibrose). Ein Steifigkeitswert über 9,2 kPa erreichte eine

Sensitivität von ca. 77 % und eine Spezifität von ca. 75 % für das Vorliegen von LGE-Läsionen (Isaak et al., 2020). Dieser Zusammenhang zwischen bildgebungsbasierter hepatischer und myokardialer Erkrankungsschwere deutet darauf hin, dass Leberzirrhose-vermittelte systemische Mechanismen der Inflammation und Fibrogenese zur Bildung der zirrhotischen Kardiomyopathie führen könnten.

Die Relevanz der modernen kardialen MRT zeigt sich in Bezug auf die Diagnostik erworbener bzw. sekundärer Kardiomyopathie schließlich auch in der aktuellen Pandemie der Coronavirus-Krankheit (COVID-19). Diese spielt derzeit inklusive ihrer quantitativen Techniken eine wesentliche Rolle bei der Erforschung COVID-19-assoziiierter Herzmuskelveränderungen (Clerkin et al., 2020; Puntmann et al., 2020; Starekova et al., 2021). Unsere Gruppe konnte den diagnostischen Wert der quantitativen Kardio-MRT im akuten Erkrankungsstadium (Luetkens et al., 2020; Luetkens et al., 2021) (Myokardschädigung nach aktuellen Hypothesen durch direkten Virusbefall oder Zytokin-Freisetzungssyndrom bzw. Zytokinsturm (Clerkin et al., 2020)), bei Nachsorgeuntersuchungen nach durchgemachter Infektion und persistierender Symptomatik (Kravchenko et al., 2021) oder bei potenziellen Impfnebenwirkungen (Isaak et al., 2021b; Kravchenko et al., 2022) aufzeigen. In Anbetracht des diffus-inflammatorischen myokardialen Erkrankungsmusters, der im Zusammenhang mit systemisch-inflammatorischen Immunreaktionen diskutiert wird, zeigt sich der besondere Wert der Mapping-Techniken (Luetkens et al., 2020). Hier sind weitere Studien zur prognostischen Relevanz dieser Befunde in Bezug auf die unmittelbare und langfristige Patientenversorgung notwendig.

Die der vorgelegten Habilitationsschrift zugrunde liegenden Arbeiten weisen gewisse Limitationen auf. Die Studien haben eine limitierte Gruppengröße, die teilweise auf die Seltenheit der Entitäten zurückzuführen ist, und einen primär explorativen Ansatz. Folgestudien sind notwendig, bevor unsere Ergebnisse generalisiert werden können. Insgesamt konnte dennoch ein diagnostischer Nutzen durch die klinische Anwendung quantitativer Kardio-MRT Verfahren gezeigt werden. Weitere Studien mit histopathologischer Korrelation unter Einbezug verschiedener Myokarditis-Typen, insbesondere der chronisch-diffusen Inflammation, sind notwendig, um die diagnostische Wertigkeit der neuen Lake-Louise-Kriterien für sekundäre Kardiomyopathien zu bestimmen. Gleichzeitig sind Folgestudien zur prognostischen Relevanz der erhobenen Kardio-MRT Befunde erforderlich. In Anbetracht der Seltenheit mancher Entitäten sind insbesondere bei sekundären

Kardiomyopathien weitere Multicenterstudien oder Registerstudien wünschenswert, um noch detailliertere Korrelationen zwischen klinischen und bildgebenden Parametern der jeweiligen Grund- bzw. Systemerkrankung zu ermöglichen. Dabei können die Methoden der quantitativen kardialen MRT durch den Einsatz neuer Verfahren basierend auf der künstlichen Intelligenz und „Radionomics“ nochmals erweitert werden und dazu beitragen, in Zukunft noch spezifischere strukturelle und funktionelle Charakteristika in der heterogenen Gruppe der nicht-ischämischen Kardiomyopathien zu erkennen.

## 5. Zusammenfassung

Die Gruppe der erworbenen primären und sekundären Kardiomyopathien hat über die Kardiologie hinaus eine erhebliche klinische Relevanz für unterschiedliche Fachrichtungen. Kardiale Beteiligungen im Rahmen von Systemerkrankungen oder Systemtherapien bleiben oft unerkannt. Aufgrund des Fehlens von einfach detektierbaren phänotypischen Merkmalen ist für ihre Diagnose eine umfassende myokardiale Gewebecharakterisierung essenziell, die mittels moderner kardialer MRT gelingen könnte. Zusammenfassend wurden in der vorgelegten Habilitationsschrift neuartige quantitative Methoden der kardialen MRT für die klinische Anwendung bei erworbenen primären und sekundären Kardiomyopathien evaluiert. Ein besonderer Schwerpunkt lag dabei auf der Detektion von diffuser myokardialer Inflammation.

Dazu wurden die neuen MRT-Diagnosekriterien (2018 Lake-Louise-Kriterien) für nicht-ischämische myokardiale Inflammation in einer spezifischen Kohorte (pädiatrische Myokarditis) validiert und ein Mehrwert für die Basis- und Verlaufsdagnostik in Bezug auf konventionelle MRT-Parameter aufgezeigt. Vor dem Hintergrund der aktuellen Kontrastmitteldebatte konnte unter Verwendung der Mapping-Techniken eine gute diagnostische Performance eines kontrastmittelfreien Scores bei Kindern und Jugendlichen gezeigt werden.

Bei der peripartalen Kardiomyopathie wurde neben der systolischen Funktionsstörung das diffuse Myokardödem als wichtiges strukturelles Erkrankungsmerkmal herausgearbeitet, welches darüber hinaus auch einen prognostischen Mehrwert aufwies. Aufgrund des Fehlens visuell fassbarer struktureller Myokardpathologien bei dieser seltenen Kardiomyopathie zeigte die quantitative kardiale MRT hier einen wichtigen diagnostischen Wert.

Übergreifend zu den sekundären Kardiomyopathien unterstreichen die vorgelegten Ergebnisse den hohen Stellenwert der quantitativen MRT-Techniken bei subklinisch verlaufenden Myokarderkrankungen. Die vorgelegten Ergebnisse charakterisieren zum einen die subklinische Form der ICI-Myokarditis und zeigen darüber hinaus, dass die quantitativen Techniken diffuse inflammatorische Myokardveränderungen unter ICI-Therapie bereits frühzeitig detektieren können. Obwohl die ICI-vermittelte Myokarditis eine äußerst seltene immuntherapeutische Komplikation ist, zeigen sich im Falle ihres Auftretens meist fulminante Verläufe, die so unter Umständen früher erkannt und im Verlauf überwacht werden können.



Ferner wurde anhand der zirrhotischen Kardiomyopathie demonstriert, dass eine gleichzeitige Untersuchung sowohl der sekundären kardialen Beteiligung als auch der Grunderkrankung selbst mittels multiparametrischer MRT klinisch realisierbar ist und eine organübergreifende Korrelation bildgebender Biomarker ermöglicht. Neben dem Vorliegen von myokardialer Fibrose konnten wir auch Zeichen der diffusen myokardialen Inflammation nachweisen, die eine mögliche neue wichtige Komponente der zirrhotischen Kardiomyopathie sein könnte und bestehende Hypothesen zur systemischen Inflammation stützt. Darüber hinaus konnten wir eine Zunahme der Herzveränderungen mit Zunahme des klinischen und bildgebenden Grades der Leberzirrhose aufzeigen. Diese Ergebnisse können zu einem besseren Verständnis der Leberzirrhose-vermittelten systemischen Inflammation und Fibrogenese beitragen.

Zusammenfassend erweitern diese Arbeiten das Verständnis für die klinische Anwendung der quantitativen kardialen MRT bei spezifischen nicht-ischämischen Kardiomyopathien und verdeutlichen die wichtige Rolle der neuen MRT-Biomarker im Rahmen der Diagnostik von diffuser myokardialer Inflammation.

## **6. Inhaltliche Überlappung mit anderen kumulativen Habilitationsschriften**

Inhaltliche Überlappungen mit anderen kumulativen Habilitationsschriften sind ausgeschlossen, da alle aufgeführten Originalarbeiten ausschließlich dieser und keiner anderen kumulativen Habilitationsschrift zugrunde liegen.

## 7. Bibliographie

Amiri-Kordestani, L., Moslehi, J., Cheng, J., Tang, S., Schroeder, R., Sridhara, R., Karg, K., Connolly, J., Beaver, J.A., and Blumenthal, G.M., et al. (2018). Cardiovascular adverse events in immune checkpoint inhibitor clinical trials: A U.S. Food and Drug Administration pooled analysis. *JCO* 36, 3009. [https://doi.org/10.1200/JCO.2018.36.15\\_suppl.3009](https://doi.org/10.1200/JCO.2018.36.15_suppl.3009).

Ammirati, E., Cipriani, M., Moro, C., Raineri, C., Pini, D., Sormani, P., Mantovani, R., Varrenti, M., Pedrotti, P., and Conca, C., et al. (2018). Clinical Presentation and Outcome in a Contemporary Cohort of Patients With Acute Myocarditis: Multicenter Lombardy Registry. *Circulation* 138, 1088-1099. <https://doi.org/10.1161/CIRCULATIONAHA.118.035319>.

Ammirati, E., Frigerio, M., Adler, E.D., Basso, C., Birnie, D.H., Brambatti, M., Friedrich, M.G., Klingel, K., Lehtonen, J., and Moslehi, J.J., et al. (2020). Management of Acute Myocarditis and Chronic Inflammatory Cardiomyopathy: An Expert Consensus Document. *Circulation. Heart failure* 13, e007405. <https://doi.org/10.1161/circheartfailure.120.007405>.

Aquaro, G.D., Ghebru Habtemicael, Y., Camastra, G., Monti, L., Dellegrottaglie, S., Moro, C., Lanzillo, C., Scatteia, A., Di Roma, M., and Pontone, G., et al. (2019). Prognostic Value of Repeating Cardiac Magnetic Resonance in Patients With Acute Myocarditis. *Journal of the American College of Cardiology* 74, 2439-2448. <https://doi.org/10.1016/j.jacc.2019.08.1061>.

Aquaro, G.D., Perfetti, M., Camastra, G., Monti, L., Dellegrottaglie, S., Moro, C., Pepe, A., Todiere, G., Lanzillo, C., and Scatteia, A., et al. (2017). Cardiac MR With Late Gadolinium Enhancement in Acute Myocarditis With Preserved Systolic Function: ITAMY Study. *Journal of the American College of Cardiology* 70, 1977-1987. <https://doi.org/10.1016/j.jacc.2017.08.044>.

Arola, A., Pikkarainen, E., Sipilä, J.O.T., Pykäri, J., Rautava, P., and Kytö, V. (2017). Occurrence and Features of Childhood Myocarditis: A Nationwide Study in Finland. *Journal of the American Heart Association* 6. <https://doi.org/10.1161/JAHA.116.005306>.

Bauersachs, J., König, T., van der Meer, P., Petrie, M.C., Hilfiker-Kleiner, D., Mbakwem, A., Hamdan, R., Jackson, A.M., Forsyth, P., and Boer, R.A. de, et al. (2019). Pathophysiology, diagnosis and management of peripartum cardiomyopathy: a position statement from the Heart Failure Association of the European Society of Cardiology Study Group on peripartum

cardiomyopathy. *European journal of heart failure* 21, 827-843. <https://doi.org/10.1002/ejhf.1493>.

Bernardi, M., Moreau, R., Angeli, P., Schnabl, B., and Arroyo, V. (2015). Mechanisms of decompensation and organ failure in cirrhosis: From peripheral arterial vasodilation to systemic inflammation hypothesis. *Journal of hepatology* 63, 1272-1284. <https://doi.org/10.1016/j.jhep.2015.07.004>.

Birnie, D.H., Nery, P.B., Ha, A.C., and Beanlands, R.S.B. (2016). Cardiac Sarcoidosis. *Journal of the American College of Cardiology* 68, 411-421. <https://doi.org/10.1016/j.jacc.2016.03.605>.

Bluemke, D.A., and Teague, S.D. (2019). *Diseases of the Chest, Breast, Heart and Vessels 2019-2022: Diagnostic and Interventional Imaging. Imaging of Nonischemic Cardiomyopathy (Cham (CH))*.

Bonaca, M.P., Olenchock, B.A., Salem, J.-E., Wiviott, S.D., Ederhy, S., Cohen, A., Stewart, G.C., Choueiri, T.K., Di Carli, M., and Allenbach, Y., et al. (2019). Myocarditis in the Setting of Cancer Therapeutics: Proposed Case Definitions for Emerging Clinical Syndromes in Cardio-Oncology. *Circulation* 140, 80-91. <https://doi.org/10.1161/circulationaha.118.034497>.

Buss, S.J., Breuninger, K., Lehrke, S., Voss, A., Galuschky, C., Lossnitzer, D., Andre, F., Ehlermann, P., Franke, J., and Taeger, T., et al. (2015). Assessment of myocardial deformation with cardiac magnetic resonance strain imaging improves risk stratification in patients with dilated cardiomyopathy. *European heart journal. Cardiovascular Imaging* 16, 307-315. <https://doi.org/10.1093/ehjci/jeu181>.

Cadour, F., Cautela, J., Rapacchi, S., Varoquaux, A., Habert, P., Arnaud, F., Jacquier, A., Meilhac, A., Paganelli, F., and Lalevée, N., et al. (2022). Cardiac MRI Features and Prognostic Value in Immune Checkpoint Inhibitor-induced Myocarditis. *Radiology*, 211765. <https://doi.org/10.1148/radiol.211765>.

Canter, C.E., Simpson, K.E., and Simpson, K.P. (2014). Diagnosis and treatment of myocarditis in children in the current era. *Circulation* 129, 115-128. <https://doi.org/10.1161/circulationaha.113.001372>.

Clerkin, K.J., Fried, J.A., Raikhelkar, J., Sayer, G., Griffin, J.M., Masoumi, A., Jain, S.S., Burkhoff, D., Kumaraiah, D., and Rabbani, L., et al. (2020). COVID-19 and Cardiovascular Disease. *Circulation* 141, 1648-1655. <https://doi.org/10.1161/CIRCULATIONAHA.120.046941>.

(2006). *Clinical magnetic resonance imaging* (Philadelphia, Pa.: Saunders Elsevier).

Collet, J.-P., Thiele, H., Barbato, E., Barthélémy, O., Bauersachs, J., Bhatt, D.L., Dendale, P., Dorobantu, M., Edvardsen, T., and Folliguet, T., et al. (2021). 2020 ESC Guidelines for the management of acute coronary syndromes in patients presenting without persistent ST-segment elevation. *European heart journal* 42, 1289-1367. <https://doi.org/10.1093/eurheartj/ehaa575>.

Corbalan, R., Bassand, J.-P., Illingworth, L., Ambrosio, G., Camm, A.J., Fitzmaurice, D.A., Fox, K.A.A., Goldhaber, S.Z., Goto, S., and Haas, S., et al. (2019). Analysis of Outcomes in Ischemic vs Nonischemic Cardiomyopathy in Patients With Atrial Fibrillation: A Report From the GARFIELD-AF Registry. *JAMA cardiology* 4, 526-548. <https://doi.org/10.1001/jamacardio.2018.4729>.

Cornicelli, M.D., Rigsby, C.K., Rychlik, K., Pahl, E., and Robinson, J.D. (2019). Diagnostic performance of cardiovascular magnetic resonance native T1 and T2 mapping in pediatric patients with acute myocarditis. *Journal of cardiovascular magnetic resonance : official journal of the Society for Cardiovascular Magnetic Resonance* 21. <https://doi.org/10.1186/s12968-019-0550-7>.

Corrado, D. (2001). Sudden cardiac death in young people with apparently normal heart. *Cardiovascular Research* 50, 399-408. [https://doi.org/10.1016/S0008-6363\(01\)00254-1](https://doi.org/10.1016/S0008-6363(01)00254-1).

Crouser, E.D., Ruden, E., Julian, M.W., and Raman, S.V. (2016). Resolution of abnormal cardiac MRI T2 signal following immune suppression for cardiac sarcoidosis. *Journal of investigative medicine : the official publication of the American Federation for Clinical Research* 64, 1148-1150. <https://doi.org/10.1136/jim-2016-000144>.

Dabir, D., Child, N., Kalra, A., Rogers, T., Gebker, R., Jabbour, A., Plein, S., Yu, C.-Y., Otton, J., and Kidambi, A., et al. (2014). Reference values for healthy human myocardium using a T1 mapping methodology: results from the International T1 Multicenter cardiovascular magnetic resonance study. *Journal of cardiovascular magnetic resonance : official journal of the Society for Cardiovascular Magnetic Resonance* 16, 69. <https://doi.org/10.1186/s12968-014-0069-x>.

Dabir, D., Luetkens, J., Kuetting, D., Nadal, J., Schild, H.H., and Thomas, D. (2021). Myokardiales Mapping bei systemischer Sarkoidose: ein Vergleich zweier Messansätze. *RoFo : Fortschritte*

auf dem Gebiete der Röntgenstrahlen und der Nuklearmedizin 193, 68-76.  
<https://doi.org/10.1055/a-1174-0537>.

Dabir, D., Luetkens, J., Kuetting, D.L.R., Feisst, A., Isaak, A., Schild, H.H., and Thomas, D. (2019a). Cardiac magnetic resonance including parametric mapping in acute Takotsubo syndrome: Preliminary findings. *European journal of radiology* 113, 217-224.  
<https://doi.org/10.1016/j.ejrad.2019.02.026>.

Dabir, D., Vollbrecht, T.M., Luetkens, J.A., Kuetting, D.L.R., Isaak, A., Feisst, A., Fimmers, R., Sprinkart, A.M., Schild, H.H., and Thomas, D. (2019b). Multiparametric cardiovascular magnetic resonance imaging in acute myocarditis: a comparison of different measurement approaches. *Journal of cardiovascular magnetic resonance : official journal of the Society for Cardiovascular Magnetic Resonance* 21, 54. <https://doi.org/10.1186/s12968-019-0568-x>.

DeFilippis, E.M., Beale, A., Martyn, T., Agarwal, A., Elkayam, U., Lam, C.S.P., and Hsieh, E. (2022). Heart Failure Subtypes and Cardiomyopathies in Women. *Circulation research* 130, 436-454. <https://doi.org/10.1161/CIRCRESAHA.121.319900>.

de Simone, F., De Simone, S.J., Messroghli, D., Andre, F., Lossnitzer, D., Seitz, S., Keller, M., Schnabel, P.A., Giannitsis, E., and Korosoglou, G., et al. (2015). T1 mapping in dilated cardiomyopathy with cardiac magnetic resonance: quantification of diffuse myocardial fibrosis and comparison with endomyocardial biopsy. *European heart journal. Cardiovascular Imaging* 16, 210-216. <https://doi.org/10.1093/ehjci/jeu183>.

Desai, A.S., Fang, J.C., Maisel, W.H., and Baughman, K.L. (2004). Implantable defibrillators for the prevention of mortality in patients with nonischemic cardiomyopathy: a meta-analysis of randomized controlled trials. *JAMA* 292, 2874-2879.  
<https://doi.org/10.1001/jama.292.23.2874>.

Disertori, M., Rigoni, M., Pace, N., Casolo, G., Masè, M., Gonzini, L., Lucci, D., Nollo, G., and Ravelli, F. (2016). Myocardial Fibrosis Assessment by LGE Is a Powerful Predictor of Ventricular Tachyarrhythmias in Ischemic and Nonischemic LV Dysfunction: A Meta-Analysis. *JACC. Cardiovascular imaging* 9, 1046-1055. <https://doi.org/10.1016/j.jcmg.2016.01.033>.

Dispenzieri, A., Kyle, R.A., Gertz, M.A., Therneau, T.M., Miller, W.L., Chandrasekaran, K., McConnell, J.P., Burritt, M.F., and Jaffe, A.S. (2003). Survival in patients with primary systemic

amyloidosis and raised serum cardiac troponins. *The Lancet* 361, 1787-1789. [https://doi.org/10.1016/S0140-6736\(03\)13396-X](https://doi.org/10.1016/S0140-6736(03)13396-X).

Dunlay, S.M., Givertz, M.M., Aguilar, D., Allen, L.A., Chan, M., Desai, A.S., Deswal, A., Dickson, V.V., Kosiborod, M.N., and Lekavich, C.L., et al. (2019). Type 2 Diabetes Mellitus and Heart Failure: A Scientific Statement From the American Heart Association and the Heart Failure Society of America: This statement does not represent an update of the 2017 ACC/AHA/HFSA heart failure guideline update. *Circulation* 140, e294-e324. <https://doi.org/10.1161/CIR.0000000000000691>.

Eitel, I., and Friedrich, M.G. (2011). T2-weighted cardiovascular magnetic resonance in acute cardiac disease. *Journal of cardiovascular magnetic resonance : official journal of the Society for Cardiovascular Magnetic Resonance* 13, 13. <https://doi.org/10.1186/1532-429X-13-13>.

Elliott, P., Andersson, B., Arbustini, E., Bilinska, Z., Cecchi, F., Charron, P., Dubourg, O., Kühl, U., Maisch, B., and McKenna, W.J., et al. (2008). Classification of the cardiomyopathies: a position statement from the European Society Of Cardiology Working Group on Myocardial and Pericardial Diseases. *European heart journal* 29, 270-276. <https://doi.org/10.1093/eurheartj/ehm342>.

Ersbøll, A.S., Bojer, A.S., Hauge, M.G., Johansen, M., Damm, P., Gustafsson, F., and Vejlstrup, N.G. (2018). Long-Term Cardiac Function After Peripartum Cardiomyopathy and Preeclampsia: A Danish Nationwide, Clinical Follow-Up Study Using Maximal Exercise Testing and Cardiac Magnetic Resonance Imaging. *Journal of the American Heart Association* 7, e008991. <https://doi.org/10.1161/JAHA.118.008991>.

Escudier, M., Cautela, J., Malissen, N., Ancedy, Y., Orabona, M., Pinto, J., Monestier, S., Grob, J.-J., Scemama, U., and Jacquier, A., et al. (2017). Clinical Features, Management, and Outcomes of Immune Checkpoint Inhibitor-Related Cardiotoxicity. *Circulation* 136, 2085-2087. <https://doi.org/10.1161/CIRCULATIONAHA.117.030571>.

Faron, A., Isaak, A., Mesropyan, N., Reinert, M., Schwab, K., Sirokay, J., Sprinkart, A.M., Bauernfeind, F.-G., Dabir, D., and Pieper, C.C., et al. (2021). Cardiac MRI Depicts Immune Checkpoint Inhibitor-induced Myocarditis: A Prospective Study. *Radiology* 301, 602-609. <https://doi.org/10.1148/radiol.2021210814>.



Felker, G., Shaw, L.K., and O'Connor, C.M. (2002). A standardized definition of ischemic cardiomyopathy for use in clinical research. *Journal of the American College of Cardiology* 39, 210-218. [https://doi.org/10.1016/S0735-1097\(01\)01738-7](https://doi.org/10.1016/S0735-1097(01)01738-7).

Ferreira, V.M., Schulz-Menger, J., Holmvang, G., Kramer, C.M., Carbone, I., Sechtem, U., Kindermann, I., Gutberlet, M., Cooper, L.T., and Liu, P., et al. (2018). Cardiovascular Magnetic Resonance in Nonischemic Myocardial Inflammation: Expert Recommendations. *Journal of the American College of Cardiology* 72, 3158-3176. <https://doi.org/10.1016/j.jacc.2018.09.072>.

Fischer, K., Obrist, S.J., Erne, S.A., Stark, A.W., Marggraf, M., Kaneko, K., Guensch, D.P., Huber, A.T., Greulich, S., and Aghayev, A., et al. (2020). Feature Tracking Myocardial Strain Incrementally Improves Prognostication in Myocarditis Beyond Traditional CMR Imaging Features. *JACC. Cardiovascular imaging* 13, 1891-1901. <https://doi.org/10.1016/j.jcmg.2020.04.025>.

Flett, A.S., Hayward, M.P., Ashworth, M.T., Hansen, M.S., Taylor, A.M., Elliott, P.M., McGregor, C., and Moon, J.C. (2010). Equilibrium contrast cardiovascular magnetic resonance for the measurement of diffuse myocardial fibrosis: preliminary validation in humans. *Circulation* 122, 138-144. <https://doi.org/10.1161/circulationaha.109.930636>.

Follath, F. (1999). Nonischemic heart failure: epidemiology, pathophysiology, and progression of disease. *Journal of cardiovascular pharmacology* 33 Suppl 3, S31-5. <https://doi.org/10.1097/00005344-199906003-00004>.

Gavazzi, A., Maria, R. de, Parolini, M., and Porcu, M. (2000). Alcohol abuse and dilated cardiomyopathy in men. *The American Journal of Cardiology* 85, 1114-1118. [https://doi.org/10.1016/S0002-9149\(00\)00706-2](https://doi.org/10.1016/S0002-9149(00)00706-2).

Giri, S., Chung, Y.-C., Merchant, A., Mihai, G., Rajagopalan, S., Raman, S.V., and Simonetti, O.P. (2009). T2 quantification for improved detection of myocardial edema. *Journal of cardiovascular magnetic resonance : official journal of the Society for Cardiovascular Magnetic Resonance* 11, 56. <https://doi.org/10.1186/1532-429X-11-56>.

Glikson, M., Nielsen, J.C., Kronborg, M.B., Michowitz, Y., Auricchio, A., Barbash, I.M., Barrabés, J.A., Boriani, G., Braunschweig, F., and Brignole, M., et al. (2021). 2021 ESC Guidelines on

cardiac pacing and cardiac resynchronization therapy. *European heart journal* 42, 3427-3520. <https://doi.org/10.1093/eurheartj/ehab364>.

Gräni, C., Eichhorn, C., Bière, L., Kaneko, K., Murthy, V.L., Agarwal, V., Aghayev, A., Steigner, M., Blankstein, R., and Jerosch-Herold, M., et al. (2019). Comparison of myocardial fibrosis quantification methods by cardiovascular magnetic resonance imaging for risk stratification of patients with suspected myocarditis. *Journal of cardiovascular magnetic resonance : official journal of the Society for Cardiovascular Magnetic Resonance* 21, 14. <https://doi.org/10.1186/s12968-019-0520-0>.

Greulich, S., Deluigi, C.C., Gloekler, S., Wahl, A., Zürn, C., Kramer, U., Nothnagel, D., Bültel, H., Schumm, J., and Grün, S., et al. (2013). CMR imaging predicts death and other adverse events in suspected cardiac sarcoidosis. *JACC. Cardiovascular imaging* 6, 501-511. <https://doi.org/10.1016/j.jcmg.2012.10.021>.

Gulati, A., Jabbour, A., Ismail, T.F., Guha, K., Khwaja, J., Raza, S., Morarji, K., Brown, T.D.H., Ismail, N.A., and Dweck, M.R., et al. (2013). Association of fibrosis with mortality and sudden cardiac death in patients with nonischemic dilated cardiomyopathy. *JAMA* 309, 896-908. <https://doi.org/10.1001/jama.2013.1363>.

Hahn, V.S., Lenihan, D.J., and Ky, B. (2014). Cancer therapy-induced cardiotoxicity: basic mechanisms and potential cardioprotective therapies. *Journal of the American Heart Association* 3, e000665. <https://doi.org/10.1161/JAHA.113.000665>.

Halliday, B.P., Gulati, A., Ali, A., Guha, K., Newsome, S., Arzanauskaite, M., Vassiliou, V.S., Lota, A., Izgi, C., and Tayal, U., et al. (2017). Association Between Midwall Late Gadolinium Enhancement and Sudden Cardiac Death in Patients With Dilated Cardiomyopathy and Mild and Moderate Left Ventricular Systolic Dysfunction. *Circulation* 135, 2106-2115. <https://doi.org/10.1161/CIRCULATIONAHA.116.026910>.

Hammersley, D.J., and Halliday, B.P. (2020). Sudden Cardiac Death Prediction in Non-ischemic Dilated Cardiomyopathy: a Multiparametric and Dynamic Approach. *Current cardiology reports* 22, 85. <https://doi.org/10.1007/s11886-020-01343-9>.

Hantson, P. (2019). Mechanisms of toxic cardiomyopathy. *Clinical toxicology (Philadelphia, Pa.)* 57, 1-9. <https://doi.org/10.1080/15563650.2018.1497172>.

Harmon, K.G., Drezner, J.A., Maleszewski, J.J., Lopez-Anderson, M., Owens, D., Prutkin, J.M., Asif, I.M., Klossner, D., and Ackerman, M.J. (2014). Pathogenesises of sudden cardiac death in national collegiate athletic association athletes. *Circulation. Arrhythmia and electrophysiology* 7, 198-204. <https://doi.org/10.1161/CIRCEP.113.001376>.

Harries, I., Liang, K., Williams, M., Berlot, B., Biglino, G., Lancellotti, P., Plana, J.C., and Bucciarelli-Ducci, C. (2020). Magnetic Resonance Imaging to Detect Cardiovascular Effects of Cancer Therapy: JACC CardioOncology State-of-the-Art Review. *JACC. CardioOncology* 2, 270-292. <https://doi.org/10.1016/j.jaccao.2020.04.011>.

Hashimura, H., Kimura, F., Ishibashi-Ueda, H., Morita, Y., Higashi, M., Nakano, S., Iguchi, A., Uotani, K., Sugimura, K., and Naito, H. (2017). Radiologic-Pathologic Correlation of Primary and Secondary Cardiomyopathies: MR Imaging and Histopathologic Findings in Hearts from Autopsy and Transplantation. *Radiographics : a review publication of the Radiological Society of North America, Inc* 37, 719-736. <https://doi.org/10.1148/rg.2017160082>.

Hermans, M.C.E., Faber, C.G., Bekkers, S.C.A.M., Die-Smulders, C.E.M. de, Gerrits, M.M., Merkies, I.S.J., Snoep, G., Pinto, Y.M., and Schalla, S. (2012). Structural and functional cardiac changes in myotonic dystrophy type 1: a cardiovascular magnetic resonance study. *Journal of cardiovascular magnetic resonance : official journal of the Society for Cardiovascular Magnetic Resonance* 14, 48. <https://doi.org/10.1186/1532-429X-14-48>.

Hor, K.N., Gottliebson, W.M., Carson, C., Wash, E., Cnota, J., Fleck, R., Wansapura, J., Klimeczek, P., Al-Khalidi, H.R., and Chung, E.S., et al. (2010). Comparison of magnetic resonance feature tracking for strain calculation with harmonic phase imaging analysis. *JACC. Cardiovascular imaging* 3, 144-151. <https://doi.org/10.1016/j.jcmg.2009.11.006>.

Hundley, W.G., Bluemke, D.A., Finn, J.P., Flamm, S.D., Fogel, M.A., Friedrich, M.G., Ho, V.B., Jerosch-Herold, M., Kramer, C.M., and Manning, W.J., et al. (2010). ACCF/ACR/AHA/NASCI/SCMR 2010 expert consensus document on cardiovascular magnetic resonance: a report of the American College of Cardiology Foundation Task Force on Expert Consensus Documents. *Journal of the American College of Cardiology* 55, 2614-2662. <https://doi.org/10.1016/j.jacc.2009.11.011>.

Isaak, A., Ayub, T.H., Merz, W.M., Faron, A., Endler, C., Sprinkart, A.M., Pieper, C.C., Kuetting, D., Dabir, D., and Attenberger, U., et al. (2022). Peripartum Cardiomyopathy: Diagnostic and

Prognostic Value of Cardiac Magnetic Resonance in the Acute Stage. *Diagnostics (Basel, Switzerland)* 12. <https://doi.org/10.3390/diagnostics12020378>.

Isaak, A., Bischoff, L.M., Faron, A., Endler, C., Mesropyan, N., Sprinkart, A.M., Pieper, C.C., Kuetting, D., Dabir, D., and Attenberger, U., et al. (2021a). Multiparametric cardiac magnetic resonance imaging in pediatric and adolescent patients with acute myocarditis. *Pediatric radiology* 51, 2470-2480. <https://doi.org/10.1007/s00247-021-05169-7>.

Isaak, A., Feisst, A., and Luetkens, J.A. (2021b). Myocarditis Following COVID-19 Vaccination. *Radiology* 301, E378-E379. <https://doi.org/10.1148/radiol.2021211766>.

Isaak, A., Praktijnjo, M., Jansen, C., Faron, A., Sprinkart, A.M., Pieper, C.C., Chang, J., Fimmers, R., Meyer, C., and Dabir, D., et al. (2020). Myocardial Fibrosis and Inflammation in Liver Cirrhosis: MRI Study of the Liver-Heart Axis. *Radiology* 297, 51-61. <https://doi.org/10.1148/radiol.2020201057>.

Jia, G., Hill, M.A., and Sowers, J.R. (2018). Diabetic Cardiomyopathy: An Update of Mechanisms Contributing to This Clinical Entity. *Circulation research* 122, 624-638. <https://doi.org/10.1161/circresaha.117.311586>.

Johnson, D.B., Balko, J.M., Compton, M.L., Chalkias, S., Gorham, J., Xu, Y., Hicks, M., Puzanov, I., Alexander, M.R., and Bloomer, T.L., et al. (2016). Fulminant Myocarditis with Combination Immune Checkpoint Blockade. *The New England journal of medicine* 375, 1749-1755. <https://doi.org/10.1056/nejmoa1609214>.

Kadish, A., Dyer, A., Daubert, J.P., Quigg, R., Estes, N.A.M., Anderson, K.P., Calkins, H., Hoch, D., Goldberger, J., and Shalaby, A., et al. (2004). Prophylactic defibrillator implantation in patients with nonischemic dilated cardiomyopathy. *The New England journal of medicine* 350, 2151-2158. <https://doi.org/10.1056/NEJMoa033088>.

Kammerlander, A.A., Marzluf, B.A., Zotter-Tufaro, C., Aschauer, S., Duca, F., Bachmann, A., Knechtelsdorfer, K., Wiesinger, M., Pfaffenberger, S., and Greiser, A., et al. (2016). T1 Mapping by CMR Imaging: From Histological Validation to Clinical Implication. *JACC. Cardiovascular imaging* 9, 14-23. <https://doi.org/10.1016/j.jcmg.2015.11.002>.

Karamitsos, T.D., Arvanitaki, A., Karvounis, H., Neubauer, S., and Ferreira, V.M. (2020). Myocardial Tissue Characterization and Fibrosis by Imaging. *JACC. Cardiovascular imaging* 13, 1221-1234. <https://doi.org/10.1016/j.jcmg.2019.06.030>.

Karamitsos, T.D., Francis, J.M., Myerson, S., Selvanayagam, J.B., and Neubauer, S. (2009). The role of cardiovascular magnetic resonance imaging in heart failure. *Journal of the American College of Cardiology* 54, 1407-1424. <https://doi.org/10.1016/j.jacc.2009.04.094>.

Klein, I., and Danzi, S. (2007). Thyroid disease and the heart. *Circulation* 116, 1725-1735. <https://doi.org/10.1161/circulationaha.106.678326>.

Knockaert, D.C. (2007). Cardiac involvement in systemic inflammatory diseases. *European heart journal* 28, 1797-1804. <https://doi.org/10.1093/eurheartj/ehm193>.

Køber, L., Thune, J.J., Nielsen, J.C., Haarbo, J., Videbæk, L., Korup, E., Jensen, G., Hildebrandt, P., Steffensen, F.H., and Bruun, N.E., et al. (2016). Defibrillator Implantation in Patients with Nonischemic Systolic Heart Failure. *The New England journal of medicine* 375, 1221-1230. <https://doi.org/10.1056/NEJMoa1608029>.

Kowalski, H.J., and Abelmann, W.H. (1953). The cardiac output at rest in Laennec's cirrhosis. *The Journal of clinical investigation* 32, 1025-1033. <https://doi.org/10.1172/JCI102813>.

Kravchenko, D., Isaak, A., Mesropyan, N., Endler, C., Bischoff, L., Vollbrecht, T., Pieper, C.C., Sedaghat, A., Kuetting, D., and Hart, C., et al. (2022). Befunde der kardialen MRT bei Patienten mit Verdacht auf eine akute Myokarditis nach COVID-19-mRNA-Impfung. *RoFo : Fortschritte auf dem Gebiete der Röntgenstrahlen und der Nuklearmedizin*. <https://doi.org/10.1055/a-1752-0951>.

Kravchenko, D., Isaak, A., Zimmer, S., Mesropyan, N., Reinert, M., Faron, A., Pieper, C.C., Heine, A., Velten, M., and Nattermann, J., et al. (2021). Cardiac MRI in Patients with Prolonged Cardiorespiratory Symptoms after Mild to Moderate COVID-19. *Radiology* 301, E419-E425. <https://doi.org/10.1148/radiol.2021211162>.

Kuruvilla, S., Adenaw, N., Katwal, A.B., Lipinski, M.J., Kramer, C.M., and Salerno, M. (2014). Late gadolinium enhancement on cardiac magnetic resonance predicts adverse cardiovascular outcomes in nonischemic cardiomyopathy: a systematic review and meta-analysis. *Circulation. Cardiovascular imaging* 7, 250-258. <https://doi.org/10.1161/CIRCIMAGING.113.001144>.

Li, S., Di Zhou, Sirajuddin, A., He, J., Xu, J., Zhuang, B., Huang, J., Yin, G., Fan, X., and Wu, W., et al. (2022). T1 Mapping and Extracellular Volume Fraction in Dilated Cardiomyopathy: A

Prognosis Study. *JACC. Cardiovascular imaging* 15, 578-590. <https://doi.org/10.1016/j.jcmg.2021.07.023>.

Li, S., Duan, X., Feng, G., Sirajuddin, A., Yin, G., Zhuang, B., He, J., Xu, J., Yang, W., and Wu, W., et al. (2021). Multiparametric Cardiovascular Magnetic Resonance in Acute Myocarditis: Comparison of 2009 and 2018 Lake Louise Criteria With Endomyocardial Biopsy Confirmation. *Frontiers in cardiovascular medicine* 8, 739892. <https://doi.org/10.3389/fcvm.2021.739892>.

Liang, Y.-D., Xu, Y.-W., Li, W.-H., Wan, K., Sun, J.-Y., Lin, J.-Y., Zhang, Q., Zhou, X.-Y., and Chen, Y.-C. (2020). Left ventricular function recovery in peripartum cardiomyopathy: a cardiovascular magnetic resonance study by myocardial T1 and T2 mapping. *Journal of cardiovascular magnetic resonance : official journal of the Society for Cardiovascular Magnetic Resonance* 22, 2. <https://doi.org/10.1186/s12968-019-0590-z>.

Look, D.C., and Locker, D.R. (1970). Time Saving in Measurement of NMR and EPR Relaxation Times. *Review of Scientific Instruments* 41, 250-251. <https://doi.org/10.1063/1.1684482>.

Lossnitzer, D., Steen, H., Zahn, A., Lehrke, S., Weiss, C., Weiss, K.H., Giannitsis, E., Stremmel, W., Sauer, P., and Katus, H.A., et al. (2010). Myocardial late gadolinium enhancement cardiovascular magnetic resonance in patients with cirrhosis. *Journal of cardiovascular magnetic resonance : official journal of the Society for Cardiovascular Magnetic Resonance* 12, 47. <https://doi.org/10.1186/1532-429x-12-47>.

Lota, A.S., Tsao, A., Owen, R., Halliday, B.P., Auger, D., Vassiliou, V.S., Tayal, U., Almogheer, B., Vilches, S., and Al-Balah, A., et al. (2021). Prognostic Significance of Nonischemic Myocardial Fibrosis in Patients With Normal LV Volumes and Ejection-Fraction. *JACC. Cardiovascular imaging* 14, 2353-2365. <https://doi.org/10.1016/j.jcmg.2021.05.016>.

Luetkens, J.A., Doerner, J., Schwarze-Zander, C., Wasmuth, J.-C., Boesecke, C., Sprinkart, A.M., Schmeel, F.C., Homs, R., Gieseke, J., and Schild, H.H., et al. (2016a). Cardiac Magnetic Resonance Reveals Signs of Subclinical Myocardial Inflammation in Asymptomatic HIV-Infected Patients. *Circulation. Cardiovascular imaging* 9, e004091. <https://doi.org/10.1161/CIRCIMAGING.115.004091>.

Luetkens, J.A., Faron, A., Isaak, A., Dabir, D., Kuetting, D., Feisst, A., Schmeel, F.C., Sprinkart, A.M., and Thomas, D. (2019a). Comparison of Original and 2018 Lake Louise Criteria for



Diagnosis of Acute Myocarditis: Results of a Validation Cohort. *Radiology. Cardiothoracic imaging* 1, e190010. <https://doi.org/10.1148/ryct.2019190010>.

Luetkens, J.A., Homsy, R., Dabir, D., Kuetting, D.L., Marx, C., Doerner, J., Schlesinger-Irsch, U., Andrié, R., Sprinkart, A.M., and Schmeel, F.C., et al. (2016b). Comprehensive Cardiac Magnetic Resonance for Short-Term Follow-Up in Acute Myocarditis. *Journal of the American Heart Association* 5. <https://doi.org/10.1161/JAHA.116.003603>.

Luetkens, J.A., Homsy, R., Sprinkart, A.M., Doerner, J., Dabir, D., Kuetting, D.L., Block, W., Andrié, R., Stehning, C., and Fimmers, R., et al. (2016c). Incremental value of quantitative CMR including parametric mapping for the diagnosis of acute myocarditis. *European heart journal. Cardiovascular Imaging* 17, 154-161. <https://doi.org/10.1093/ehjci/jev246>.

Luetkens, J.A., Isaak, A., Öztürk, C., Mesropyan, N., Monin, M., Schlabe, S., Reinert, M., Faron, A., Heine, A., and Velten, M., et al. (2021). Cardiac MRI in Suspected Acute COVID-19 Myocarditis. *Radiology. Cardiothoracic imaging* 3, e200628. <https://doi.org/10.1148/ryct.2021200628>.

Luetkens, J.A., Isaak, A., Zimmer, S., Nattermann, J., Sprinkart, A.M., Boesecke, C., Rieke, G.J., Zachoval, C., Heine, A., and Velten, M., et al. (2020). Diffuse Myocardial Inflammation in COVID-19 Associated Myocarditis Detected by Multiparametric Cardiac Magnetic Resonance Imaging. *Circulation. Cardiovascular imaging* 13, e010897. <https://doi.org/10.1161/circimaging.120.010897>.

Luetkens, J.A., Landenberg, C. von, Isaak, A., Faron, A., Kuetting, D., Gliem, C., Dabir, D., Kornblum, C., and Thomas, D. (2019b). Comprehensive Cardiac Magnetic Resonance for Assessment of Cardiac Involvement in Myotonic Muscular Dystrophy Type 1 and 2 Without Known Cardiovascular Disease. *Circulation. Cardiovascular imaging* 12, e009100. <https://doi.org/10.1161/CIRCIMAGING.119.009100>.

Luetkens, J.A., Schlesinger-Irsch, U., Kuetting, D.L., Dabir, D., Homsy, R., Doerner, J., Schmeel, F.C., Fimmers, R., Sprinkart, A.M., and Naehle, C.P., et al. (2017). Feature-tracking myocardial strain analysis in acute myocarditis: diagnostic value and association with myocardial oedema. *European radiology* 27, 4661-4671. <https://doi.org/10.1007/s00330-017-4854-4>.

Lurz, P., Luecke, C., Eitel, I., Föhrenbach, F., Frank, C., Grothoff, M., Waha, S. de, Rommel, K.-P., Lurz, J.A., and Klingel, K., et al. (2016). Comprehensive Cardiac Magnetic Resonance

Imaging in Patients With Suspected Myocarditis: The MyoRacer-Trial. *Journal of the American College of Cardiology* 67, 1800-1811. <https://doi.org/10.1016/j.jacc.2016.02.013>.

Lyon, A.R., Yousaf, N., Battisti, N.M.L., Moslehi, J., and Larkin, J. (2018). Immune checkpoint inhibitors and cardiovascular toxicity. *The Lancet Oncology* 19, e447-e458. [https://doi.org/10.1016/S1470-2045\(18\)30457-1](https://doi.org/10.1016/S1470-2045(18)30457-1).

Ma, Z., and Lee, S.S. (1996). Cirrhotic cardiomyopathy: getting to the heart of the matter. *Hepatology (Baltimore, Md.)* 24, 451-459. <https://doi.org/10.1002/hep.510240226>.

Mahrholdt, H., Wagner, A., Judd, R.M., Sechtem, U., and Kim, R.J. (2005). Delayed enhancement cardiovascular magnetic resonance assessment of non-ischaemic cardiomyopathies. *European heart journal* 26, 1461-1474. <https://doi.org/10.1093/eurheartj/ehi258>.

Marian, A.J., and Braunwald, E. (2017). Hypertrophic Cardiomyopathy: Genetics, Pathogenesis, Clinical Manifestations, Diagnosis, and Therapy. *Circulation research* 121, 749-770. <https://doi.org/10.1161/CIRCRESAHA.117.311059>.

Maron, B.J., Towbin, J.A., Thiene, G., Antzelevitch, C., Corrado, D., Arnett, D., Moss, A.J., Seidman, C.E., and Young, J.B. (2006). Contemporary definitions and classification of the cardiomyopathies: an American Heart Association Scientific Statement from the Council on Clinical Cardiology, Heart Failure and Transplantation Committee; Quality of Care and Outcomes Research and Functional Genomics and Translational Biology Interdisciplinary Working Groups; and Council on Epidemiology and Prevention. *Circulation* 113, 1807-1816. <https://doi.org/10.1161/circulationaha.106.174287>.

Matyas, C., Erdelyi, K., Trojnar, E., Zhao, S., Varga, Z.V., Paloczi, J., Mukhopadhyay, P., Nemeth, B.T., Haskó, G., and Cinar, R., et al. (2020). Interplay of Liver-Heart Inflammatory Axis and Cannabinoid 2 Receptor Signaling in an Experimental Model of Hepatic Cardiomyopathy. *Hepatology (Baltimore, Md.)* 71, 1391-1407. <https://doi.org/10.1002/hep.30916>.

McDonagh, T.A., Metra, M., Adamo, M., Gardner, R.S., Baumbach, A., Böhm, M., Burri, H., Butler, J., Čelutkienė, J., and Chioncel, O., et al. (2021). 2021 ESC Guidelines for the diagnosis and treatment of acute and chronic heart failure. *European heart journal* 42, 3599-3726. <https://doi.org/10.1093/eurheartj/ehab368>.

- McKenna, W.J., Maron, B.J., and Thiene, G. (2017). Classification, Epidemiology, and Global Burden of Cardiomyopathies. *Circulation research* 121, 722-730. <https://doi.org/10.1161/CIRCRESAHA.117.309711>.
- Merlo, M., Ammirati, E., Gentile, P., Artico, J., Cannatà, A., Finocchiaro, G., Barbati, G., Sormani, P., Varrenti, M., and Perkan, A., et al. (2019). Persistent left ventricular dysfunction after acute lymphocytic myocarditis: Frequency and predictors. *PloS one* 14, e0214616. <https://doi.org/10.1371/journal.pone.0214616>.
- Messroghli, D.R., Moon, J.C., Ferreira, V.M., Grosse-Wortmann, L., He, T., Kellman, P., Mascherbauer, J., Nezafat, R., Salerno, M., and Schelbert, E.B., et al. (2017). Clinical recommendations for cardiovascular magnetic resonance mapping of T1, T2, T2\* and extracellular volume: A consensus statement by the Society for Cardiovascular Magnetic Resonance (SCMR) endorsed by the European Association for Cardiovascular Imaging (EACVI). *Journal of cardiovascular magnetic resonance : official journal of the Society for Cardiovascular Magnetic Resonance* 19, 75. <https://doi.org/10.1186/s12968-017-0389-8>.
- Messroghli, D.R., Radjenovic, A., Kozerke, S., Higgins, D.M., Sivananthan, M.U., and Ridgway, J.P. (2004). Modified Look-Locker inversion recovery (MOLLI) for high-resolution T1 mapping of the heart. *Magnetic resonance in medicine* 52, 141-146. <https://doi.org/10.1002/mrm.20110>.
- Miller, C.A., Naish, J.H., Bishop, P., Coutts, G., Clark, D., Zhao, S., Ray, S.G., Yonan, N., Williams, S.G., and Flett, A.S., et al. (2013). Comprehensive validation of cardiovascular magnetic resonance techniques for the assessment of myocardial extracellular volume. *Circulation. Cardiovascular imaging* 6, 373-383. <https://doi.org/10.1161/CIRCIMAGING.112.000192>.
- Møller, S., and Bernardi, M. (2013). Interactions of the heart and the liver. *European heart journal* 34, 2804-2811. <https://doi.org/10.1093/eurheartj/eh246>.
- Møller, S., and Henriksen, J.H. (2010). Cirrhotic cardiomyopathy. *Journal of hepatology* 53, 179-190. <https://doi.org/10.1016/j.jhep.2010.02.023>.
- Neilan, T.G., Coelho-Filho, O.R., Danik, S.B., Shah, R.V., Dodson, J.A., Verdini, D.J., Tokuda, M., Daly, C.A., Tedrow, U.B., and Stevenson, W.G., et al. (2013). CMR quantification of myocardial scar provides additive prognostic information in nonischemic cardiomyopathy. *JACC. Cardiovascular imaging* 6, 944-954. <https://doi.org/10.1016/j.jcmg.2013.05.013>.

Patel, A.R., and Kramer, C.M. (2017). Role of Cardiac Magnetic Resonance in the Diagnosis and Prognosis of Nonischemic Cardiomyopathy. *JACC. Cardiovascular imaging* 10, 1180-1193. <https://doi.org/10.1016/j.jcmg.2017.08.005>.

Pereira, N.L., Grogan, M., and Dec, G.W. (2018). Spectrum of Restrictive and Infiltrative Cardiomyopathies: Part 1 of a 2-Part Series. *Journal of the American College of Cardiology* 71, 1130-1148. <https://doi.org/10.1016/j.jacc.2018.01.016>.

Petersen, S.E., and Khanji, M.Y. (2021). Bright Is (Not Too) Bad: "Incidental" Nonischemic Fibrosis Associated With Good Outcomes in "Normal" Hearts. *JACC. Cardiovascular imaging* 14, 2366-2368. <https://doi.org/10.1016/j.jcmg.2021.06.009>.

Plana, J.C., Thavendiranathan, P., Bucciarelli-Ducci, C., and Lancellotti, P. (2018). Multi-Modality Imaging in the Assessment of Cardiovascular Toxicity in the Cancer Patient. *JACC. Cardiovascular imaging* 11, 1173-1186. <https://doi.org/10.1016/j.jcmg.2018.06.003>.

Praktiknjo, M., Monteiro, S., Grandt, J., Kimer, N., Madsen, J.L., Werge, M.P., William, P., Brol, M.J., Turco, L., and Schierwagen, R., et al. (2020). Cardiodynamic state is associated with systemic inflammation and fatal acute-on-chronic liver failure. *Liver international : official journal of the International Association for the Study of the Liver* 40, 1457-1466. <https://doi.org/10.1111/liv.14433>.

Prasad, M., Hermann, J., Gabriel, S.E., Weyand, C.M., Mulvagh, S., Mankad, R., Oh, J.K., Matteson, E.L., and Lerman, A. (2015). Cardiorheumatology: cardiac involvement in systemic rheumatic disease. *Nature reviews. Cardiology* 12, 168-176. <https://doi.org/10.1038/nrcardio.2014.206>.

Puntmann, V.O., Carerj, M.L., Wieters, I., Fahim, M., Arendt, C., Hoffmann, J., Shchendrygina, A., Escher, F., Vasa-Nicotera, M., and Zeiher, A.M., et al. (2020). Outcomes of Cardiovascular Magnetic Resonance Imaging in Patients Recently Recovered From Coronavirus Disease 2019 (COVID-19). *JAMA cardiology* 5, 1265-1273. <https://doi.org/10.1001/jamacardio.2020.3557>.

Puntmann, V.O., D'Cruz, D., Smith, Z., Pastor, A., Choong, P., Voigt, T., Carr-White, G., Sangle, S., Schaeffter, T., and Nagel, E. (2013). Native myocardial T1 mapping by cardiovascular magnetic resonance imaging in subclinical cardiomyopathy in patients with systemic lupus erythematosus. *Circulation. Cardiovascular imaging* 6, 295-301. <https://doi.org/10.1161/CIRCIMAGING.112.000151>.

Regitz-Zagrosek, V., Roos-Hesselink, J.W., Bauersachs, J., Blomström-Lundqvist, C., Cífková, R., Bonis, M. de, lung, B., Johnson, M.R., Kintscher, U., and Kranke, P., et al. (2018). 2018 ESC Guidelines for the management of cardiovascular diseases during pregnancy. *European heart journal* 39, 3165-3241. <https://doi.org/10.1093/eurheartj/ehy340>.

Renz, D.M., Röttgen, R., Habedank, D., Wagner, M., Böttcher, J., Pfeil, A., Dietz, R., Kivelitz, D., and Elgeti, T. (2011). New insights into peripartum cardiomyopathy using cardiac magnetic resonance imaging. *RoFo : Fortschritte auf dem Gebiete der Rontgenstrahlen und der Nuklearmedizin* 183, 834-841. <https://doi.org/10.1055/s-0031-1281600>.

Ricci, F., Innocentiis, C. de, Verrengia, E., Ceriello, L., Mantini, C., Pietrangelo, C., Irsuti, F., Gabriele, S., D'Alleva, A., and Khanji, M.Y., et al. (2020). The Role of Multimodality Cardiovascular Imaging in Peripartum Cardiomyopathy. *Frontiers in cardiovascular medicine* 7, 4. <https://doi.org/10.3389/fcvm.2020.00004>.

Roger, V.L., Go, A.S., Lloyd-Jones, D.M., Adams, R.J., Berry, J.D., Brown, T.M., Carnethon, M.R., Dai, S., Simone, G. de, and Ford, E.S., et al. (2011). Heart disease and stroke statistics--2011 update: a report from the American Heart Association. *Circulation* 123, e18-e209. <https://doi.org/10.1161/CIR.0b013e3182009701>.

Romano, S., Judd, R.M., Kim, R.J., Kim, H.W., Klem, I., Heitner, J.F., Shah, D.J., Jue, J., White, B.E., and Indorkar, R., et al. (2018). Feature-Tracking Global Longitudinal Strain Predicts Death in a Multicenter Population of Patients With Ischemic and Nonischemic Dilated Cardiomyopathy Incremental to Ejection Fraction and Late Gadolinium Enhancement. *JACC. Cardiovascular imaging* 11, 1419-1429. <https://doi.org/10.1016/j.jcmg.2017.10.024>.

Schelbert, E.B., Elkayam, U., Cooper, L.T., Givertz, M.M., Alexis, J.D., Briller, J., Felker, G.M., Chaparro, S., Kealey, A., and Pisarcik, J., et al. (2017). Myocardial Damage Detected by Late Gadolinium Enhancement Cardiac Magnetic Resonance Is Uncommon in Peripartum Cardiomyopathy. *Journal of the American Heart Association* 6. <https://doi.org/10.1161/JAHA.117.005472>.

Schmacht, L., Traber, J., Grieben, U., Utz, W., Dieringer, M.A., Kellman, P., Blaszczyk, E., Knobelsdorff-Brenkenhoff, F. von, Spuler, S., and Schulz-Menger, J. (2016). Cardiac Involvement in Myotonic Dystrophy Type 2 Patients With Preserved Ejection Fraction:

Detection by Cardiovascular Magnetic Resonance. *Circulation. Cardiovascular imaging* 9. <https://doi.org/10.1161/CIRCIMAGING.115.004615>.

Schürer, S., Klingel, K., Sandri, M., Majunke, N., Besler, C., Kandolf, R., Lurz, P., Luck, M., Hertel, P., and Schuler, G., et al. (2017). Clinical Characteristics, Histopathological Features, and Clinical Outcome of Methamphetamine-Associated Cardiomyopathy. *JACC. Heart failure* 5, 435-445. <https://doi.org/10.1016/j.jchf.2017.02.017>.

Schuster, A., Hor, K.N., Kowallick, J.T., Beerbaum, P., and Kutty, S. (2016). Cardiovascular Magnetic Resonance Myocardial Feature Tracking: Concepts and Clinical Applications. *Circulation. Cardiovascular imaging* 9, e004077. <https://doi.org/10.1161/CIRCIMAGING.115.004077>.

Schwartz, B.G., Rezkalla, S., and Kloner, R.A. (2010). Cardiovascular effects of cocaine. *Circulation* 122, 2558-2569. <https://doi.org/10.1161/CIRCULATIONAHA.110.940569>.

Seferović, P.M., Polovina, M., Bauersachs, J., Arad, M., Gal, T.B., Lund, L.H., Felix, S.B., Arbustini, E., Caforio, A.L.P., and Farmakis, D., et al. (2019). Heart failure in cardiomyopathies: a position paper from the Heart Failure Association of the European Society of Cardiology. *European journal of heart failure* 21, 553-576. <https://doi.org/10.1002/ejhf.1461>.

Seward, J.B., and Casacang-Verzosa, G. (2010). Infiltrative cardiovascular diseases: cardiomyopathies that look alike. *Journal of the American College of Cardiology* 55, 1769-1779. <https://doi.org/10.1016/j.jacc.2009.12.040>.

Sprinkart, A.M., Luetkens, J.A., Träber, F., Doerner, J., Gieseke, J., Schnackenburg, B., Schmitz, G., Thomas, D., Homsy, R., and Block, W., et al. (2015). Gradient Spin Echo (GraSE) imaging for fast myocardial T2 mapping. *Journal of cardiovascular magnetic resonance : official journal of the Society for Cardiovascular Magnetic Resonance* 17, 12. <https://doi.org/10.1186/s12968-015-0127-z>.

Starekova, J., Bluemke, D.A., Bradham, W.S., Eckhardt, L.L., Grist, T.M., Kusmirek, J.E., Purtell, C.S., Schiebler, M.L., and Reeder, S.B. (2021). Evaluation for Myocarditis in Competitive Student Athletes Recovering From Coronavirus Disease 2019 With Cardiac Magnetic Resonance Imaging. *JAMA cardiology* 6, 945-950. <https://doi.org/10.1001/jamacardio.2020.7444>.



Templin, C., Ghadri, J.R., Diekmann, J., Napp, L.C., Bataiosu, D.R., Jaguszewski, M., Cammann, V.L., Sarcon, A., Geyer, V., and Neumann, C.A., et al. (2015). Clinical Features and Outcomes of Takotsubo (Stress) Cardiomyopathy. *The New England journal of medicine* 373, 929-938. <https://doi.org/10.1056/NEJMoa1406761>.

Thavendiranathan, P., Zhang, L., Zafar, A., Drobni, Z.D., Mahmood, S.S., Cabral, M., Awadalla, M., Nohria, A., Zlotoff, D.A., and Thuny, F., et al. (2021). Myocardial T1 and T2 Mapping by Magnetic Resonance in Patients With Immune Checkpoint Inhibitor-Associated Myocarditis. *Journal of the American College of Cardiology* 77, 1503-1516. <https://doi.org/10.1016/j.jacc.2021.01.050>.

Towbin, J.A., Lorts, A., and Jefferies, J.L. (2015). Left ventricular non-compaction cardiomyopathy. *The Lancet* 386, 813-825. [https://doi.org/10.1016/S0140-6736\(14\)61282-4](https://doi.org/10.1016/S0140-6736(14)61282-4).

Tschöpe, C., Ammirati, E., Bozkurt, B., Caforio, A.L.P., Cooper, L.T., Felix, S.B., Hare, J.M., Heidecker, B., Heymans, S., and Hübner, N., et al. (2021). Myocarditis and inflammatory cardiomyopathy: current evidence and future directions. *Nature reviews. Cardiology* 18, 169-193. <https://doi.org/10.1038/s41569-020-00435-x>.

Vermes, E., Childs, H., Faris, P., and Friedrich, M.G. (2014). Predictive value of CMR criteria for LV functional improvement in patients with acute myocarditis. *European heart journal. Cardiovascular Imaging* 15, 1140-1144. <https://doi.org/10.1093/ehjci/jeu099>.

Vogel-Claussen, J., Rochitte, C.E., Wu, K.C., Kamel, I.R., Foo, T.K., Lima, J.A.C., and Bluemke, D.A. (2006). Delayed enhancement MR imaging: utility in myocardial assessment. *Radiographics : a review publication of the Radiological Society of North America, Inc* 26, 795-810. <https://doi.org/10.1148/rg.263055047>.

Vos, T., Barber, R.M., Bell, B., Bertozzi-Villa, A., Biryukov, S., Bolliger, I., Charlson, F., Davis, A., Degenhardt, L., and Dicker, D., et al. (2015). Global, regional, and national incidence, prevalence, and years lived with disability for 301 acute and chronic diseases and injuries in 188 countries, 1990–2013: a systematic analysis for the Global Burden of Disease Study 2013. *The Lancet* 386, 743-800. [https://doi.org/10.1016/S0140-6736\(15\)60692-4](https://doi.org/10.1016/S0140-6736(15)60692-4).

Weintraub, R.G., Semsarian, C., and Macdonald, P. (2017). Dilated cardiomyopathy. *The Lancet* 390, 400-414. [https://doi.org/10.1016/S0140-6736\(16\)31713-5](https://doi.org/10.1016/S0140-6736(16)31713-5).

Wiese, S., Hove, J., Mo, S., Mookerjee, R.P., Petersen, C.L., Vester-Andersen, M.K., Mygind, N.D., Goetze, J.P., Kjaer, A., and Bendtsen, F., et al. (2018). Myocardial extracellular volume quantified by magnetic resonance is increased in cirrhosis and related to poor outcome. *Liver international : official journal of the International Association for the Study of the Liver* 38, 1614-1623. <https://doi.org/10.1111/liv.13870>.

Wiese, S., Voiosu, A., Hove, J.D., Danielsen, K.V., Voiosu, T., Grønbaek, H., Møller, H.J., Genovese, F., Reese-Petersen, A.L., and Mookerjee, R.P., et al. (2020). Fibrogenesis and inflammation contribute to the pathogenesis of cirrhotic cardiomyopathy. *Alimentary pharmacology & therapeutics* 52, 340-350. <https://doi.org/10.1111/apt.15812>.

Zamorano, J.L., Lancellotti, P., Rodriguez Muñoz, D., Aboyans, V., Asteggiano, R., Galderisi, M., Habib, G., Lenihan, D.J., Lip, G.Y.H., and Lyon, A.R., et al. (2016). 2016 ESC Position Paper on cancer treatments and cardiovascular toxicity developed under the auspices of the ESC Committee for Practice Guidelines: The Task Force for cancer treatments and cardiovascular toxicity of the European Society of Cardiology (ESC). *European heart journal* 37, 2768-2801. <https://doi.org/10.1093/eurheartj/ehw211>.

Zardi, E.M., Abbate, A., Zardi, D.M., Dobrina, A., Margiotta, D., van Tassel, B.W., van Tassel, B.W., Afeltra, A., and Sanyal, A.J. (2010). Cirrhotic cardiomyopathy. *Journal of the American College of Cardiology* 56, 539-549. <https://doi.org/10.1016/j.jacc.2009.12.075>.

Zhang, L., Awadalla, M., Mahmood, S.S., Nohria, A., Hassan, M.Z.O., Thuny, F., Zlotoff, D.A., Murphy, S.P., Stone, J.R., and Golden, D.L.A., et al. (2020). Cardiovascular magnetic resonance in immune checkpoint inhibitor-associated myocarditis. *European heart journal* 41, 1733-1743. <https://doi.org/10.1093/eurheartj/ehaa051>.

Zorzi, A., Perazzolo Marra, M., Rigato, I., Lazzari, M. de, Susana, A., Niero, A., Pilichou, K., Migliore, F., Rizzo, S., and Giorgi, B., et al. (2016). Nonischemic Left Ventricular Scar as a Substrate of Life-Threatening Ventricular Arrhythmias and Sudden Cardiac Death in Competitive Athletes. *Circulation. Arrhythmia and electrophysiology* 9. <https://doi.org/10.1161/circep.116.004229>.

## 8. Danksagung

Mein erster und besonderer Dank gilt Prof. Dr. Ulrike Attenberger. Sie haben mir seit dem ersten Tag Ihrer Amtszeit Vertrauen und Wertschätzung entgegengebracht und mich mit Ihren motivierenden Impulsen immerfort in meiner wissenschaftlichen Arbeit bestärkt und so die Vollendung dieser Arbeit ermöglicht.

Meinen tiefen Dank möchte ich Prof. Dr. Hans Schild aussprechen, der mir den klinischen Einstieg in die Radiologie erst ermöglichte. Ich danke Ihnen für Ihr Vertrauen und dafür, dass Sie früh die Weichen für meine wissenschaftliche Laufbahn gestellt haben.

Ein herzlicher Dank gilt Prof. Dr. Daniel Thomas, der mir die klinische und wissenschaftliche Arbeit in der Herzbildgebung ermöglichte, die mich bis heute tagtäglich begeistert.

Als nächstes möchte ich mich bei Priv.-Doz. Dr. Darius Dabir, einem ganz besonderen Menschen und Freund bedanken. Du hast mich damals im MRT schnell unter deine Fittiche genommen und die Herzbildgebung für mich zur Herzenssache gemacht. Danke für Deine wertvollen und konstruktiven Ratschläge, deine Großzügigkeit und deine Herzlichkeit.

Für die größtmögliche Unterstützung bei meiner wissenschaftlichen Laufbahn bedanke ich mich bei meinem Mentor Priv.-Doz. Dr. Julian Luetkens. Du hast bereits in meinem ersten Jahr das wissenschaftliche Feuer in mir entfacht. Durch Deine inspirierende, motivierende, fokussierte und teamorientierte Art hast du es geschafft, dass ich bis heute an keinem Tag den Spaß am wissenschaftlichen Arbeiten verloren habe. Danke für Deine unschätzbar wertvolle und fortwährende Unterstützung und Förderung, ohne die diese Arbeit so nicht möglich gewesen wäre.

Für das wertvolle Mentoring und die zahlreichen Hilfestellungen und Unterstützungen gilt ein außerordentlicher Dank Priv.-Doz. Dr. Alois Martin Sprinkart, Priv.-Doz. Dr. Daniel Kütting, Dr. Patrick Kupczyk, Priv.-Doz. Dr. Claus Pieper und Dr. Andreas Feisst.

Ohne Teamgeist wäre diese Arbeit so nicht möglich gewesen. Ich danke meiner gesamten Arbeitsgruppe, ganz besonders Priv.-Doz. Dr. Anton Faron, Dr. Christoph Endler, Dr. Narine Mesropyan, Dr. Dmitrij Kravchenko, Dr. Thomas Vollbrecht und Leon Bischoff, für den produktiven wissenschaftlichen Austausch und die Kameradschaft bei den täglichen Herausforderungen von Klinik und Wissenschaft.

Ein riesiger Dank gebührt natürlich auch dem gesamten radiologischen Team, ganz besonders dem MRT-Team. Auch wenn ich nicht alle Kolleginnen und Kollegen einzeln benennen kann, möchte ich, dass sich wirklich jede und jeder Einzelne des gesamten MRT-Teams angesprochen fühlt: Danke für Eure Unterstützung bei der alltäglichen Umsetzung meiner prospektiven Projekte, für die zahlreichen Projekt- und Terminkoordinierungen, für die praktischen Hilfestellungen am Scanner und für den Spaß bei und an der Arbeit!

Für die wertvolle technische Unterstützung am MRT, die zahlreichen Sequenzoptimierungen und den wichtigen klinisch-technischen Austausch möchte ich mich ganz herzlich bei Dr. Shuo Zhang, Christoph Katemann und Dr. Oliver Weber bedanken.

Vielen Dank an die zahlreichen interdisziplinären Kooperationspartner für die produktive Zusammenarbeit, insbesondere Dr. Johannes Chang, Dr. Christian Jansen und Priv.-Doz. Dr. Michael Praktiknjo aus der Hepatologie, Prof. Dr. Rainer Surges, Dr. Jan Pukropski und Dr. Elisa Volmering aus der Epileptologie, Priv.-Doz. Dr. Stefan Kreyer aus der Anästhesiologie/Intensivmedizin sowie Frau Dr. Leonie Weinhold aus dem Institut für Medizinische Biometrie, Informatik und Epidemiologie.

Zum Schluss möchte ich mich bei meiner *gesamten* Familie bedanken, insbesondere bei meinen Großeltern und meinen Schwiegereltern. Allen voran aber bei meinen Eltern und meinem Bruder, ohne deren immerwährende Unterstützung über alle bisherigen Lebensabschnitte hinweg das alles nicht möglich gewesen wäre. Ihr habt mir gezeigt, was man mit Einsatz und Fleiß alles erreichen kann und mich bis heute geprägt. Danke für Euer Vertrauen, Eure Zuversicht, Eure selbstlose Liebe und dafür, dass Ihr mir jederzeit ermöglicht, meine Träume zu verwirklichen. Von Herzen danke ich schließlich meiner Frau Marie-Luise: für Deine Liebe, Deinen motivierenden Antrieb, Dein Verständnis und für den bedingungslosen Rückhalt, den Du mir jeden Tag gibst!